



Title	A study on growth processes of sea ice in the southern region of the Okhotsk Sea, evaluated from heat budget and sea ice sample analysis
Author(s)	Toyota, Takenobu
Citation	北海道大学. 博士(地球環境科学) 甲第4579号
Issue Date	1998-12-25
DOI	10.11501/3146358
Doc URL	<a href="http://hdl.handle.net/2115/32520">http://hdl.handle.net/2115/32520</a>
Type	theses (doctoral)
File Information	4579.pdf



[Instructions for use](#)

A study on growth processes of sea ice  
in the southern region of the Okhotsk Sea,  
evaluated from heat budget and sea ice sample analysis

(熱収支と海氷サンプルの解析による  
オホーツク海南部の海氷の成長過程に関する研究)

A dissertation submitted to Hokkaido University  
for the degree of Doctor of Environmental Earth Science

by

Takenobu Toyota

(November, 1998)

## Abstract

In order to investigate the characteristics of the sea ice extent in the southern region of the Okhotsk Sea, we conducted ice observations in connection with meteorological and hydrographical observation from 3 to 5 February of 1996 and from 2 to 9 February of 1997. In ice observations, ice concentration and thickness are quantitatively estimated through video analysis, and in-situ sea ice pieces are sampled. Meteorological observation contains air temperature, wind, and albedo. The result of albedo analysis shows that surface albedo is well correlated with ice concentration and has a statistically significant correlation with solar zenith angle and ice thickness and that daily integrated sea ice albedo is estimated as  $0.63 \pm 0.03$ . This value is somewhat lower than that observed in the polar land fast ice region. The developed snow grains on sea ice may be responsible for this low value. On the basis of the estimated sea ice albedo and meteorological observation, the heat budget and ice growth rate are calculated with a thermodynamical model. The result indicates that the averaged ice growth rate is limited to below 0.5 cm/day and that sea ice area in this region works as a heating source to atmosphere although the turbulent heat flux is a half of that without sea ice. The latter of these results is attributed to thinner ice thickness. It is shown from ice sample analysis that these characteristics influence the ice structure. First, it is found for thick ice that granular structure occupies greater part than columnar one and many ice samples are composed of several ice sheets of 5 to 10 cm thickness/layer on average. These results indicate that dynamical processes are more essential for ice growth than thermodynamical ones in this region. Second, the nilas samples of about 1 cm thickness with almost vertically oriented c-axes were found out. Laboratory experiments are carried out to examine the feature of this structure. As a result, it is shown that less saline water than normal sea water is required for the c-axis vertical layer, which forms near the ice surface, to develop up to about 1 cm. It is suggested from heat budget calculation that such less saline water can possibly be produced due to melting at daytime in this region. Therefore, those nilas samples may be affected by this less saline water. All these results of ice sample analysis indicate that the structure of sea ice is much influenced by the heat budget characteristics in this region.

## Acknowledgements

The author would like to express his heartfelt gratitude to Prof.M.Wakatsuchi of the Institute of Low Temperature Science of Hokkaido University (ILTS) for the invaluable suggestions and the encouragement throughout his research. He is also deeply grateful to Dr.T.Kawamura, who always gave helpful suggestions to him during the course of ice sample analysis and laboratory experiments and stimulated his interest, and to Dr.K.I.Ohshima and Dr.Y.Fukamachi for their generous support and helpful discussions throughout his research. He is also indebted to Prof.M.Ikeda, Prof.K.Takeuchi, Prof.K.Yamazaki, and Prof.T.Yamanouchi for critical reading of this paper and valuable comments and to Dr.J.Ukita, the co-worker at cruise observation, for valuable discussions. Thanks are extended to all the members of the oceanographical division of ILTS for precious comments at the seminars. He is much obliged to Mr.M.Ohi for the GPS instrument and to Mr.H.Ishii and Mr.T.Segawa for the apparatus of laboratory experiments.

All the crew of *P/V SOYA*, Marine Safety Agency, kindly cooperated with us throughout the cruise observation. Dr.N.Iwasaka of Tokyo Merchant Vessel University kindly offered the pyranometers to us. Mr.H.Shimoda of Ship Research Institute kindly helped him through the technical support of the observation and analysis of video monitoring. Mr.Y.Nabae of First Regional Maritime Safety Headquarters kindly helped him with the calculation of solar position. Mr.N.Okada of Sapporo Sun-piazza aquarium kindly offered sea water used for laboratory experiments. He would like to take this opportunity to express sincere gratitude to all of them. Finally, he expresses his profound thanks to Ms.A.Tonedachi who always encouraged him in making his decision in his life.

GFD-Dennou Club Library is used for graph drawing. The program developed by Prof.Muramoto is used for ice concentration analysis. This study was supported partly by a special fund, Center of Excellence (COE), for scientific research and partly by the Grant-in-Aid for Scientific Research on Priority Areas (Nos. 08241201 and 09227201), from the Ministry of Education, Science, Sports and Culture of Japan.



# Contents

1. Introduction		1
2. Observations	2.1 Conditions	6
	2.2 Meteorological observation	8
	2.3 Sea ice observation	10
3. Albedo	3.1 Introduction	21
	3.2 Measurement	22
	3.2.1 Measurement errors	
	3.2.2 Comparison of observation areas	
	3.3 Turning Experiment	25
	3.4 Results	30
	3.5 Summary and Discussion	43
4. Heat Budget	4.1 Introduction	47
	4.2 Method of calculation	48
	4.3 Results	56
	4.4 Summary and Discussion	68
5. Ice Sample Analysis	5.1 Introduction	70
	5.2 Method of Analysis	75
	5.3 Results	77
	5.3.1 General characteristics	
	5.3.2 First-year ice and Young ice	
	5.3.3 Nilas	
	5.3.4 Pancake ice	
	5.4 Summary and Discussion	105
6. Laboratory Experiments	6.1 Introduction	106
	6.2 Apparatus and Experimental procedures	107
	6.3 Results	111
	6.4 Summary and Discussion	130
7. Conclusion		134
References		137

## Chapter 1. Introduction

The southern region of the Okhotsk Sea is characterized by sea ice which covers this area in winter. The sea ice in this region is located at the lowest latitude in the world and has been drawing lots of scientists' interests. Hence a lot of researches concerning the sea ice in this region have been made so far mainly from the analysis of the in-situ ice samples near Hokkaido coast and the coastal radar observation. For example, *Ono (1965)* has examined the thermal properties and *Tabata (1966)* has examined the mechanical properties with the in-situ sea ice. From the radar observation, mainly the sea ice motion (e.g. *Tabata et al., 1969; Kawamura et al., 1975*) and the annual variation of sea ice amount off Hokkaido (*Aota et al., 1988*) have been investigated. However, the observation has been limited to the coastal region, and sea ice in the interior pack ice region has been little investigated. Although the ship-based ice thickness measurements have been continued since 1991 by Ship Research Institute, Ministry of Transport, the structural analysis of sea ice, which gives an important information of ice growth history, has not been done so far. Therefore, the ice growth processes in this region still remains unknown.

From the viewpoint of atmospheric circulation, this region is worth noticing. This region is one of the main cyclone tracks in winter over East Asia (*Chen et al., 1991*), and it is shown that especially developing cyclones often pass over this region (*Nakamura et al., 1986*). Therefore, it may be possible that heat exchange between the atmosphere and the sea ice area over this region has a significant effect on the cyclone activities there. The possibility that sea ice area in the Okhotsk Sea influences the atmospheric circulation has been pointed out mainly from numerical studies. For example, *Honda et al. (1996)* showed using the general circulation model that sea ice area has an effect on a global scale atmospheric circulation through the propagation of wave activities. For a local scale, *Sasaki and Deguchi (1988)* showed that the sea ice area can affect the convergent

band off the western Hokkaido coast in winter, and *Okubo and Mannoji (1994)* showed that the sea ice area can affect the wind pattern in Hokkaido. However, because of the lack of in-situ observational data, it is still unknown how much effect sea ice area has on the heat budget in the Okhotsk Sea. Recently, the decrease of the sea ice cover over the southern region of the Okhotsk Sea has been reported (*Tachibana et al., 1996*). In order to discuss its effect on the atmosphere, the qualitative estimation of heat budget on the basis of observation is required.

This region is an important area also to the ocean circulation. It has recently been pointed out the southwestern Okhotsk Sea is a possible origin of the North Pacific Intermediate Water (*Watanabe and Wakatsuchi, 1998*). Therefore, the representative ice growth rate there is an important information because the expelled dense brine may affect the ocean structure.

Fortunately, we had the opportunity to conduct ice observations over this region in early February of 1996 and 1997 on board the ice breaker, *SOYA* (Figure 1.1). In this paper, on the basis of this in-situ observational data, we estimate heat budget and representative ice growth rate, and discuss the characteristics of sea ice, particularly its ice growth processes. In calculating heat budget, sea ice albedo is an important parameter especially at such low latitude as this region. Since the in-situ observation of sea ice albedo in the pack ice region has not been done so far, we take the estimation of sea ice albedo to be also one of the themes in this study.

Our main interests in this paper can be summarized as follows:

- (1) How does sea ice in the southern region of the Okhotsk Sea develop ?
- (2) How much effect does the existence of sea ice have on the heat exchange between the atmosphere and the ocean over this region ?
- (3) Are there any different features of sea ice between at a relatively low latitude and in the polar regions ?

It is known that the heat budget remarkably changes according to ice thickness especially

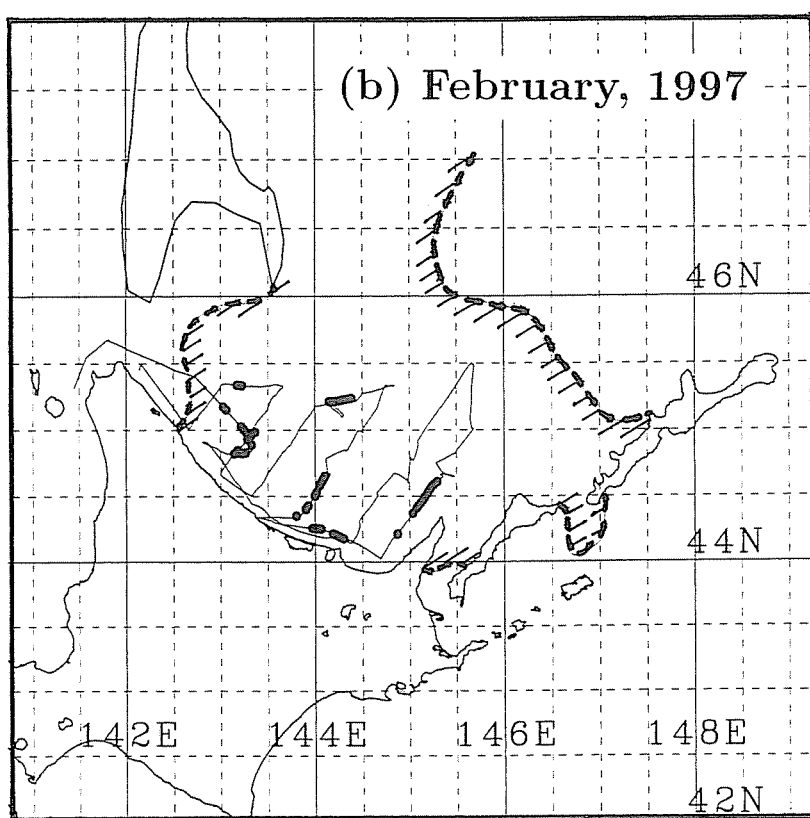
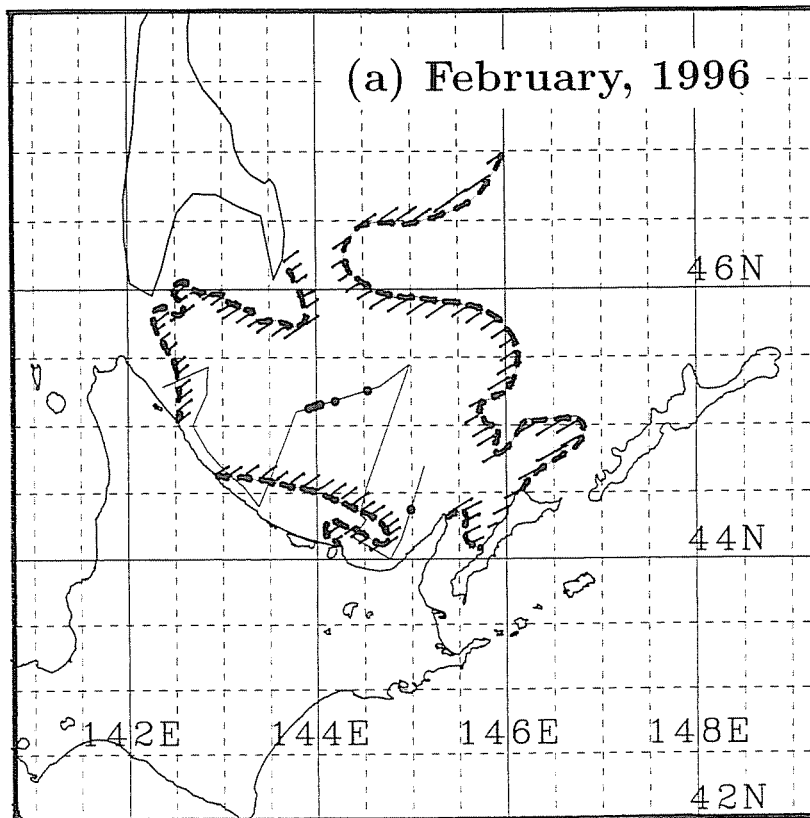
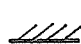


Figure 1.1 Geographical map of the southwestern Okhotsk Sea with the location of the samples used for albedo analysis (black circles) and ship tracks (thin lines).

 : Ice area.

when ice is thin (*Maykut, 1978*). Since the southern Okhotsk Sea contains many kinds of thin sea ice, the widely spread quantitative ice observations are required to answer these questions. For this reason, the observation was conducted over relatively wide area in the southern Okhotsk Sea. To quantitatively obtain the ice data, ice conditions were monitored by video cameras during the cruise, and ice concentration and thickness are analyzed from these video images. In addition, several ice samples are taken at different locations and examined through thin/thick section analysis. These analyzed data are discussed in connection with heat budget analysis.

In the other polar regions, extensive observations of ice and heat budget have been done so far especially for thick ice. From these observations, the structural characteristics of thick ice and its growth history have been clarified to some extent. However, over the marginal ice zones where young ice is dominant, both the ice structural analysis and, particularly, the heat budget observation are relatively limited except for some Antarctic regions. Although *Andreas and Makhtas (1985)* carried out the detailed heat budget observation over the Antarctic Ocean, ice observations were not included. Therefore, our observation seems to be one of the first trials of ice observations in connection with meteorological and hydrographical observation over the marginal ice zones. Considering the fact that the marginal ice zones vary year by year and interact much with the atmospheric circulation (e.g. *Walsh and Johnson, 1979; Overland and Pease, 1982*), it is important to investigate the growth processes from in-situ observation. Therefore, we believe that our observational study in the southern Okhotsk Sea also serves to understand the characteristics of sea ice in the marginal ice zone.

The main purpose of this study is through in-situ observation to find out the characteristics of sea ice, particularly its growth processes, in the southern region of the Okhotsk Sea. This paper is organized as follows:

The outline of our observation and the technical method of analysis will be described in Chapter 2. In Chapter 3, sea ice albedo will be estimated and heat budget will be

discussed with this estimated albedo in Chapter 4. In Chapter 5, the results of ice sample analysis will be shown and ice growth processes will be discussed in connection with the result of heat budget. Chapter 6 will present the result of laboratory experiments which were conducted to examine the characteristic thin ice found out in this region. Finally, the conclusion of this paper will be described in Chapter 7.

## Chapter 2. Observations

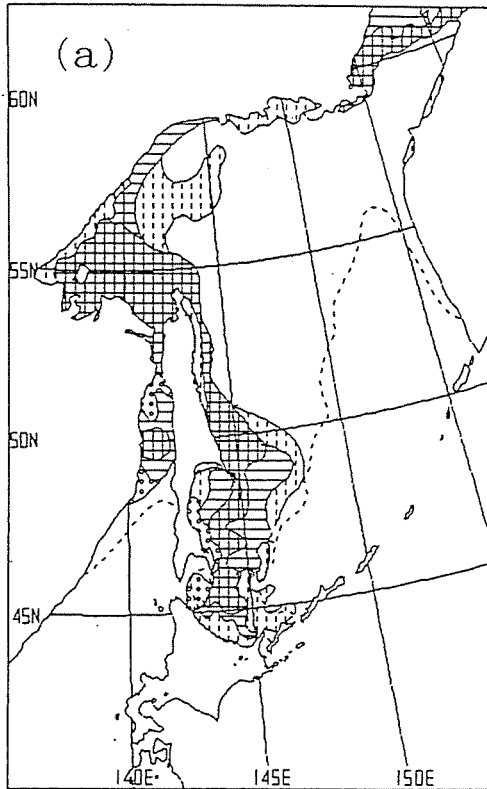
During 3 to 5 February of 1996 and 2 to 9 February of 1997, we have carried out ice observations aboard an ice breaker *SOYA* in the southern region of the Okhotsk Sea (Figure 1.1) as one of collaborative observations with the Marine Safety Agency. In these cruises, we have done direct measurements of both meteorological and ice conditions, in particular ice concentration and thickness. In addition, we took sea ice samples to investigate their structure.

### 2.1 Conditions

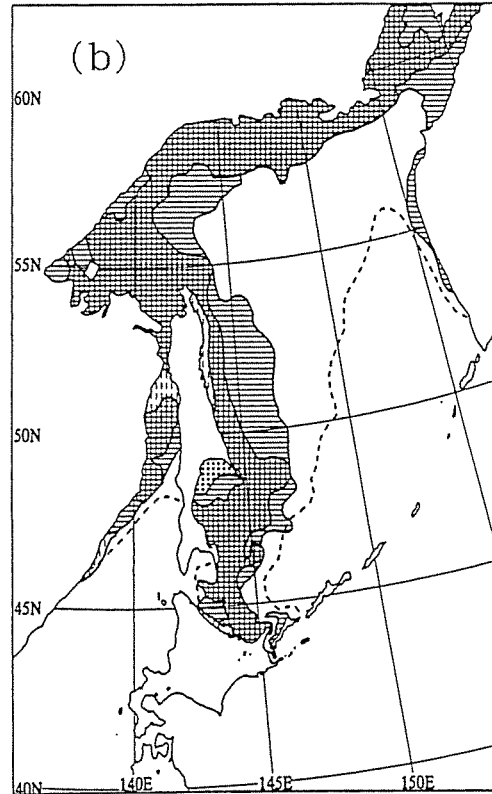
During the observation period in 1996, the weather was relatively calm with mostly clear to cloudy sky and neither snowstorm nor big swells. The air temperature ranged from  $-6$  to  $-1^{\circ}\text{C}$ , and the wind was 4 to 10 m/s, changing from northwestern to northeastern direction. In 1997, the weather was also relatively calm. The air temperature ranged from  $-10$  to  $-2^{\circ}\text{C}$ , and the wind speed was 1 to 10 m/s. Neither snowstorm nor big swells occurred during the observation period.

Ice charts are shown in Figure 2.1.1 (published by *Japan Meteorological Agency*). In 1996, the sea ice extent in the Okhotsk Sea was record-breakingly small until early February, since the data became available in 1971. The sea ice extent in the southern region of the Okhotsk Sea was also below normal until late January, while it spread nearly to the normal in early February. In 1997, sea ice extended almost normally from January to February in the southern region of the Okhotsk Sea.

Ship positions were monitored by the GPS instrument used for ship navigation and recorded manually at one minute's interval in 1996. The ship's speed and head direction were calculated from the ship displacement for one minute. In 1997, ship positions were measured by the GPS instrument which we prepared. It stocked the data on the hard



5 February 1996



5 February 1997

Ice concentration (in tenths)

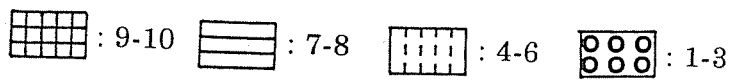


Figure 2.1.1 Sea ice extent at the observation time in the Okhotsk Sea.

Broken lines mean the normal average of ice edge from 1971 to 1990.



disk of our personal computer at ten seconds' intervals. The ship's speed and head direction were similarly calculated at one minute's interval. The ship track in Figure 1.1 is drawn using these data.

## 2.2 Meteorological observation

### *Air temperature and Relative humidity*

We measured air temperature and relative humidity with a thermo-/hydro-meter with a ventilating motor fan. The data were recorded on a logger at five minute's interval. This instrument was mounted at the ship mast of 15 m height above the sea level so as to avoid the ship body effect.

### *Short wave radiation*

Upward and downward short wave radiation was measured with two pyranometers. Their instrument type is S-185 which is designed for measurement on ships by the Ishikawa Sangyou KK. They measure short wave radiation of the wavelength region 300-2800 nm from omni directions within a hemisphere with the accuracy of  $\pm 2\%$ , using thermo-piles. Their surfaces were kept horizontal by a gimbaling mechanism (see Figure 2.2.1a). The response time is six seconds. They were calibrated with the instrument of Japan Meteorological Agency for the solar altitude higher than 10 degrees. Since the accuracy is not guaranteed for the solar altitude less than 10 degrees, we used here only the data which were taken at the solar altitude greater than 10 degrees.

Installing these two pyranometers at the top and the bottom of the gimbaling cylinder, we mounted these instruments at the tip of the ship bow with a ladder of 3 m length to avoid the shadow effect by the ship structures (see Figure 2.2.1b and c).

We did the measurements during the period from February 3 to 5 in 1996 and from February 2 to 9 in 1997. The radiation data were accumulated successively during the time interval of 10 minutes in 1996 and one minute in 1997 and averaged values were

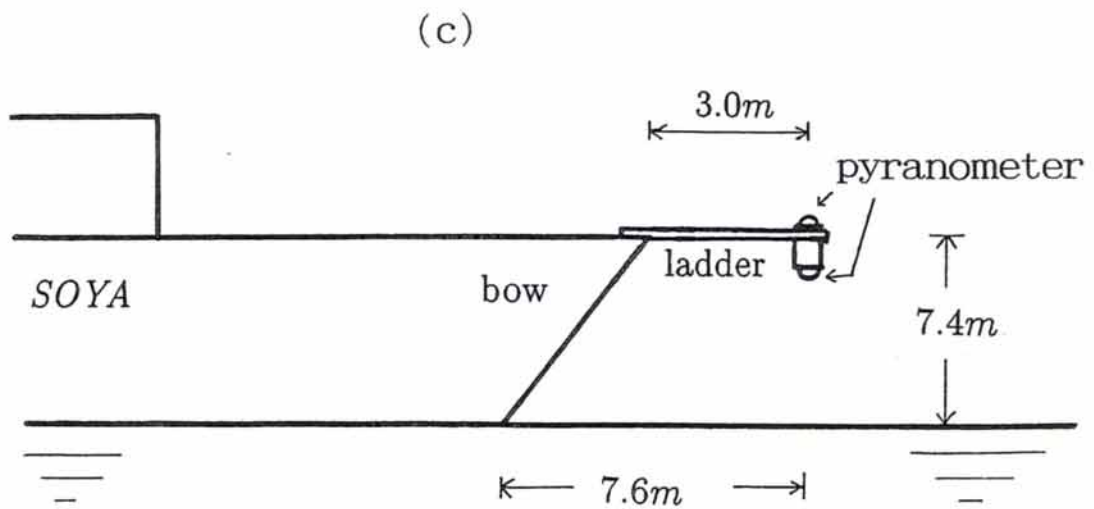
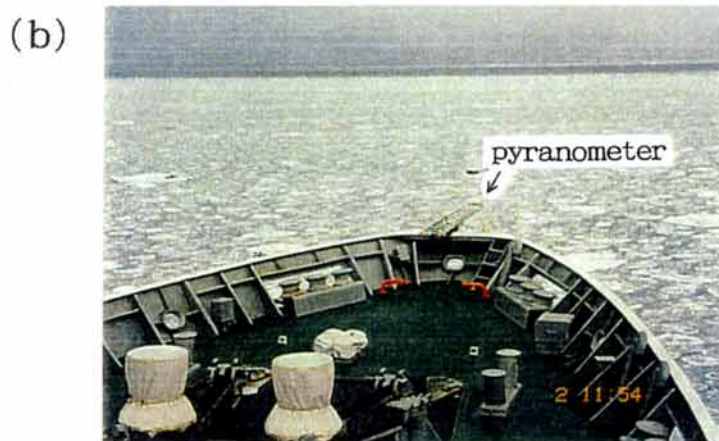
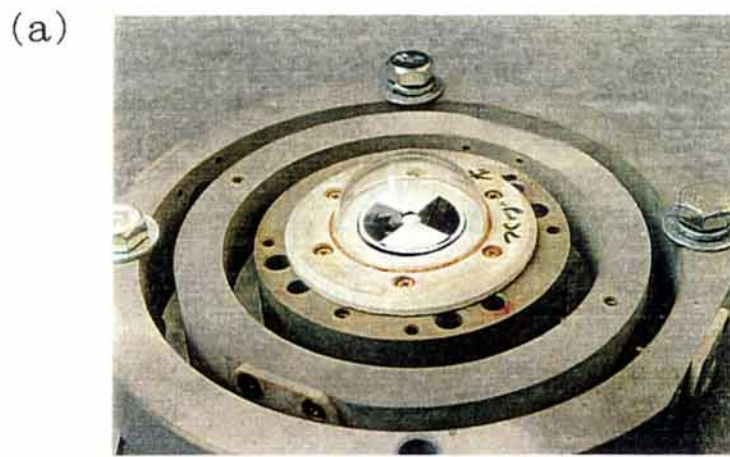


Figure 2.2.1 Measurement of short wave radiation.

- (a) Pyranometers mounted on gimbal.
- (b) Photograph of observation.
- (c) Geometric picture of observation.

recorded on data loggers every time interval. After obtaining incident and reflected short wave radiation, we calculated the averaged albedo by taking their ratio.

### *Wind*

Anemometers installed at the top of the ship mast, 22 m above the sea level were used to get wind data. The absolute wind data were obtained by subtracting the ship speed from the measured values. This observation was conducted by the ship's crew of 'SOYA' at hourly intervals and recorded on a log-book in the form of wind force. We used this recorded data for analysis.

### *Cloud and weather*

Cloud amount (in tenths) and weather were observed visually and recorded at hourly intervals during the cruise. Due to visual observation, the accuracy of the data cannot be expected to be high.

### *Solar positions*

Solar zenith and azimuth angles were calculated at hourly intervals as a function of time and ship position utilizing the program developed by Marine Safety Agency, which is used for the publication on daily solar position. Then we interpolated with a fourth polynomial expression to get the data at the observation time. It is shown from this calculation that at this season of the year, the culmination time is around 11:30 a.m.JST and its zenith angle is about 60 degrees at the observation area. The sun rises about at 07h00m and sets about at 16h30m.

## **2.3 Sea ice observation**

### *Ice concentration*

During the cruise, ice concentration was monitored by a forward-looking video camera

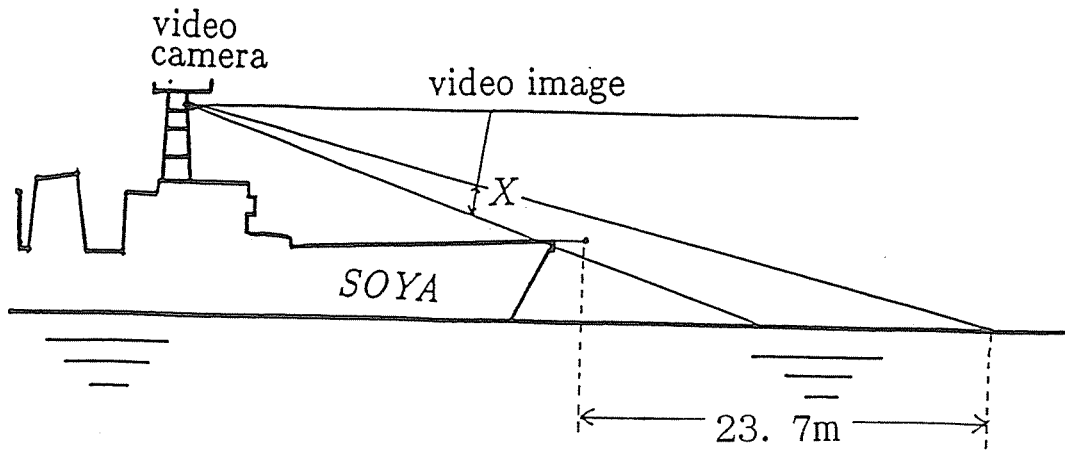
mounted at the front mast of the ship with an angle of about 10 degrees downward from the level (see Figure 2.3.1a). The video image data were then recorded on 8-mm video tapes of the video controller equipped in the bridge room.

To process video images for ice concentration, we used a one-dimensional method developed by *Muramoto et al.(1993)*. First, the continuous video images were sampled at the interval of one second through an image processor to make digital data set of individual scenes. Then on a fixed row in each scene we estimated the ratio of sea ice to the row length by dissecting this line into 256 segments and discriminating ice from water according to brightness (see Figure 2.3.1b). In determining the location of the row on a video image, the further away from the ship we set it, the wider range can be contained for analysis. But on the other hand, the worse the resolution becomes. Here we selected the row so that the real width across the scene became approximately 50 m in principle because the observed size of ice floes was mostly a few to a few tens of meters (Figure 2.3.6b) and the resolution was enough for discriminating ice from water. Finally by averaging these successive values over a certain interval, area mean ice concentration could be obtained along the ship track during the averaging period. We found that thus estimated ice concentration were in good agreement with the daily operational ice charts compiled by the Marine Safety Agency.

In order to make the above analysis possible, the following conditions should be satisfied:

- (1) The video image is bright enough to discriminate sea ice from water.
- (2) The ship is moving because successively averaged data are meaningless while the ship stops.
- (3) The outline of sea ice is clear enough to discriminate it from water (i.e. frazil or dark ice is not appropriate).
- (4) The ridging of the sea ice surface is not so big as to make considerable dark shadows.

(a)



(b)



(Black area: Sea Ice)

Figure 2.3.1 Ice concentration analysis.

(a) Video monitoring.

(b) Digitalized Video image.

Black area corresponds to ice, while white area shows open area.

'X' denotes the distance of the analysis row

from the bottom of the video image.

(5) The direct solar radiation does not make the image saturated.

Among these constraints, (2) was the strongest. Our ship had to stop for hydrographical observation occasionally, which resulted in the relatively limited number of samples. As for (3), more or less dark ice floes which do not have clear outlines were included in many cases. Here we treated only the cases where they were not predominant for more than half of the sampling period, if any.

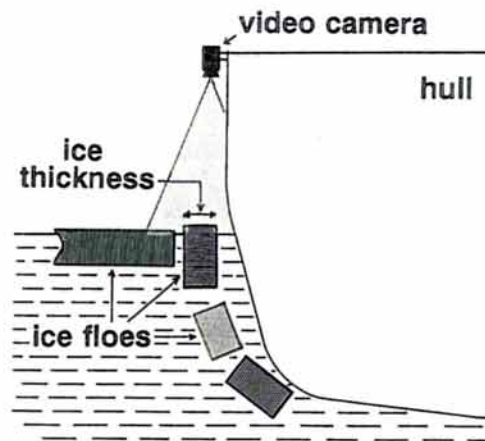
When the above constraints were satisfied, measurement errors seemed to be small. All the same, some errors may be contained because this method includes subjective judgment in determining the threshold of ice and water. In order to reduce the errors due to subjectivity, we repeated this measurement three times and used their averaged values for analysis.

#### *Ice thickness*

Ice thickness was also monitored by a downward-looking video camera mounted at the side deck of the ship. Some of ice floes which were broken at the bow were found to turn into side-up positions (Figure 2.3.2a). For such ice floes we measured their ice thicknesses manually on each video image (Figure 2.3.2b). To determine the scale on video images, we sometimes put crossed sticks of one meter length on an ice floe so that they were photographed in a video image. The measuring method is same as that described in *Shimoda et al.(1997)*. As is shown in Figure 2.3.2b, we refer to ice thickness as the sum of snow depth and the thickness of underlying ice in this paper.

After all, 153 and 4119 samples were obtained in total in 1996 and 1997, respectively. As a whole, sea ice was much thicker in 1997 than in 1996. This difference of ice thickness is remarkably found in histograms (Figure 2.3.3a-b). Ice thicknesses were mostly below 30 cm and their averaged value was 18.5 cm in 1996, while it ranged from 10 cm to 150 cm and the averaged value amounted to 54.9 cm in 1997. According to the observation of ice thickness in the other years, which have been continued since 1991 by Ship Research

(a)



(b)

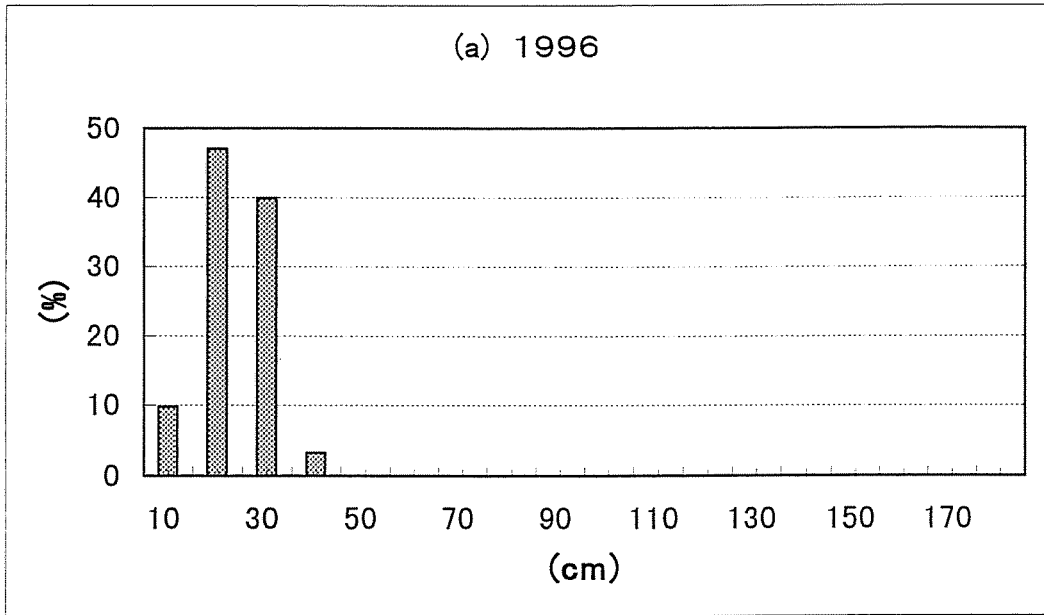


Ice thickness

Figure 2.3.2 Ice thickness measurement.

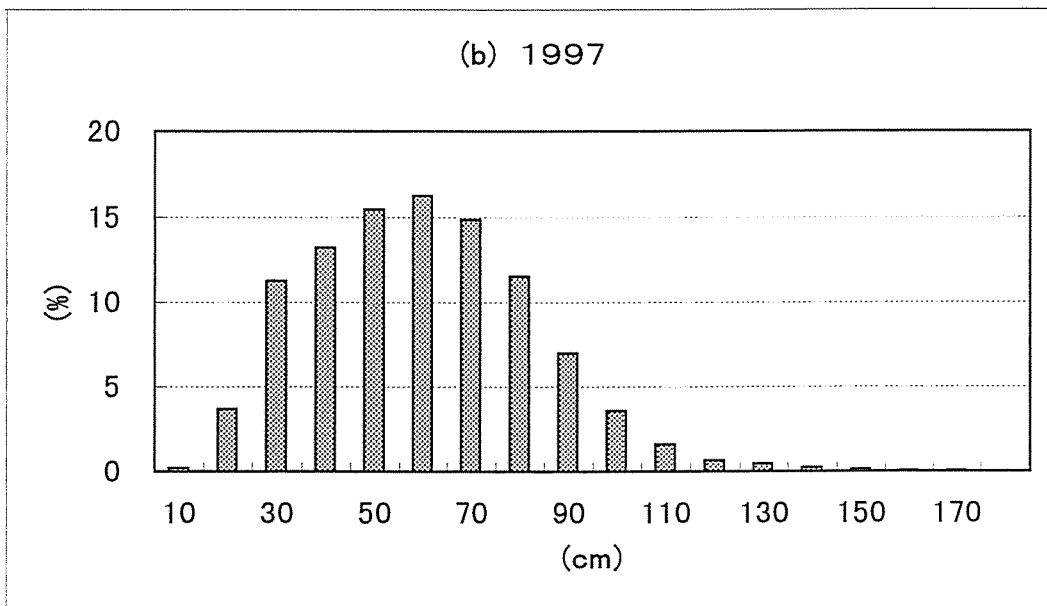
(a) Schematic picture of the measurement (cited from *Shimoda et al. (1997)*).

(b) Photograph of the scene where ice floes turned into side-up positions.



N= 153

mean = 18.5 cm



N= 4119

mean = 54.9 cm

Figure 2.3.3 Histograms of ice thickness.

(a) 1996

(b) 1997



Institute, Ministry of Transport, ice thickness ranges from 25 to 45 cm. It may be said that the 1996 and 1997 data give the minimum and maximum ice thickness in recent years, respectively.

One example of time series of measured ice thicknesses is shown with a 10-minutes averaged line in Figure 2.3.4a. We can see from this figure that ice thickness varies on small time scale, but the averaged values represent the distribution of ice thicknesses as a whole. We mapped ice thickness distribution along the ship track using the averaged values(see Figure 2.3.4b). The geographical features of ice thickness in the southern region of the Okhotsk Sea is markedly represented. In this figure, thicker ice is noticeable in the eastern part where ice floes flowed southward piling up each other from the coastal region off Sakhalin, while thinner ice are found in the western part where in-situ frozen ice is dominant.

Since there were a lot of ice floes which were thick enough to discriminate snow depth on video images in 1997, we also measured snow depth utilizing the difference of brightness. Although its accuracy was not high compared with that of ice thickness, we obtained the result that the snow depth ranged from 5 to 15 cm. We did not notice marked geographical features as those of ice thickness.

### *Sea ice sampling*

Thick sea ice samples were taken with sticks and a rope reinforced with wire (Figure 2.3.5a). When sampling, we brought an ice floe toward our position with long sticks and put it into a ring of the rope, and then pulled it up to the shipboard. A fishery net was used for thin ice sampling. They were kept at the ship's freezing room during the cruise. Quickly after the cruise, we took them into the cold temperature laboratory of our institute and kept them at  $-16^{\circ}C$  until ready for sectioning.

We also took several snow samples tentatively with a cylindrical stick to examine the features of snow on a sea ice floe during the cruise in 1997. Figure 2.3.5b shows the

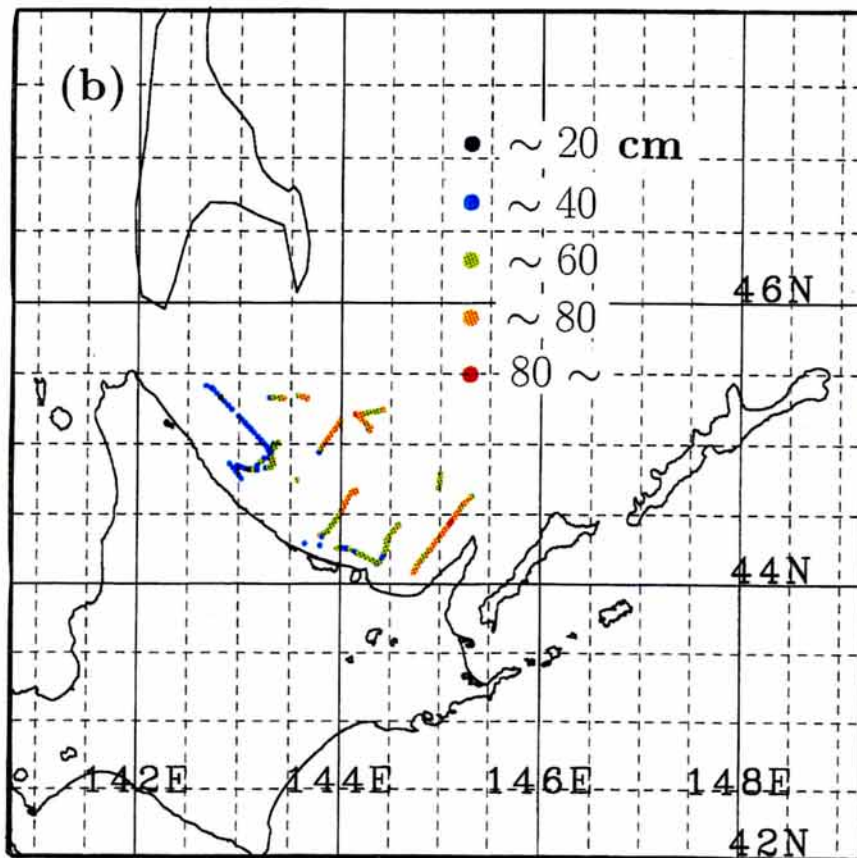
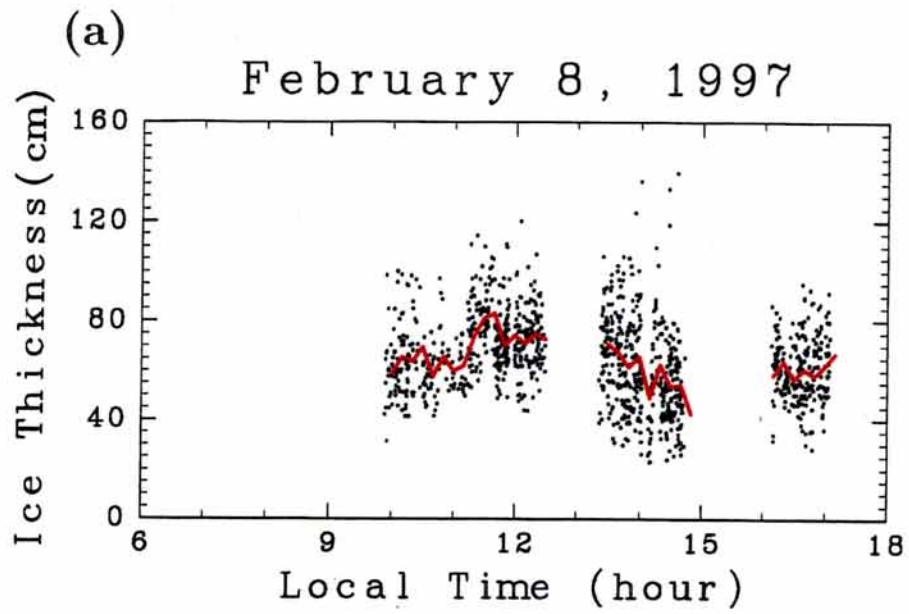


Figure 2.3.4 Ice thickness distribution in 1997.

(a) Daily time series of ice thickness on February 8, 1997.

(b) Geographical distribution.



Figure 2.3.5 Scene of sampling observation.

(a) Ice sampling

(b) Snow sampling.

sampling scene. We measured density and salinity, and estimated their grain sizes with a scale in millimeters. Because of the observational difficulty, the number of samples was only limited to eleven.

### *Visual observation*

We aimed for quantitative measurement of ice conditions in this observation. However, such ice conditions as surface roughness, floe size, and ice concentration of nilas cannot be measured quantitatively by the above method. These data were compensated by visual observation at hourly intervals at daytime. Detailed observation was started in 1997. The observation points are shown in Figure 2.3.6a. Since the observation covers large sea ice area, the result may be representative of this ice area.

The observation consists of partial ice concentration, ice thickness, floe size and sail height of individual ice types. Basically, we followed the classification of *WMO(1970)* and the method of *Allison et al.(1993)*. In 1997, observation was conducted at 42 locations. Ridging was particularly prominent in this year, and its area occupied 24% of all the ice floe area and the visually estimated mean sail height was 0.47 m. These results are comparable to those in the Antarctic Ocean (*Worby et al., 1996*). This result also shows that sea ice was remarkably developed in 1997. Since similar observation has been continued in the Antarctic Ocean since 1992 (*Allison and Worby, 1994*), we consider that it will be possible to compare the sea ice characteristics between in the Okhotsk Sea and in the Antarctic Ocean in more details when the data are accumulated enough in the Okhotsk Sea. Here, we show only the result of the observation of ice floe size in Figure 2.3.6b. As mentioned in section 2.3.1, this figure shows that ice floes of a few to one hundred meters in diameter were predominant.

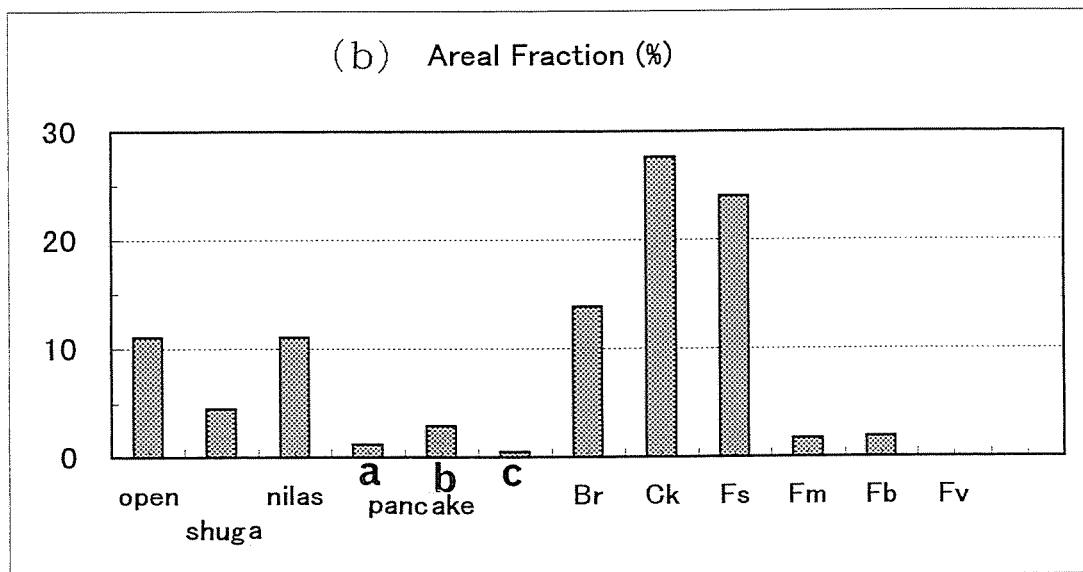
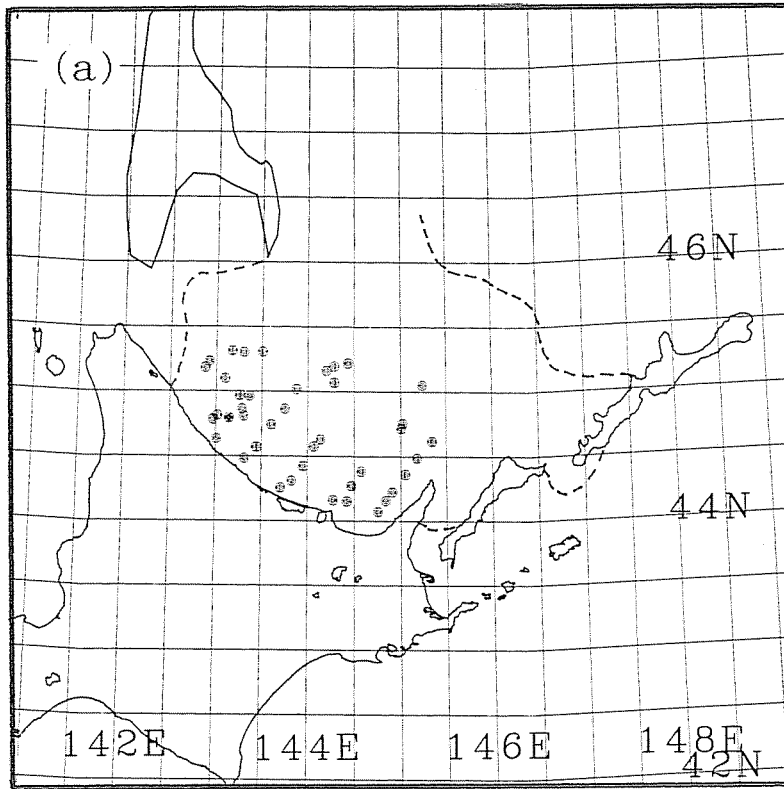


Figure 2.3.6 Visual observation in 1997.

(a) Locations with ice edge (broken lines).

(b) Areal fraction of each ice type.

Br : Brush ice ( $\phi \leq 2m$ )

Ck : Ice cakes ( $2m \leq \phi \leq 20m$ )

Fs : Small floe ( $20m \leq \phi \leq 100m$ )

Fm : Medium floe ( $100m \leq \phi \leq 500m$ )

Fb : Big floe ( $500m \leq \phi \leq 2km$ )

Fv : Vast floe ( $2km \leq \phi \leq 10km$ )

Pancake ice is further divided into (a)  $\phi \leq 40cm$ , (b)  $\leq 1.5m$ , (c)  $\leq 3m$ .

## Chapter 3. Albedo

### 3.1 Introduction

In this chapter, we estimate sea ice albedo which will be used for the heat budget calculation in the next chapter. Since the southern region of the Okhotsk Sea is located at relatively low latitude, solar radiation is abundant even in mid winter compared with that in the polar regions. Therefore, sea ice albedo is expected to be a more significant parameter in heat budget. Around the Okhotsk Sea, albedo measurements have been carried out on Saroma Lake, located at the northeastern part of Hokkaido, (*Ishikawa and Kobayashi, 1984*). However, the in-situ observation has not been done in the pack ice regions.

The in-situ observation of sea ice albedo is also scarce in the polar regions. Although the potential importance of sea ice albedo to climate system has been pointed out from model studies (e.g. *Shine and Henderson-Sellers, 1985; Ingram et al. , 1989*), the in-situ observation of sea ice albedo has been relatively limited to land fast ice regions so far (e.g. *Grenfell and Maykut (1977), Grenfell and Perovich (1984), Perovich (1994), Schlosser (1988)*). *Andreas and Makshtas (1985)* have measured the incident and reflected short wave radiation over the pack ice region in the Antarctic for heat budget calculation, little attention being paid to the value of sea ice albedo. *Allison et al.(1993)* estimate sea ice albedo in the pack ice region of the Antarctic Ocean, but their values are based on visually determined ice concentration with a priori set albedo values for various surface conditions.

Thus there seems to be yet no direct measurement of sea ice albedo for pack ice regions with varying ice conditions. Given a large extent of areas with such conditions (i.e. marginal and seasonal ice zones), it seems to be important to estimate sea ice albedo from in-situ observation. Therefore, we believe that our estimation here can be applied to other marginal pack ice regions.

In our observation, surface albedo data were continuously obtained from two pyranometers mounted at the bow of the ship. Each pyranometer was looking upward and downward, thus recording incident and reflected radiation. In order to check the effect of the ship shadow, a ship turning experiment was also carried out under a clear sky condition.

In addition to ice conditions, solar altitude will be taken into account to estimate sea ice albedo. The major purpose of this chapter is to quantitatively estimate sea ice albedo which will be useful to calculate heat budgets and to show how much effect ice conditions and solar altitude have on sea ice albedo. Therefore, our interest here is toward the estimation of representative sea ice albedo over relatively large area (more than one kilometer), rather than exact measurement at a limited spot. According to *Warren(1982)*, snow albedo is also affected by snow grains and cloud cover. Since most of the ice floes over the observation area were covered with snow, these effects seems significant. However, we will not mention about the effects of these factors in detail here because it was difficult to take successive data during the cruise.

In section 3.2, we will discuss the measurement error and compare the observation areas of ice concentration and albedo. In section 3.3, we will examine the ship shadow effect from the results of a ship turning experiment. The results of analysis will be presented in section 3.4.

## **3.2 Measurement**

Since we described the method of the albedo measurement in Chapter 2, we here discuss the errors associated with the measurement and examine the observation area for analysis.

### *3.2.1 Measurement errors*

We here discuss three kinds of errors associated with the albedo measurement. The

first one is the effect of a systematic bias introduced by the shielding of the ship on upward short wave radiation (see Figure 3.2.1). To estimate it, we calculated the upward radiant flux ( $F(S)$ ) incident from the shielded solid angle ( $S$ ) on the sphere centered on a pyranometer, assuming that radiance ( $I$ ) is isotropic in direction.

$$\begin{aligned} F(S) &= \int \int_S I \sin\theta \cos\theta d\varphi d\theta = \int_{\theta=0}^{\theta_0} \int_{-\varphi(\theta)}^{+\varphi(\theta)} I \cos\theta \sin\theta d\varphi d\theta \\ &= I \int_0^{\theta_0} 2\varphi(\theta) \cos\theta \sin\theta d\theta \approx 4.10 * 10^{-2} I \end{aligned}$$

,where  $I$ ,  $\theta$ , and  $\varphi$  is radiance, incident zenith angle, and azimuth measured from the ladder, respectively. Hence, the contribution of the shielded portion ( $S$ ) to the total upward radiation ( $\pi I$ ) is equal to  $4.10 * 10^{-2} I / \pi I = 1.31 * 10^{-2}$ . This implies that the measured albedo may include errors by 1.3 %. Since this value is not significant in the calculation of heat budget, we neglected this effect here.

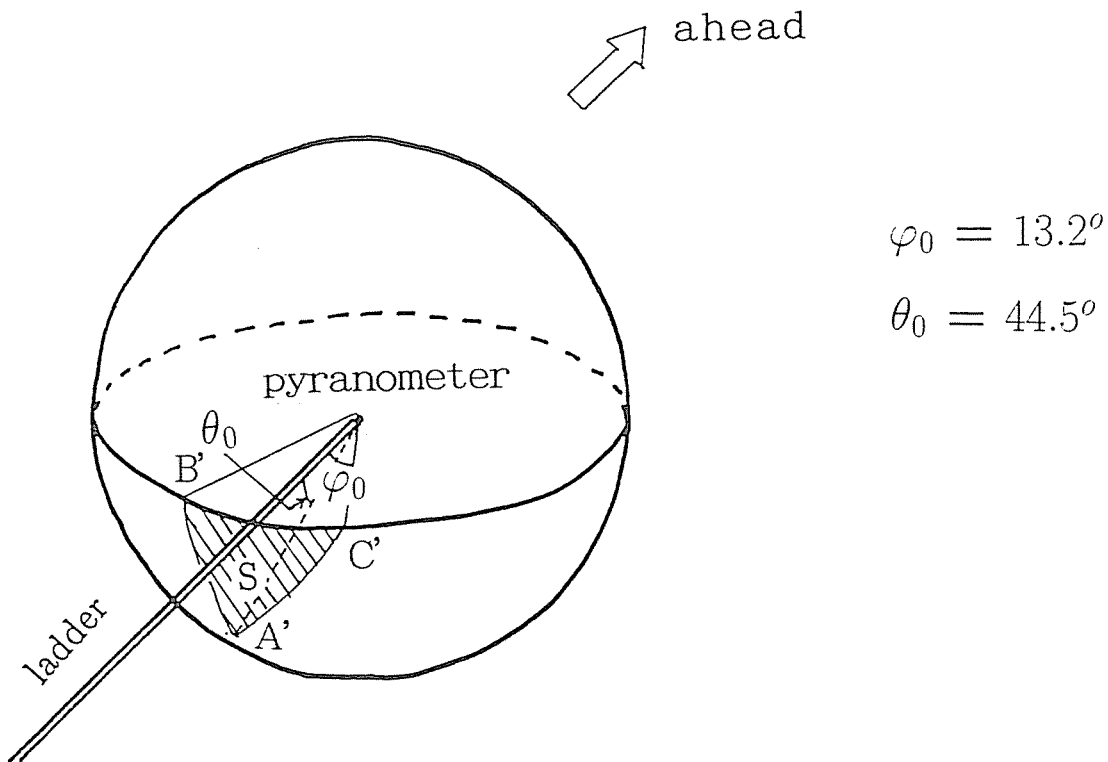
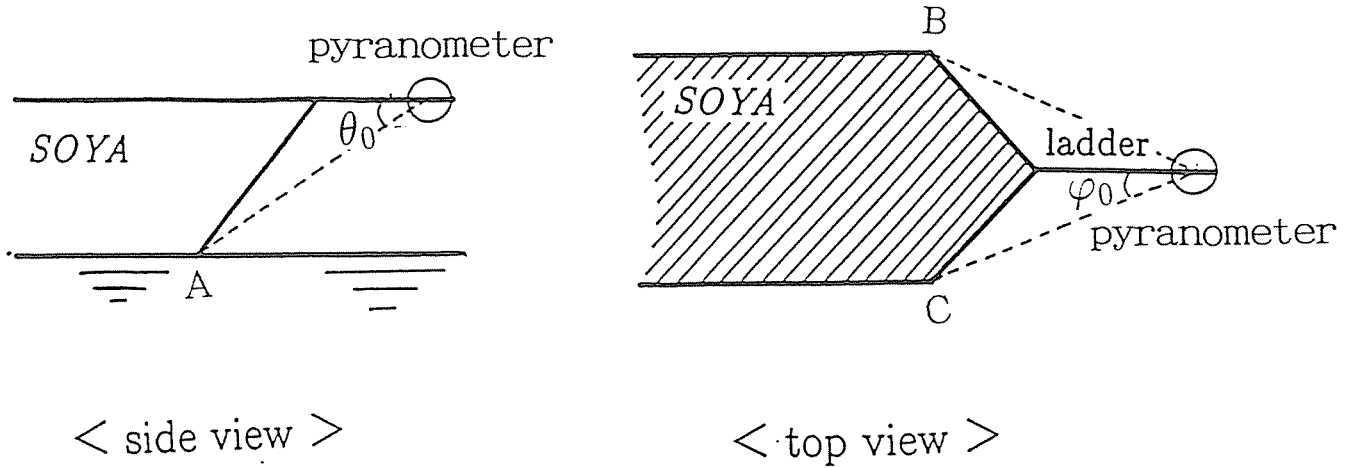
The second one is the leveling error of the instruments. As for this effect, we did not take any data. However, since the ocean surface was quite calm in the ice extent during the observation period, the gimbaling mechanism seemed to function well in response to the slight vibration. For reference, during another cruise of the same ship over ice regions of the southern Okhotsk Sea in 1997, the rolling and the pitching angles were both below 0.5 degree, according to Shimoda (personal communication). Therefore, we regarded the leveling error as negligible.

The last error is the effect of ship shadow reflected on the ice surface. We examined it by a ship turning experiment. Through this experiment, we investigated the dependence of albedo on the solar azimuth relative to the ship head. After all, it was shown that this effect should be taken into account when the sun existed behind the ship. The detailed result will be shown in the next section.

### 3.2.2 Comparison of observation areas

Although the instantaneous observation area of ice concentration is different from that





S : Solid angle shielded by the ship

Figure 3.2.1 : Schematic pictures used for calculating the shielding effect of the ship' geometry.

Slanted lines in top view denote the shielded area.

$A', B'$  and  $C'$  are the points projected to the sphere centered on a pyranometer from  $A, B$  and  $C$ , respectively.

of albedo, these areas overlap as the ship moves. To discuss the relationship between ice concentration and albedo, the overlapped area should occupy a large fraction of each observation area. For this purpose, we have to take average for an adequate period.

Since the sampling rate of radiation was 10 minutes in 1996, minimum of averaging period is required to be 10 minutes. Considering that the ship speed was about 5 m/s in the ice region, 10 minutes corresponds approximately to 3 km in distance. If we take averages over 3 km, the discrepancy of observation locations (=23.7 m) (see Figure 2.3.1) is almost negligible.

Next, we examine the width of each observation area. In Figure 3.2.2, the ratio of the upward radiant flux ( $F(\theta)$ ) emitted from the circle area just below the pyranometer to the total upward radiant flux ( $F(\pi)$ ) is shown as a function of  $D$ . Here, isotropic radiance is assumed. From this figure, it is shown that the ratio is 0.92 for  $D = 50$  m which corresponds to the real width of the row used for ice concentration analysis.

Consequently, it is considered that the observation areas of radiation and ice concentration coincide by 92%. Given that the ice extent with similar ice conditions usually spread on the scale of much more than 50 m, it is unlikely that ice concentration and albedo in the residual area (8%) were significantly different and substantially alter the result. Therefore, we regarded the 10 minutes period as sufficient for comparison of these data. In addition, this horizontal scale of approximately 3 km matches that of our interest as well. Thus 10 minutes was adopted for averaging period.

After examining all the scenes of video images, we came up with 91 ten-minute periods (14 for 1996 and 77 for 1997) in total where both data were available for analysis.

### 3.3 Turning Experiment

Prior to analysis of measured data, we should mention the effect of the ship shadow on the measured albedo. For the examination, we carried out a ship turning experiment around 44.9°N 143.3°E for eighteen minutes from 12h57m to 13h15m on February 9

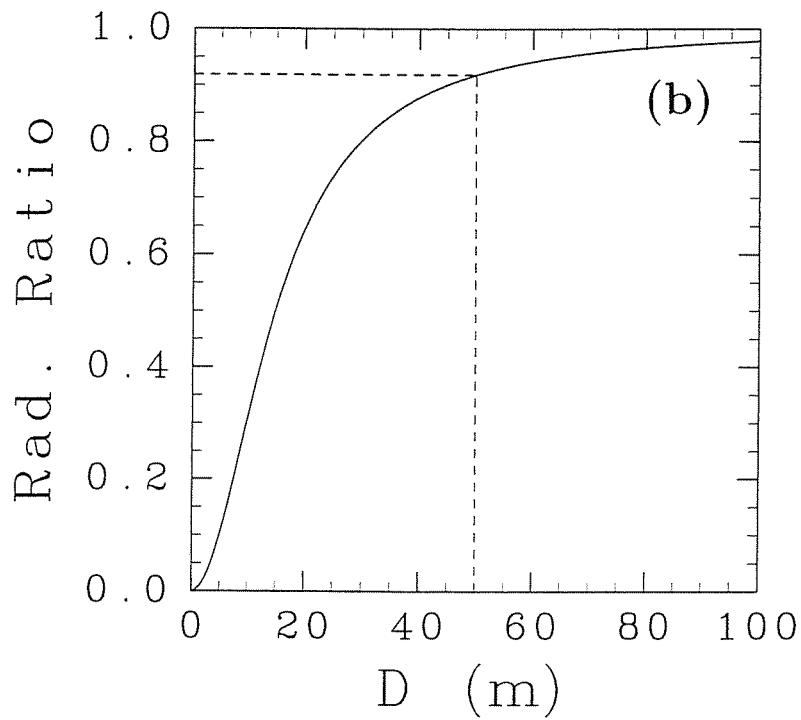
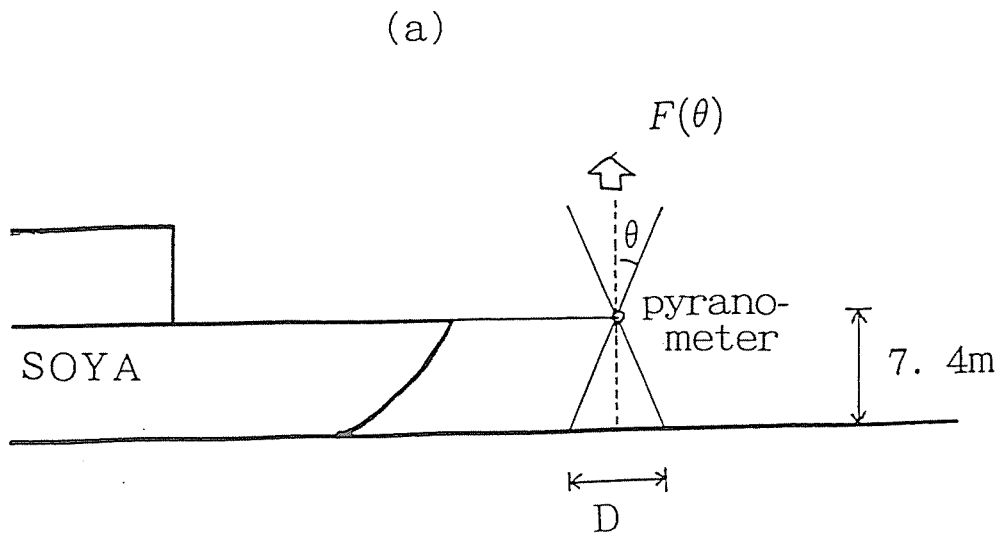


Figure 3.2.2 : Contribution of the radiation emitted from the circle area just below a pyranometer to total upward short wave radiation.  
 (a) Geometric side view.  
 (b) Geometrically calculated contribution as a function of the diameter ( $D$  m).

in 1997. This experiment was aimed at examining the dependence of albedo on the solar azimuth relative to the ship head by turning the ship around in a circle with the diameter of about 1 km (Figure 3.3.1a). If the shadow effect were substantial, with the increase of the ship shadow area, the decrease of the measured upward radiation would be detected. The downward irradiance seemed to be little affected by the shadow of the ship's structures because the instrument was mounted far enough from them. Therefore, if we consider only the effect of the ship shadow, the albedo measured is expected to change like a sinusoidal curve in response to the change of the relative solar azimuth, where the maximum (minimum) occurs when the sun exists ahead of (behind) the ship.

The conditions during the experiment was as follows: The weather was clear, and a definite shadow appeared as shown in Figure 3.3.1b. The solar altitude was 28 deg. at 13h00m. Air temperature was about  $-6^{\circ}C$ , relative humidity was 61%, wind was 1 to 3 m/s from southeast, and ocean surface was quite calm. The ice concentration was highly variable, ranging from 40 to 90%, which caused the variation of reflected radiation and accordingly albedo (see Figure 3.3.2ab).

In order to derive the ship's shadow effect, we have to correct the effect of low albedo over open water area. For this purpose, we examined the correlation between ice concentration and albedo, using all the 91 samples selected for analysis. As a result, it was found that albedo was highly correlated with ice concentration at more than 99 percent confidence level. Therefore, we calculated the regression line to predict albedo from ice concentration and used the deviation data from this regression line instead of albedo itself to examine the shadow effect. The result is shown in Figure 3.3.2c. In this figure, a four-dimensional fitted curve is also drawn to see the general trend more clearly. It is found from this figure that the deviations became relatively lower particularly for the relative solar azimuth beyond  $\pm 120$  degrees when the sun was located nearly behind the ship. For example, the deviation is lower by 0.1 to 0.2 for the relative solar azimuth of 150 to 180 degrees than for that of -90 to 90 degrees.

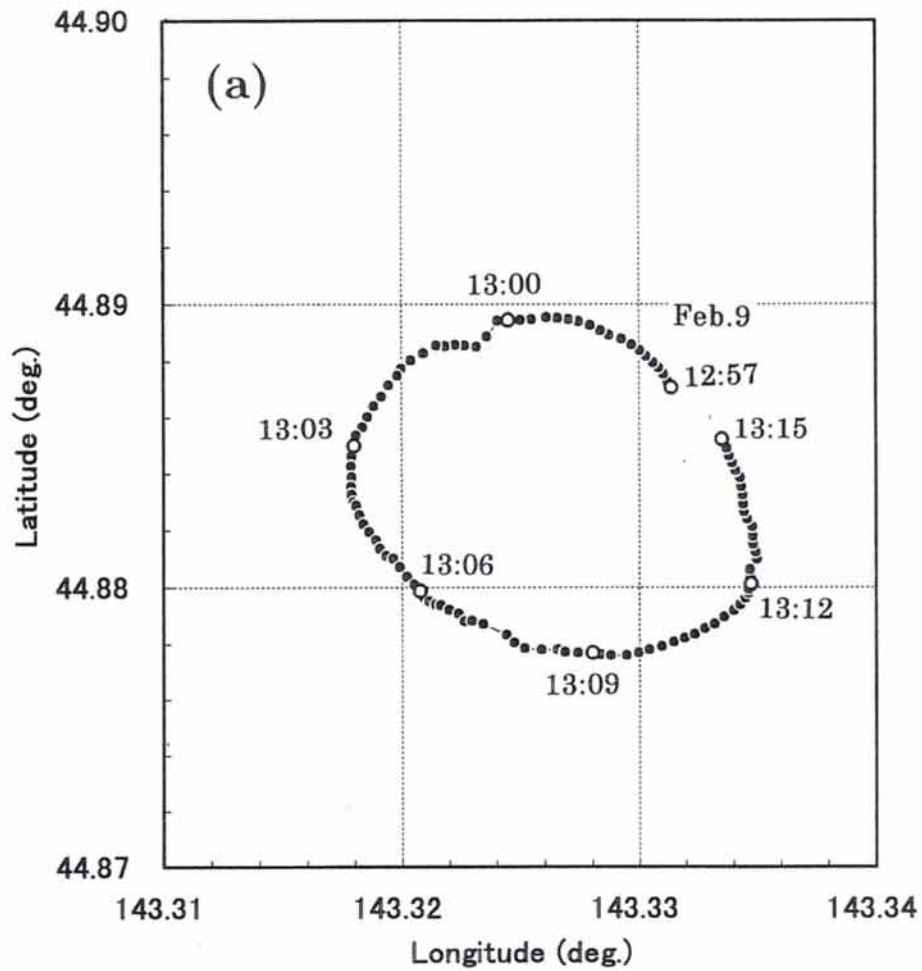


Figure 3.3.1 : Ship turning experiment conducted on February 9, 1997.

(a) Ship track.

(b) Photograph of the ice conditions.

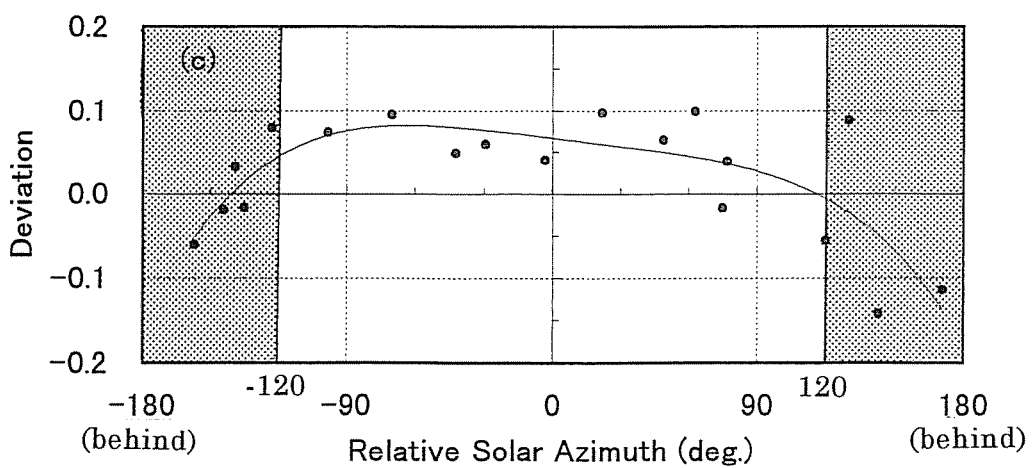
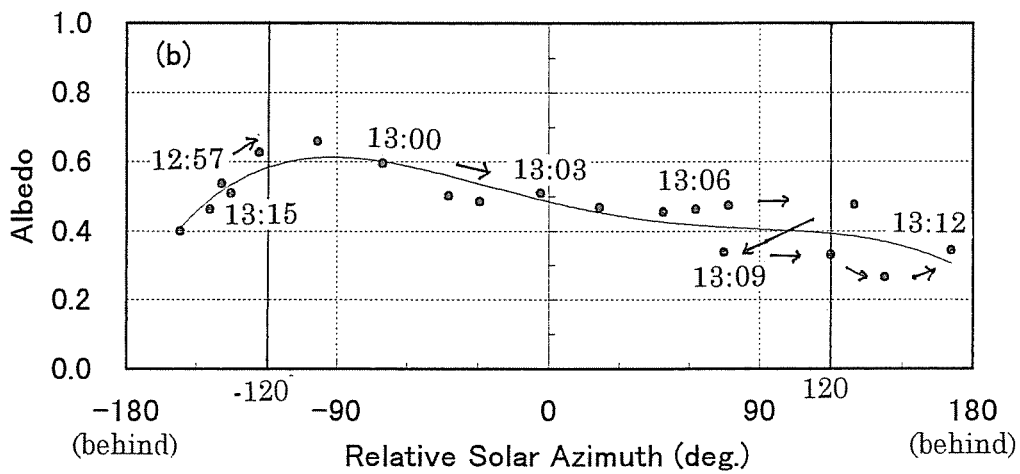
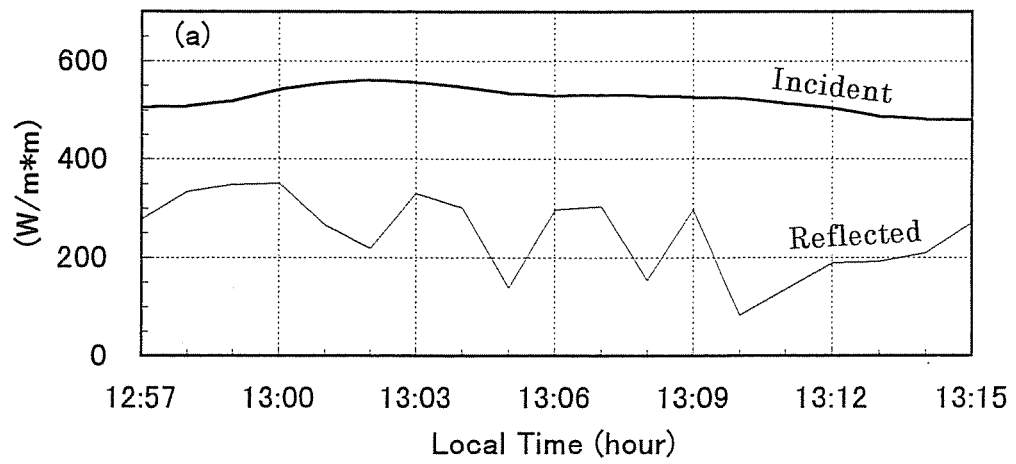


Figure 3.3.2 : Results of a ship turning experiment.

- (a) Time series of incident and reflected solar radiation during the experiment.
- (b) Plots of every minute surface albedo.
- (c) Plots of every minute deviation of albedo from the linear regression.

This result indicates that the ship shadow could affect the albedo significantly when the sun existed nearly behind the ship under clear sky conditions. Although the decrease of albedo by ship shadow was 0.1 to 0.2 unit in the case of this experiment, this value would vary depending on the sky conditions. We consider that it would be difficult to estimate it exactly. Therefore, the data which were taken for the relative solar azimuth of greater than 120 degrees or less than -120 degrees, i.e. in the case the sun was located behind the ship, were all excluded from this analysis. After all, the number of the samples used for analysis was reduced to 59 in total (6 for 1996, 53 for 1997). Their locations were plotted in Figure 1.1. They all existed within the pack ice region.

Besides the above result, it should be noticed in Figure 10a that somewhat increased incident radiation is detected especially during the period of 13h00m to 13h06m. Because it changed smoothly and occurred only when the sun was located nearly ahead of the ship, this increase is attributed to the reflected light from the ship's structures rather than the leveling error of pyranometers. This effect caused the measured albedo to become apparently lower, resulting in somewhat lower deviation when the sun was located nearly ahead of the ship (about at 13h03m). This result implies that the measured albedo may be affected by the ship structure for the case when the sun is located nearly ahead of the ship under clear sky conditions. However, since such a case was not included in the above 59 samples, we did not take this effect into account here.

### 3.4 Results

Figure 3.4.1 shows albedo as a function of ice concentration with a regression solid line. As is expected, the surface albedo for a mixed surface condition with both ice and water is linearly correlated with ice concentration at more than 99 percent confidence level. The regression line is

$$A = 0.116 + 0.527 * \frac{c}{100} \quad RMS = 0.062 \quad (1)$$

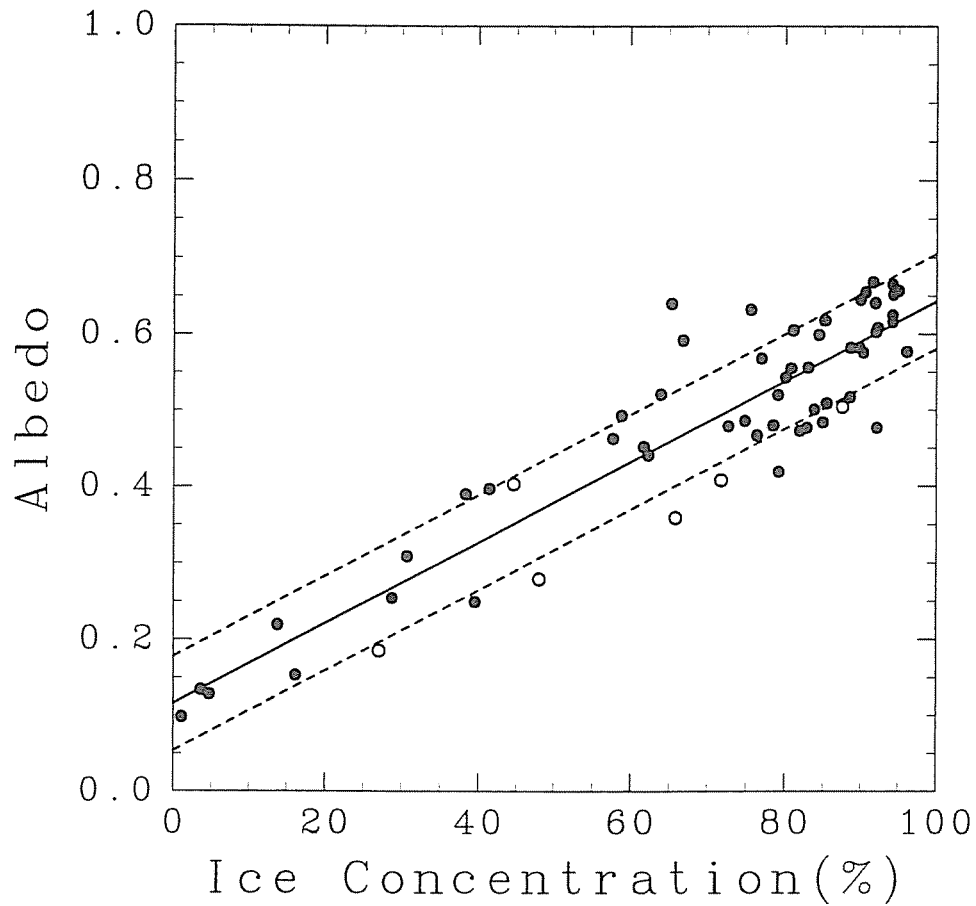


Figure 3.4.1 : Correlation between ice concentration and albedo with a regression line.

White and black circles denote the data of 1996 and 1997, respectively.

Two broken lines denote  $\pm RMS (= 0.062)$ .



where  $c$  and  $A$  are ice concentration(%) and albedo, respectively, and  $RMS$  means root mean square which shows the accuracy of the regression. Since the samples are concentrated between 60% and 100% ice concentration, sea ice albedo (100% ice cover) can be estimated with significant accuracy. The regression line allows us to estimate the sea ice albedo as  $0.64 \pm 0.03$  at the 95% confidence level.

The sea ice albedo calculated here is somewhat higher than the value of 0.61 which was similarly estimated from a regression line of ice concentration versus albedo in a region of the Antarctic by *Allison et al.(1993)*. Besides, the variation of our data from the regression line is much small compared with that of their data. These differences are attributed mainly to the existence of various ice types, in particular dark nilas in their data. The fact that we excluded the dark nilas from our analysis because it was difficult to distinguish such ice from the water is likely the reason for somewhat higher albedo and small variation from the regression.

Although surface albedo and ice concentration were highly correlated as a whole in Figure 3.4.1, the discrepancies from the regression line are also noticeable especially at high concentration. We next will consider other factors to examine the cause of these discrepancies,

Most of the ice floes but nilas were found to be covered with snow during the cruise, so that snow seemed to have significant effects on the surface albedo. According to *Warren (1982)*, a snow albedo is determined mainly by snow grain sizes, solar zenith angle, and cloud cover. Among these factors, it is solar zenith angle that we can obtain quantitatively with accuracy. Therefore, we here focus on the effect of the solar zenith angle among these factors. Although snow grain sizes and cloud cover were not measured successively, we took several snow samples and conducted the visual observation of cloud amount in tenths at hourly intervals. On the basis of these data, the effect of cloud amount and snow grain sizes will be discussed later.

In addition to these factors, it is known that sea ice albedo varies corresponding to

ice thickness (e.g. *Weller, 1972*). Therefore, we examined the correlation between the discrepancies and the 10-minute averaged total thicknesses measured by the method described in section 2.1. When ice concentration were low, the accuracy of the ice thickness measurement decreased because it became easier for thick ice floes to flow around the ship rather than to be broken and turn into the side-up positions. For this reason, here we dealt with ice thickness data only when the ice concentration was greater than 70%. Although snow depth may also affect albedo, we did not deal with this parameter directly because of an accuracy problem. (Actually, we examined the effect of measured snow depth on the discrepancies of albedo for 1997 data, but significant effect could not be found.)

The individual correlation with the deviations from the regression line (1) is shown in Figure 3.4.2ab. The trends for solar zenith cosine and ice thickness, which are drawn in these figures, are both significant at the 95% confidence level. Especially, the correlation with solar zenith cosine is significant even at the 99% confidence level.

Therefore, we again derived a linear regression adding the term of solar zenith cosine to estimate the effect of solar altitude on albedo. The linear regression is represented as

$$A = 0.256 + 0.543 * \frac{c}{100} - 0.364 * \cos\mu \quad RMS = 0.056 \quad (2)$$

where  $\mu$  is solar zenith angle. The value of *RMS* was somewhat reduced compared with that ( $=0.062$ ) of the regression (1). The correlation between observation and calculation from this regression is shown in Figure 3.4.3a. It is shown that the variation from the line is somewhat reduced compared with that in Figure 3.4.1. Figure 3.4.3b is the contour map which represents the regression (2). We see from this figure that the increase of the solar altitude by 20 degrees causes the decrease of albedo for same ice concentration approximately by 0.1. This result is consistent with the observation of snow albedo shown in Figure 12 of *Warren(1982)*. Therefore, we do not consider that regression (2) is far from the reality though the dependence on solar zenith does not appear so much strong

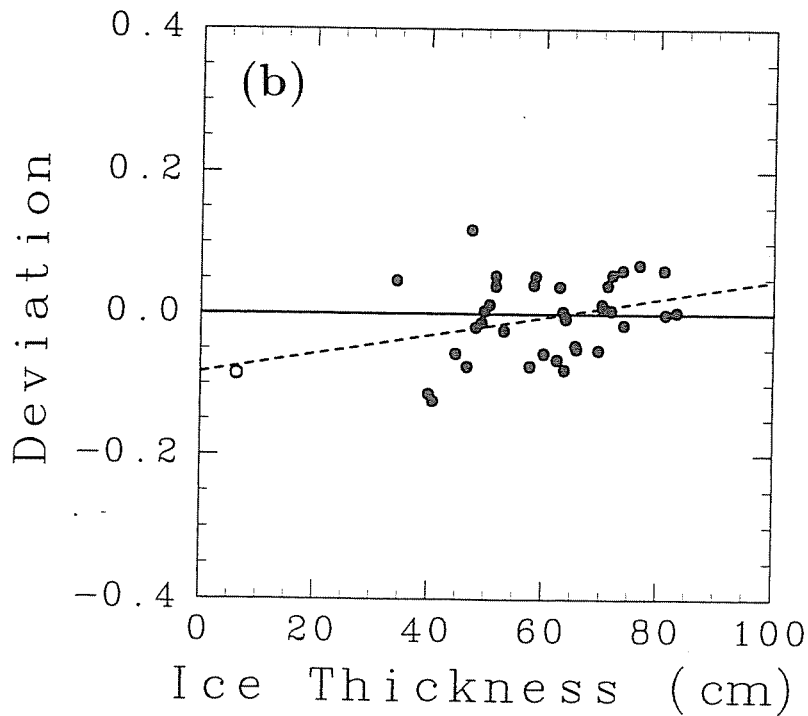
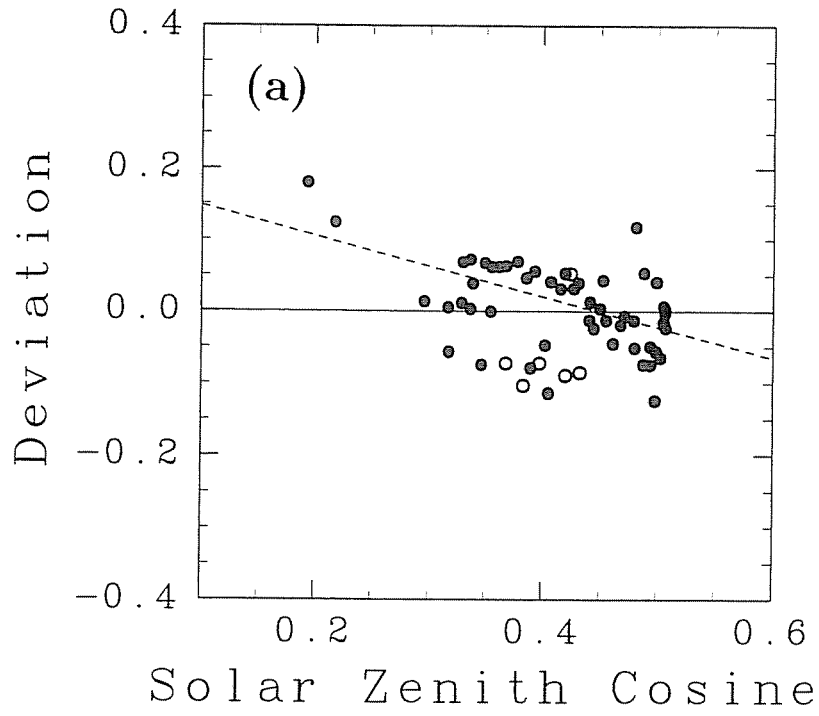


Figure 3.4.2 : Deviation of the observed albedo from the regression line in Fig.3.4.1 as a function of (a) solar zenith cosine and (b) ice thickness with each regression line.

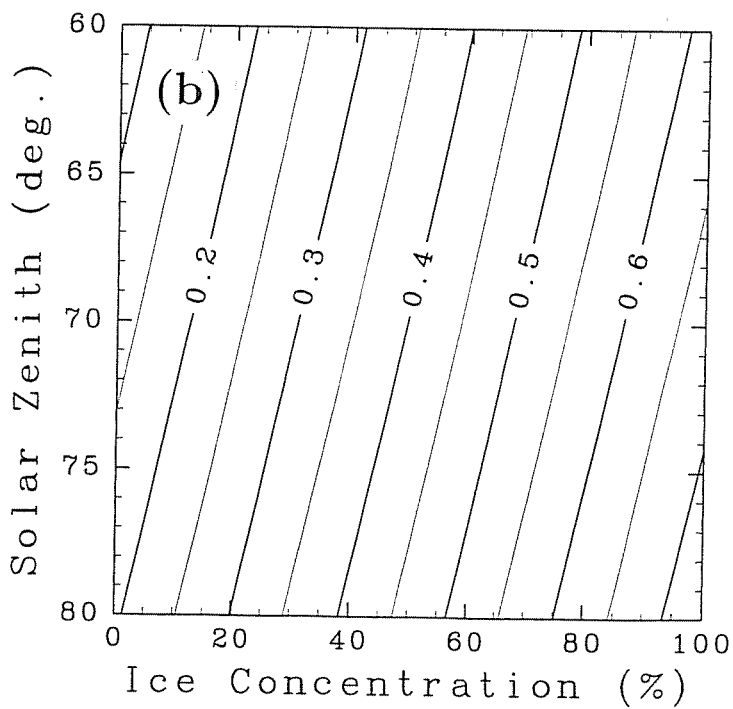
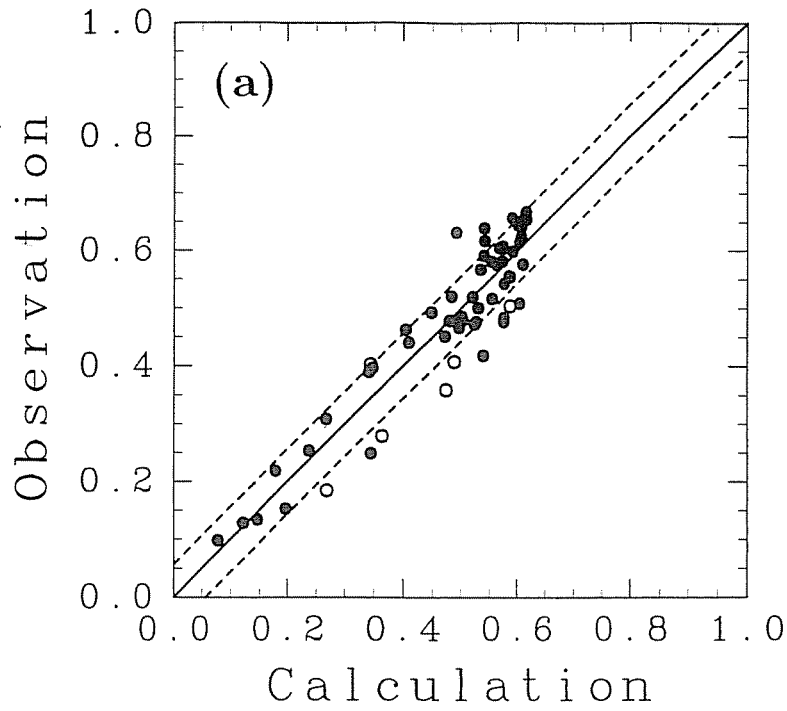


Figure 3.4.3 : Albedo calculated from ice concentration and solar zenith cosine using regression (2).

(a) Correlation between observation and calculation.

White and black circles are same as Fig.3.4.1.

Two broken lines denote  $\pm RMS (= 0.056)$ .

(b) Contour map as a function of solar zenith and ice concentration.

in Figure 3.4.2a.

Next, we will examine the effect of ice thickness which contributed weakly but significantly to albedo. We again derived the linear regression from the variables of ice concentration, solar zenith, and ice thickness. The regression line is represented as

$$A = 0.066 + 0.625 * \frac{c}{100} - 0.241 * \cos\mu + 0.109 * \frac{Hi}{100} \quad RMS = 0.050 \quad (3)$$

$$(c \geq 70\%, N = 37)$$

where  $Hi$  is ice thickness(cm). The value of  $RMS$  is slightly reduced again compared with that ( $=0.056$ ) of the regression (2). The correlation between observation and calculation is plotted with  $RMS$  line in Figure 3.4.4. Although the discrepancy between observation and prediction from the regression line is reduced again, this figure shows that there are some samples in which the discrepancies still remained. To know what caused them considerably to deviate from the regression, we examined cloud amount data and their surface conditions.

Since cloud amount data were taken only at hourly intervals, we took out the samples in which cloud amount was observed at the same time, and plotted the deviation of the observed values from the regression (3) as a function of cloud amount. The result is shown in Figure 3.4.5. The solar altitude of each sample is also plotted. The deviation is varied even for similar solar altitude and significant dependence on cloud amount can hardly be found in this figure. Besides, for the samples which deviated from the regression by more than  $RMS$ , the cloud amount data which are estimated by interpolating from the hourly data are varied from 0 to 10. This suggests that the deviation is caused mainly by other factors.

In order to examine the effect of surface conditions, we checked the monitoring video images for the cases where the observed values deviated significantly from the regression (3). In Figure 3.4.4, there are three points where the observed values are greater than the predicted values by more than  $RMS$ . The investigation with the video images

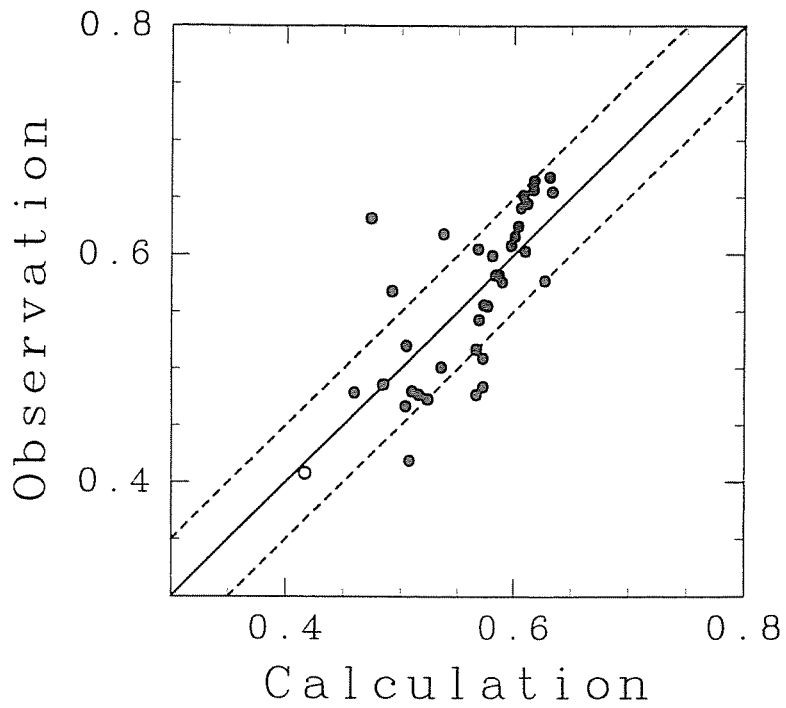


Figure 3.4.4 : Correlation between observed albedo and calculated one from ice concentration, solar zenith cosine, and ice thickness using regression (3).

White and black circles are same as Fig.3.4.1.

Broken lines denote  $\pm RMS (= 0.050)$ .

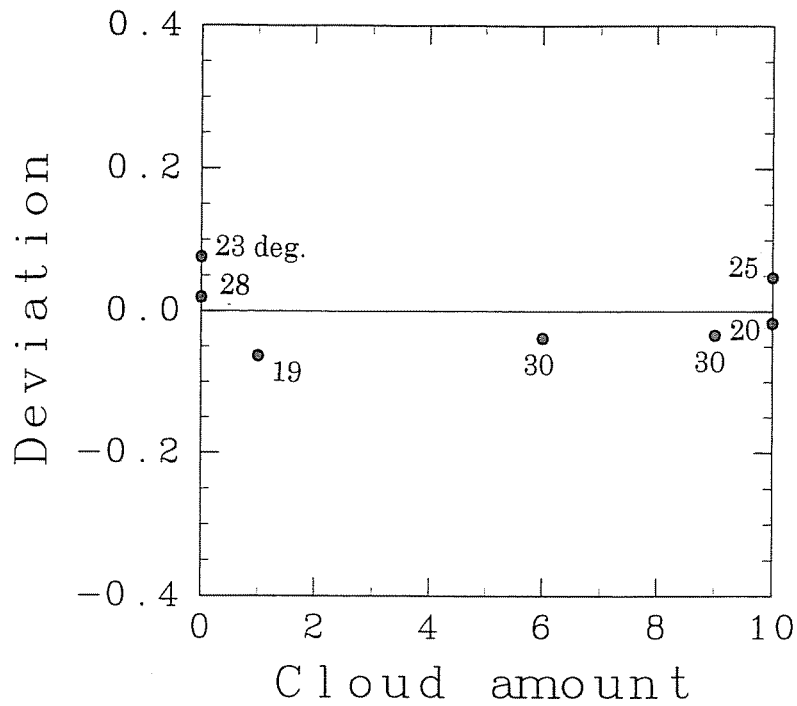


Figure 3.4.5 : Correlation between cloud amount and the deviation of observed albedo from the calculation in Fig.3.4.4.

Only the cases in which cloud amount was also observed are shown.

The numbers plotted in the figure mean solar altitude (deg.)

reveals that the common feature that there existed lots of relatively large ice floes (their diameters are greater than a few hundreds of meters) during the observation period are found in all the three cases. On the other hand, there are six points where the observed values are less than the predicted values by more than *RMS*. In these cases, thin ice with a relatively small amount of snow was predominant. We consider that these features were responsible for lowering albedo. From these results, it is suggested that ice surface conditions have a more significant effect on albedo than cloud amount. In both cases, surface roughnesses were found occasionally though their degrees and frequencies were varied. Such roughnesses may possibly weaken the effect of cloud cover because they play the role in increasing the scattered light as cloud cover does.

Finally, we will calculate the ratio of the total reflected solar radiation to the total incident one over sea ice (ice concentration = 100%) during the day (we refer to this ratio as daily integrated albedo here) using regression (2)(3) to estimate representative sea ice albedo (100% ice concentration) in this region. Since it was shown that the effect of cloud cover is weak, we estimate the daily integrated albedo of sea ice under clear sky conditions. As for the amount of incident irradiance ( $I_0$ ), we used the following formula (*Kondo, 1967*).

$$I_0 = J_0(d_m/d)^2 \cos\mu(0.3 + 0.7 * 10^B) \quad (4)$$

$$B = -0.055 * (1 + 0.04e_H) \sec\mu$$

where  $J_0$  is a solar constant,  $\mu$  is solar zenith angle,  $e_H$  is vapor pressure at the surface and  $d_m$  is the annual mean distance between the sun and the earth, and  $d$  is that at an observation time. The incident solar radiation in this region at this time of the year, which is predicted by this formula, is drawn in Figure 3.4.6a. To check this formula, we compared  $I_0$  with our data (4 samples) which were measured under definitely clear sky conditions during the cruise. This comparison revealed that calculated and observed value agreed well within  $8.6W/m^2$ .



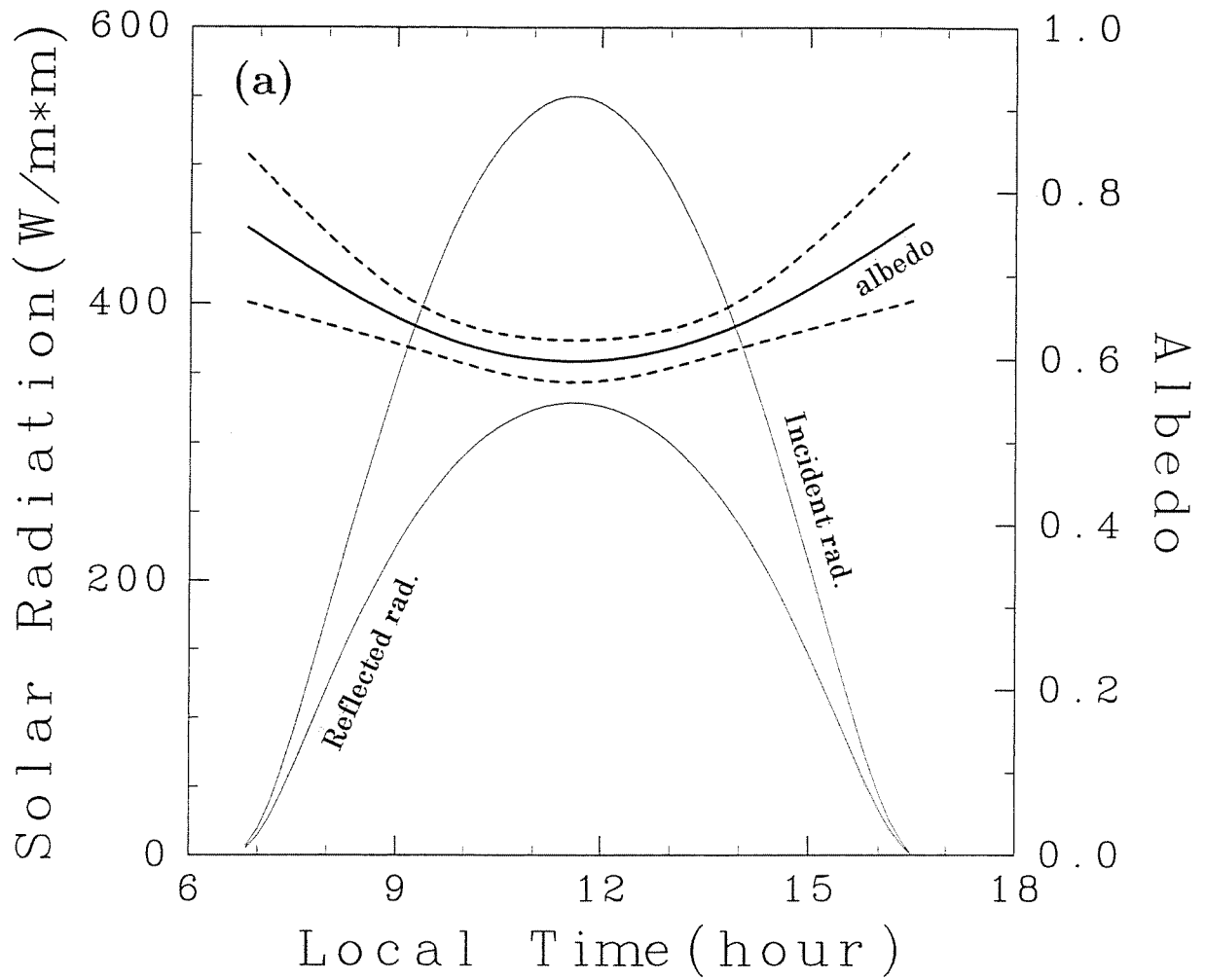


Figure 3.4.6 : (a) Diurnal change of sea ice albedo calculated from the regression (2).

Two broken curves denote 95% significance interval.

Diurnal changes of incident and reflected solar radiation are also drawn.

Reflected radiation is calculated by multiplying albedo and incident radiation at each time.

When the effect of ice thickness is not taken into account, the regression (2) can be used to obtain the daily integrated albedo. If we assume that the regression (2) holds for the solar altitude less than 10 degrees, the daily change of reflected radiation can be calculated using the formula (4) and the regression (2). The result is drawn in Figure 3.4.6a. By calculating the ratio of the daily integrated reflected radiation to irradiance, the daily averaged albedo is estimated to be  $0.63 \pm 0.03$  at the 95% confidence level.

When the effect of ice thickness is taken into account, the daily integrated albedo can be estimated as a function of ice thickness using the regression (3) and the formula (4). The result is shown in Figure 3.4.6b. This figure shows that with the increase of ice thickness, a slight increase of albedo can be detected. For example, the daily albedo is  $0.64 \pm 0.07$  for 40 cm ice thickness. This value increases to  $0.69 \pm 0.05$  for 80 cm ice thickness. We will use this daily albedo as a function of ice thickness for the calculation of heat budget in the next chapter. The significance intervals in Figure 3.4.6b will be used to estimate the error of heat flux and ice growth rate.

#### *albedo of dark nilas*

In the case of snow-free sea ice, we obtained the albedo data for dark nilas off the Shiretoko Peninsula at 10:30 a.m. ( $26^\circ$  Solar altitude) on February 5, 1996 and at  $44.9^\circ N$   $143.3^\circ E$  at 1:30 p.m. (again  $26^\circ$  Solar altitude) on February 9, 1997 while the ship was stopped for hydrographical observations. In both cases, surrounding areas were entirely covered with nilas. The ice thicknesses which were measured by taking samples with a net from the ship were 1 to 1.5 cm for the former one and 2 to 3 cm for the latter one; the observed values of albedo were 0.10 and 0.12, respectively. In the light of approximately same solar altitudes, a slight difference may be attributed to the difference of the ice thicknesses. These values of albedo were in good agreement with the earlier works. (e.g. *Weller(1972)*, *Allison et al.(1993)*).

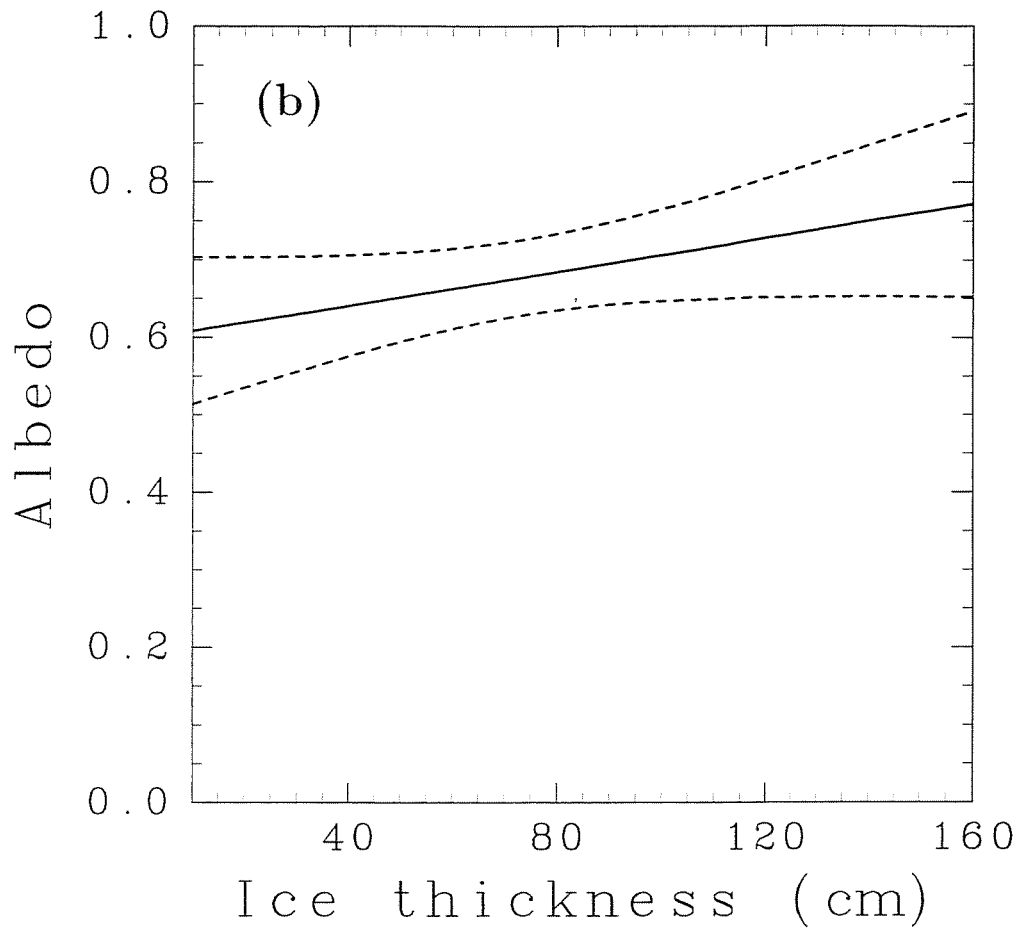


Figure 3.4.6 : *Continued.*

(b) Daily integrated albedo as a function of ice thickness (calculated from regression (3)). Two broken curves denote 95% significance interval. Daily integrated albedo is calculated by taking the ratio of the total reflected radiation to the total incident one during the day. Two broken curves denote 95% significance interval.

### 3.5 Summary and Discussion

In the southwestern region of the Okhotsk Sea, we conducted the measurements of surface albedo and ice conditions. From the analysis focusing on the horizontal scale of a few kilometers, it was found that the surface albedo was highly correlated with the ice concentration ( $RMS=0.062$ ). The deviation from the regression line had statistically significant relation with the solar zenith angle. If we include the solar zenith cosine as an additional variable in the regression, the  $RMS$  was reduced to 0.056. Ice thickness was also weakly but significantly related with the deviation from the regression. If we added ice thickness to the variables of the regression, the  $RMS$  was reduced to 0.050. The data which still deviated considerably from regression seem to be caused by surface conditions rather than cloud cover. From examination of video images, it was found that albedo of less snow covered ice floes is lowered, whereas for remarkably large ice floes albedo is heightened. If the effect of ice thickness is not taken into account, the daily integrated sea ice albedo is estimated as  $0.63\pm 0.03$ .

In addition, we could also obtain the albedos of dark nilas with snow-free surface when the ship stopped. They were estimated to be 0.10 and 0.12 for ice thickness of 1-1.5 cm and 2-3 cm, respectively.

Among these results, here we discuss especially two noticeable points. The first point is that the estimated sea ice albedo was somewhat lower than that of the previous studies on land fast ice covered with almost same snow depth. According to *Grenfell and Perovich(1984)*, 0.79 is estimated for snow covered (snow depth is 8 cm before melting) first-year ice near the shore of Alaska. On the other hand, for the interior pack ice region, nearly same albedo as ours is reported in the Antarctic Ocean by *Andreas and Makshatas(1985)*. They observed surface albedo of 0.5 to 0.6 for the sea ice area with about 90% ice concentration. Although they did not measure sea ice albedo (100% ice concentration), this result indicates it is 0.6 to 0.7 and is in good agreement with our estimation.

Therefore, it is suggested that somewhat lower albedo may be one of the characteristics of the sea ice in the pack ice regions.

Regarding the discrepancy of albedo between pack ice and land fast ice, we at first speculated as follows: it is caused by difference of snow features, especially grain size between land fast ice and pack ice. For land fast ice, snow undergoes relatively less amount of morphological processes, thus retaining fine-grained structure. On the other hand, in areas with a significant variability in ice conditions, in particular ice concentration such as a marginal ice zone, the fabric structure of a snow layer is more easily modified by sea spray and flooding, thus resulting in the growth of snow grains. According to *Warren(1982)*, the snow albedo highly depends much on its grain size. This may be why somewhat lower albedo was estimated in our case. This speculation is not inconsistent with the fact that considerably highly deviated albedo was observed where remarkably large ice floes were predominant. It is likely that the growth of snow grains on remarkably large ice floes is relatively limited because they are less influenced by sea water compared with those on small ice floes.

To confirm our speculation, we arbitrarily took 11 snow samples on small sea ice floes with a cylinder from the ship during the cruise in 1997. Grain sizes were estimated on a sampling sheet with a scale in millimeters. Salinity was measured for melted samples after the cruise. They were almost all from 0.5 to 1.0 mm in size and classified to depth hoar or granular snow. This implies that they had already grown up enough from new snow and supports our speculation.

On the other hand, salinity data were somewhat varied from less than one psu to more than ten psu (11.18, 4.37, 7.49, 0.81, 1.45, 0.31, 0.72, 1.61, 4.39, 2.33, 15.15 psu). Among them the samples of relatively high salinity seem to have been affected mainly by sea water through sea spray and/or flooding in the growing process of snow grains. In contrast, it is considered that the ones of much less salinity ( $\leq 1$  psu) were affected by other factors than sea water. Considering that abundant solar radiation and relatively

high temperature even in mid winter are the characteristics of sea ice at relatively low latitude, these factors can help the growth of snow grains. In addition to these factors, we would like to notice the strong vertical temperature gradient in snow layer which is caused by low thermal conductivity of snow. *Fukuzawa and Akitaya (1993)* showed through laboratory experiments that the growth rate of snow grain sizes increases with the temperature gradient in the snow layer. Since both snow depth and ice thickness are thin in the marginal ice zone, stronger vertical gradient of temperature is expected in the snow layer on the pack ice than on the thick land fast ice. Therefore, this effect may also be important in the pack ice region. Thus, it may be said that relatively low sea ice albedo is one of the features of sea ice in the southern part of the Okhotsk Sea, which contains a number of pack ice floes and is also located at relatively low latitude.

The second point is that ice thickness had a significant effect on sea ice albedo. From our measurement, significant positive correlation could be seen between 10-minute averaged ice thicknesses and snow depths (Figure 3.5.1). When we consider the fact that the optical extinction coefficients of visible wavelengths range 60 to  $90(m^{-1})$  for snow grain sizes of 1 mm (density is 0.41 to  $0.45 Mg/m^3$ ) (*Mellor, 1977*) and that snow depth was 5 to 15 cm in this study, it is natural to consider that the dependence of albedo on ice thickness is caused mainly by snow depth on ice floes rather than by the ice thickness below the snow. The reason why the significant effect of snow depth on albedo could not be found is probably due to accuracy problem.

From all the above discussion, it is suggested that snow on sea ice floes plays an important role in determining the albedo in the marginal pack ice regions. For better understanding, further investigation on albedo and especially the characteristics of snow on ice floes will be desired in the future.

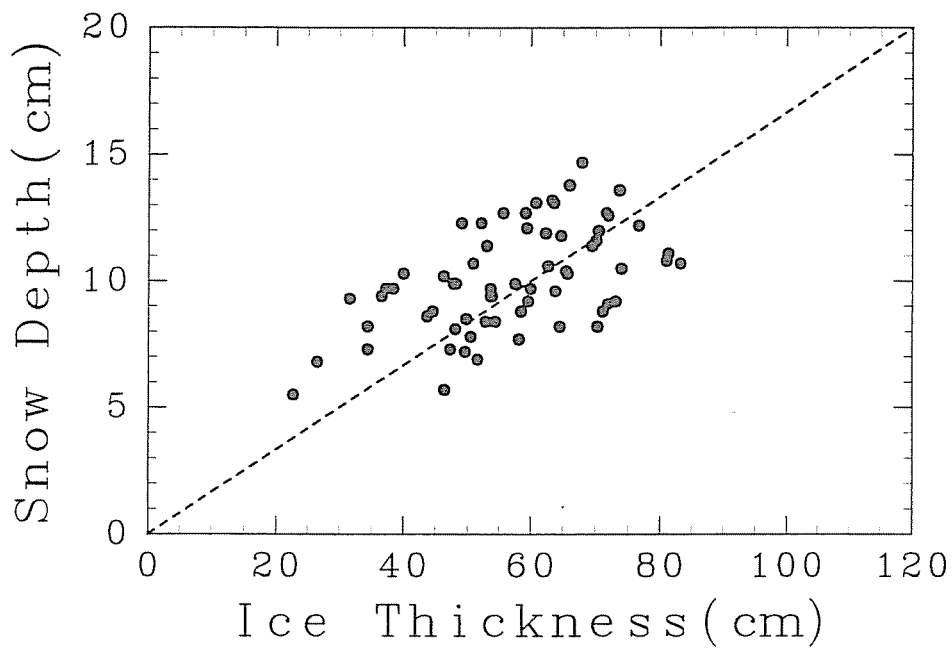


Figure 3.5.1 : Correlation between snow depth and ice thickness.  
Here, ice thickness includes snow depth.

## Chapter 4. Heat budget

### 4.1 Introduction

In winter, a northwesterly monsoon from Siberia prevails in the Okhotsk Sea. This region is characterized by strong horizontal temperature gradient between cold continent ( $T \leq -20^{\circ}C$ ) and relatively warm north Pacific Ocean ( $T \geq 0^{\circ}C$ ). It is well known that sea ice extent prevents cold air from being transformed by the ocean. The degree of prevention depends on the meteorological conditions and the ice thickness distribution. That is, the cold air is appreciably transformed over thin ice area, whereas heat exchange between ocean and atmosphere can hardly occur over thick ice extent. In the former case, the cold air is gradually transformed from the continent to the Pacific Ocean and hence the local horizontal temperature gradient around the ice margin becomes less than in the latter case. Since this region is located at one of the major paths of cyclones over east Asia from winter to spring (*Chen et al., 1991*), transformation of cold air may affect the development of cyclones. Thus it is important to know how much degree of heat is transferred from ocean to atmosphere.

Besides, this region is also an important area to ocean circulation. The dense water produced by ice formation may affect the ocean structure. This region has recently been pointed out as a possible origin of North Pacific Intermediate Water (*Watanabe and Wakatsuchi, 1998*), and hence it is important to know how much sea ice can be produced in this area. Further, the estimation of the growth amount of sea ice serves to understand ice growth processes in this region.

Thus the southern region of the Okhotsk Sea is an important area to both the atmospheric and the oceanic circulation. The major purpose of this chapter is to discuss the characteristics of sea ice extent over this area from the viewpoint of heat exchange. For this purpose, we calculate the heat budgets on the basis of the observed meteorological ice data, and estimate the turbulent heat flux from ocean to atmosphere and the ice



growth rate. In this calculation, the sea ice albedo estimated in the previous chapter is used (see Figure 3.4.6b). To estimate the error of calculated heat flux values, the 95% confidence intervals of sea ice albedo in Figure 3.4.6b are used because solar incidence is a leading factor of the heat budget in this region.

In the next section, we will explain the method of heat budget calculation. The results will be shown in section 4.3. We will discuss them in section 4.4.

## 4.2 Method of calculation

A thermodynamic ice model is used to estimate heat budgets and ice production. The model we used is similar to those of *Maykut (1978 and 1982)*, which are used to investigate the effects of ice thickness variations on heat exchange over the Central Arctic. Although he assumed ice thickness distribution obtained from a model (*Thorndike et al., 1975*), the observational data are used here for ice thickness distribution.

### *Meteorological data*

In order to grasp the general features of the heat budgets in this region, we discuss the averaged values during the observation period. For this purpose, we prepare the hourly meteorological data by taking averages at each hour during the period. The hourly data of air temperature, relative humidity, and solar radiation are shown in Figure 4.2.1a (1996) and b (1997). These data are considered to be representative of the diurnal cycle during this period. Therefore, the averaged values of these data for one day give representative daily mean data. The data of individual years are listed in Table 4.3.1. This table shows that meteorological conditions are similar in both years. Since ice conditions are much different between the two years, the resultant heat flux can be considered to directly show the effect of ice thickness distribution on heat budgets.

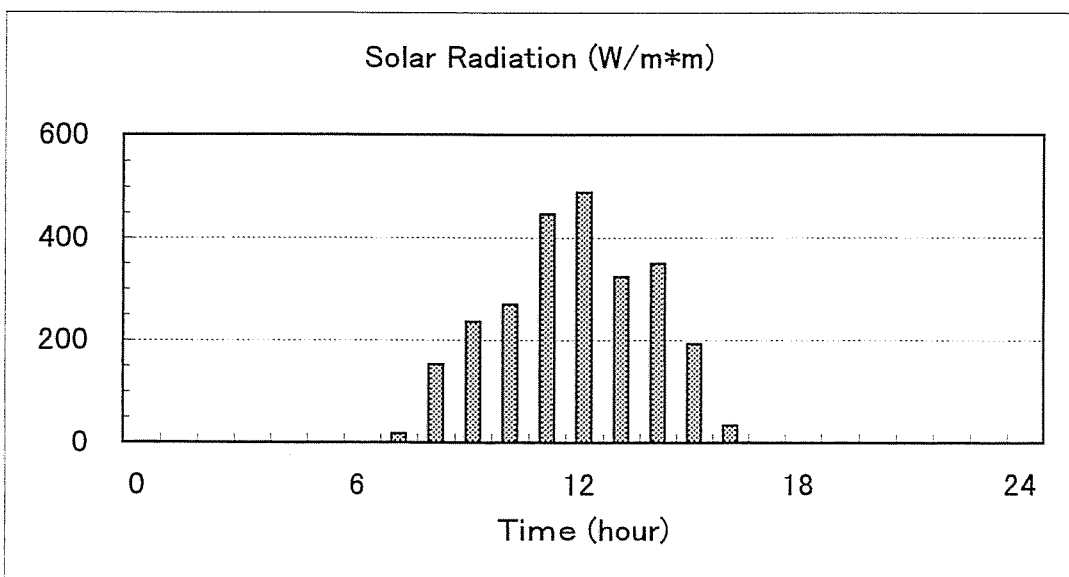
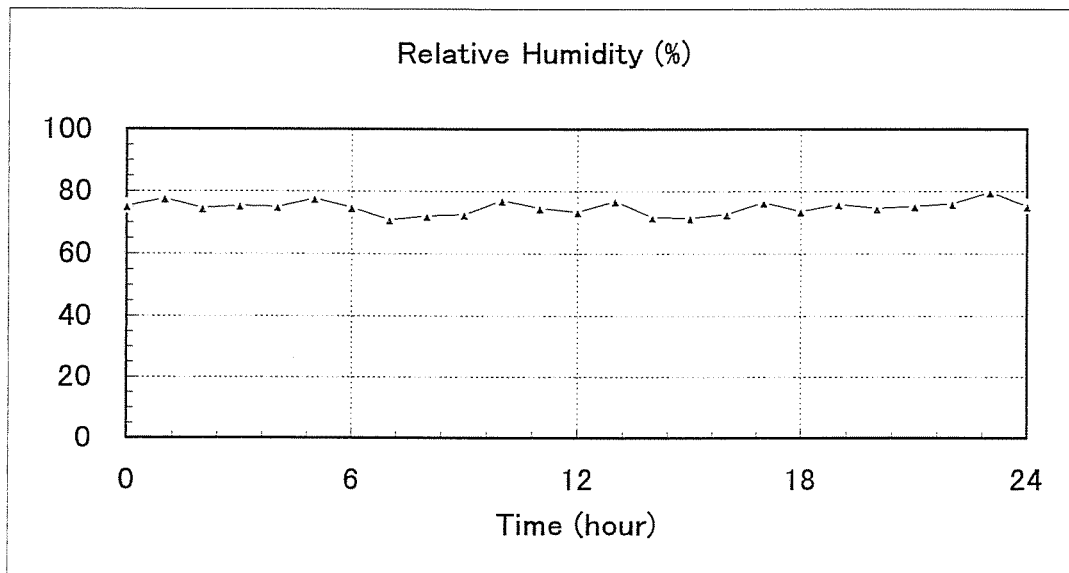
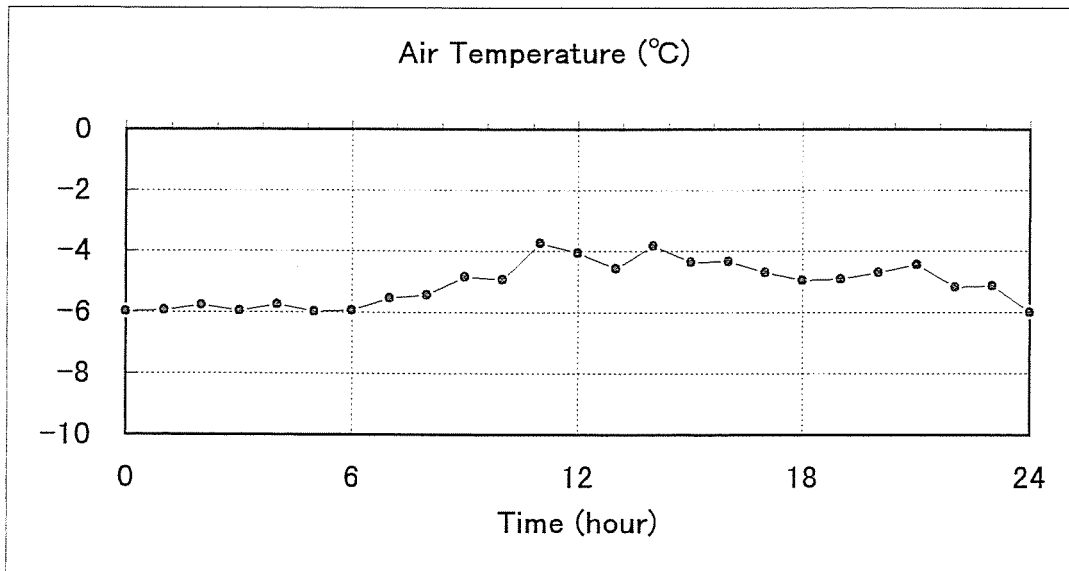


Figure 4.2.1 Averaged diurnal cycle of meteorological data.

(a) 1996.

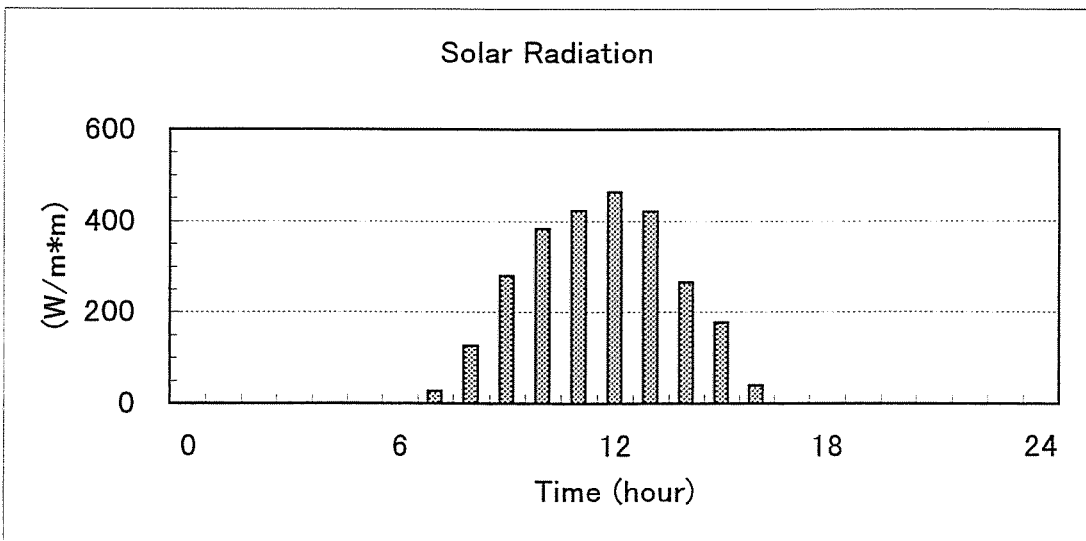
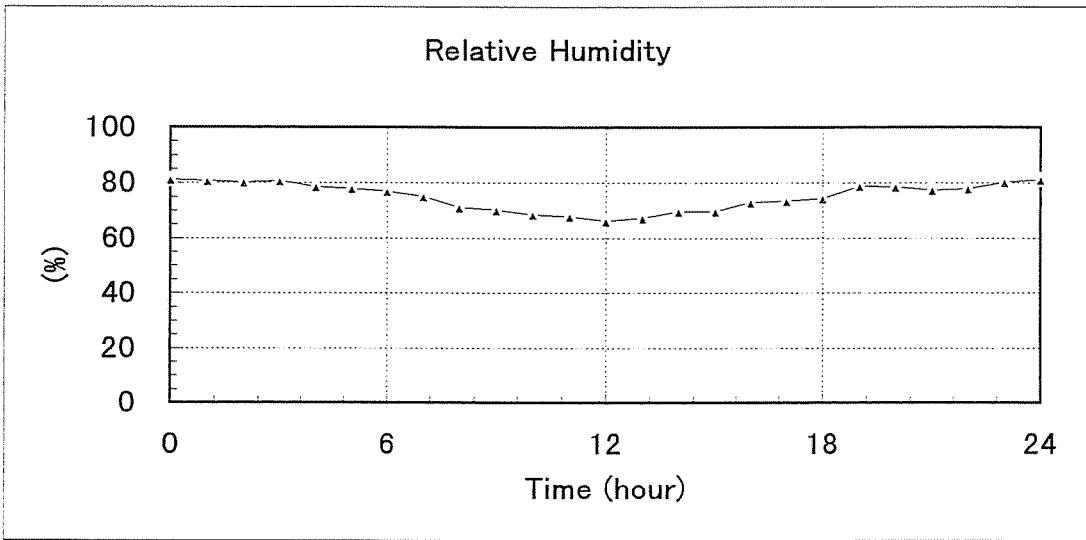
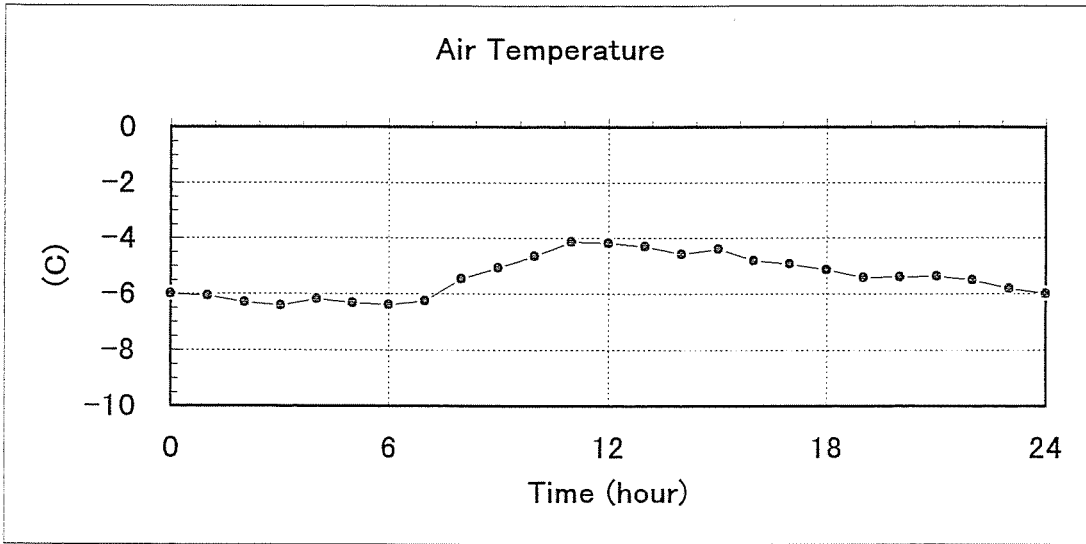


Figure 4.2.1 (Continued.)

(b) 1997.

Table 4.3.1 Daily mean meteorological conditions

Elements	1996	1997
Air temp. (C)	-5.0	-5.4
Relative Humid.(%)	74.8	74.9
Solar radiation( $W/m^2$ )	104.5	108.4
Wind speed(m/s)	6.6	4.3
Cloud amount(1/10)	7.0	6.6
Air pressure(hpa)	1013.0	1012.9

*Assumption*

Heat budgets are calculated on the following assumptions:

- (1) Vertical heat transport is predominant.
- (2) Sensible heat flux ( $FSH$ ), latent heat flux( $FLH$ ), net solar radiation ( $FSW$ ), net long radiation ( $FLW$ ), and conductive heat flux in ice ( $FCI$ ) are balanced at the surface of sea ice.
- (3) Areal ice thickness distribution is represented by the frequency of observed ice thickness (Figure 2.3.3).
- (4) Sea ice is covered with snow except for nilas and snow depth is given by one fifth of ice thickness.

Assumption (1) is approximately satisfied because the ice floe size mostly ranged from a few to one hundred meters in our observation area (Figure 2.3.6) and is much greater than ice thickness.

The full balance equation of heat flux at the surface is described as follows:

$$\rho_i \Delta H C_i \frac{\partial T_s}{\partial t} = FSH + FLH + FSW + FLW + FCI \quad (1)$$

, where  $\rho_i$ ,  $\Delta H$ ,  $C_i$ , and  $T_s$  is ice density, thickness of surface layer, specific heat, and surface temperature, respectively. According to *Ono (1967)*,  $C_i$  is  $1.57 cal g^{-1} K^{-1}$  (=

$6.57Jg^{-1}K^{-1}$ ) for  $T_S = -4^\circ C$  and  $S_i = 4psu$ . Since the change of the weekly mean temperature (the observation period is about one week) is below 5 K (That is, below 1 K/day), the left term is estimated as below  $1.4W/m^2$  if  $\Delta H$  is taken to be 2 cm. Therefore, we consider the left term of equation (1) is negligible and assumption (2) approximately holds.

When the ship chose the thin ice route, the frequency of observed ice thickness would be biased to thinner ice and assumption (3) would not be satisfied. But most of the sea ice was below the ability of the ship's ice breaking and she did not seem to take thinner route. Therefore, we consider that assumption (3) is approximately satisfied. We allocated the areal fraction of ice thickness at 10 cm intervals ( $H_i=15, 25, 35, 45, \dots$  cm) among total ice concentration (66.2% in 1996, 70.5% in 1997) which was calculated from video analysis. The areal fraction of nilas ( $H_i=5$  cm) was obtained from visual observation of nilas and the remnant was allocated to open water ( $H_i=0$  cm). The resultant ice thickness distribution is shown Figure 4.2.2. The distributions were significantly different between 1996 and 1997. Remarkably thin ice was predominant in 1996, while sea ice was remarkably thick in 1997. Therefore, the results of these two years may give maximum and minimum estimates.

Since most of the ice floes but nilas were observed to be covered with snow, assumption (4) is also satisfied. The ratio of snow depth and ice thickness was determined by the result of video analysis (Figure 3.5.1). They are well correlated and the ratio (broken line) is about 1/6. (Note that ice thickness in Figure 3.5.1 includes snow depth. Although uncertainty remains regarding snow thickness, we made sure that our results are insensitive to snow thickness.)

### *Thermodynamic ice model*

When the surface temperature ( $T_S$ ) is below freezing point, the heat balance equation

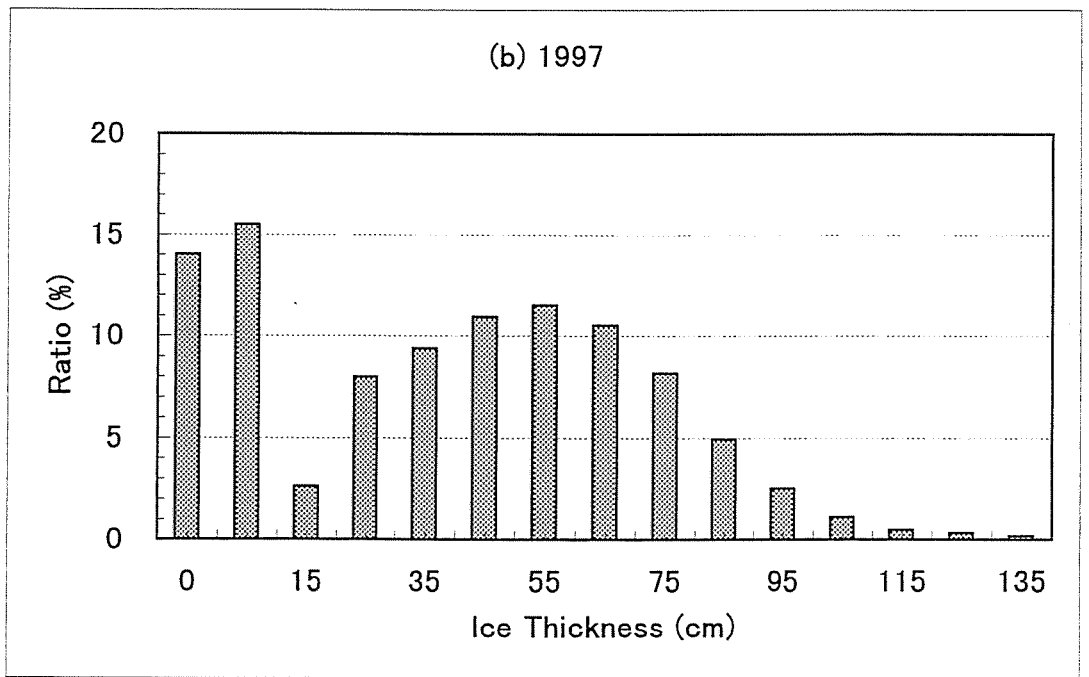
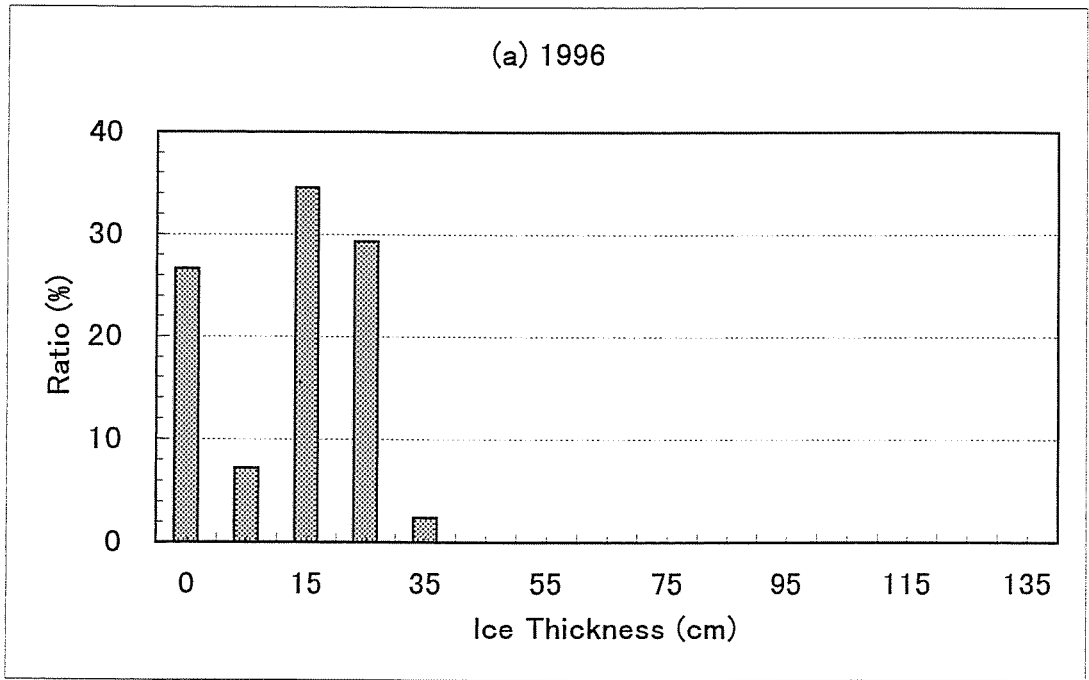


Figure 4.2.2 Areal fraction of ice thickness used for heat budget calculation.

(a) 1996      (b) 1997.

Note that substantial difference is found between two years.

at the surface can be expressed as

$$FSH(T_S) + FLH(T_S) + FSW + FLW(T_S) + FCI(T_S) = 0 \quad (2)$$

Here a flux toward the surface is taken to be positive, while one away from the surface is taken to be negative. The sensible heat flux and the latent heat flux is calculated using the bulk method.  $FSH$  is obtained from  $\rho c_p C_s u (T_a - T_S)$ , where  $T_a$  is the observed air temperature,  $\rho$  is the air density ( $1.3 \text{ kg/m}^3$ ),  $c_p$  is the specific heat of the air ( $1004 \text{ J/kg/K}$ ),  $C_s$  is the transfer coefficient for sensible heat (discussed later), and  $u$  is the observed wind speed.  $FLH$  is obtained from  $0.622 \rho L_v C_e u (r e_{sa} - e_{sS}) / p$ , where  $L_v$  is the latent heat of sublimation ( $2.84 * 10^6 \text{ J/kg}$ ; Yen, 1981),  $C_e$  is the transfer coefficient for latent heat,  $r$  is the observed relative humidity,  $p$  is the surface pressure, and  $e_s$  is the saturation vapor pressure. The dependence of  $e_s$  on air temperature is expressed as a fourth-order polynomial developed by Maykut (1978). Since the ice thickness is relatively thin in this region, we assume that temperature gradient in the ice is linear, so that the conductive heat flux ( $FCI$ ) can be written as  $\gamma (T_B - T_S)$ , where  $T_B$  is the temperature at the ice bottom and is taken to be the freezing temperature and  $\gamma$  is thermal conductance of the ice-snow slab ( $= k_i k_s / (k_s H_i + k_i H_s)$ ), where  $k$  and  $H$  is thermal conductivity and thickness, respectively, and the suffix  $i$  and  $s$  denote ice and snow, respectively.

The absorbed short wave radiation ( $FSW$ ) is described as  $F_r * (1 - \alpha) * (1 - i_o)$ , where  $F_r$  is the solar radiation reaching to the ground,  $\alpha$  is surface albedo, and  $i_o$  is the transmittance. As for albedo, 0.07 and 0.12 are used for open water and nilas ( $H_i = 5 \text{ cm}$ ), respectively, and the values estimated as a function of ice thickness in the previous chapter are used for thicker ice (see Figure 3.4.4b). Since the extinction coefficient of snow is more than  $60 \text{ m}^{-1}$  (Mellor, 1977), we set  $i_o = 0$  except for nilas ( $i_o = 0.18$ ; Grenfell and Maykut, 1977).

The incident long wave radiation ( $FLW_1$ ) is obtained from  $FLW_1 = 0.7855 * (1 + 0.2232 C^{2.75}) * \sigma T_a^4$ , which is derived from observation in the polar region by Maykut and

*Church (1973)*, where  $C$  is cloud amount ( $0 \leq C \leq 1$ ). The emitted long wave radiation ( $FLW_2$ ) is described as  $FLW_2 = \varepsilon * \sigma T_S^4$ .  $\varepsilon$  is taken to be 0.97 for open water and nilas ( $H_i=5$  cm) and 0.99 for thicker ice.

After substituting the observed values, the equation (2) is resolved for  $T_S$  using a Newton-Raphson method and then the individual fluxes are calculated by substituting the obtained  $T_S$ . For open water,  $T_S$  is taken to be freezing temperature and the residual term ( $FQ = FSH + FLH + FSW + FLW + FCI$ ) is calculated.

On the other hand, the heat balance equation at the bottom of ice is expressed as:

$$\rho_i L_f \frac{dH_i}{dt} = FCI - F_w \quad (3)$$

, where  $\rho_i$  is the ice density ( $900\text{kg}/\text{m}^3$ ),  $L_f$  is the latent heat of fusion (discussed later), and  $F_w$  is the ocean heat flux. If we set  $F_w$  to be zero, the growth rate of ice thickness can be calculated as  $FCI/\rho_i L_f$  from the equation (3). For open water, the ice growth rate is calculated as  $-FQ/\rho_i L_f$ . The heat fluxes and ice growth rate of total area are obtained by summing up the area-weighted values of individual ice thicknesses.

### *Physical parameters*

Prior to analysis, we discuss three essential physical parameters which are used in the model. The first one is the heat transfer coefficient. This parameter is taken to be  $1.37 * 10^{-3}$  for both sensible heat flux and latent heat flux after *Andreas and Makshtas (1985)* because their observation is quite similar to ours. Both are ship-based observations and the measurement heights of wind speed and air temperature are almost same (21m( $u$ ) and 11m( $T_a$ ) in their case, and 22m( $u$ ) and 15m( $T_a$ ) in our case), and the usefulness of the coefficient value is checked by the detailed observation. However, somewhat smaller values of  $1.0 * 10^{-3}$  (*Aota et al., 1989*) are used for open water and nilas because roughness is much less than thicker ice.

Second, thermal conductivity is taken to be  $0.3\text{Wm}^{-1}\text{K}^{-1}$  for snow layer and 2.0



$Wm^{-1}K^{-1}$  for ice. In general, the thermal conductivity of snow can be represented as  $k_s = 2.22362 * \rho_s^{1.885}$  (Yen, 1981). Since  $\rho_s$  is about  $0.35g/cm^3$  in our case,  $k_s$  is estimated as 0.3. The thermal conductivity of sea ice is expressed as  $k_i = k_0(T_i) + \frac{0.13S_i}{T_i - 273.15}$  (Untersteiner, 1961), where  $k_0$  is thermal conductivity of pure ice, and  $S_i$  is ice salinity. This formula gives almost constant value of  $2.0Wm^{-1}K^{-1}$  under the conditions of our observation.

The last one is latent heat of fusion. In general, latent heat of fusion of sea ice can be expressed as follows:

$$L_f = 4.19 * 10^3 [79.68 - 0.505(T_i - 273.15) - 0.0273S_i + \frac{4.3115 * S_i}{T_i - 273.15}] \quad J/kg \quad (Yen, 1981)$$

, where  $T_i$  is set to be the freezing temperature.  $S_i$  is taken to be 9.1 psu for open water, 7.0 for nilas, and 3.5 for thicker ice on the basis of ice sample analysis (see Figure 5.3.1a).

### 4.3 Results

#### *Daily mean*

The result is shown in Figure 4.3.1ab. Here,  $FQ$  is a residual term (defined as  $FSH + FLH + FCI + FSW + FLW$ ) only for open water as mentioned before. If  $FQ \leq 0$ , ice forms by the thickness of  $(-FQ/(\rho_i L_f))$  at open ocean surface. What is most impressive in these figures is that the contribution of solar radiation is much more prominent in both years than that of the turbulent heat flux. This result is in contrast with that over thin ice area in the polar region (Maykut, 1978), where the sensible heat flux dominates the heat exchange with the atmosphere, and seems one feature of sea ice at low latitude where solar radiation is abundant. The estimated turbulent heat flux ( $29.6 \pm 4.0W/m^2$  in 1996 and  $15.3 \pm 3.0W/m^2$  in 1997) is nearly same as that estimated in the Antarctic pack ice region at the beginning of melting season ( $0 \sim 60W/m^2$ ; Andreas and Makhtas, 1985). Here, the error values are determined by the 95% confidence interval of albedo (see Fig.3.4.6b). The contribution of conductive heat flux is also small,

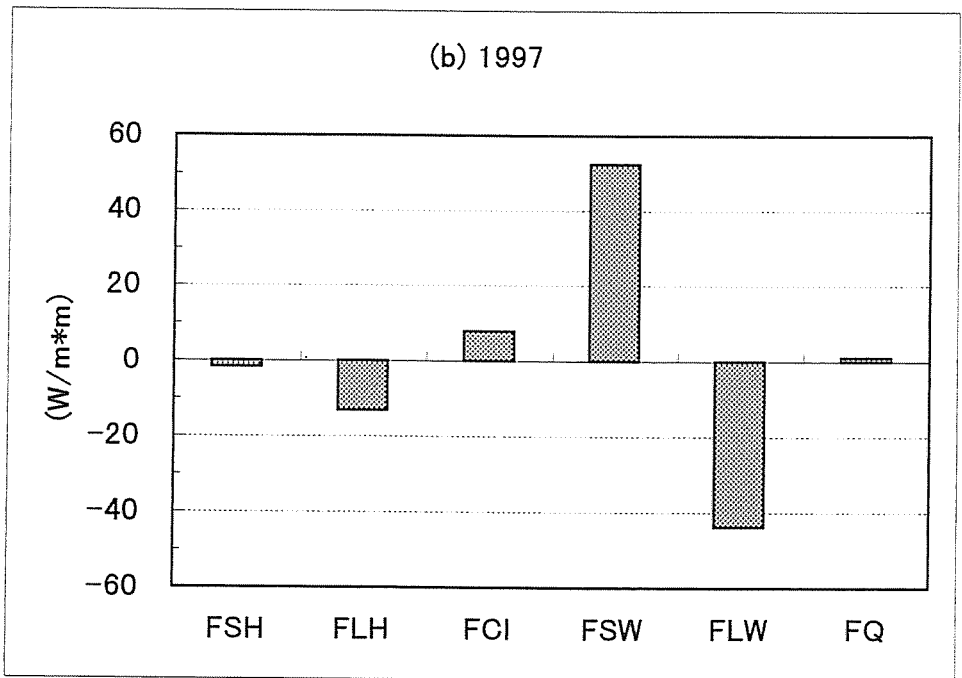
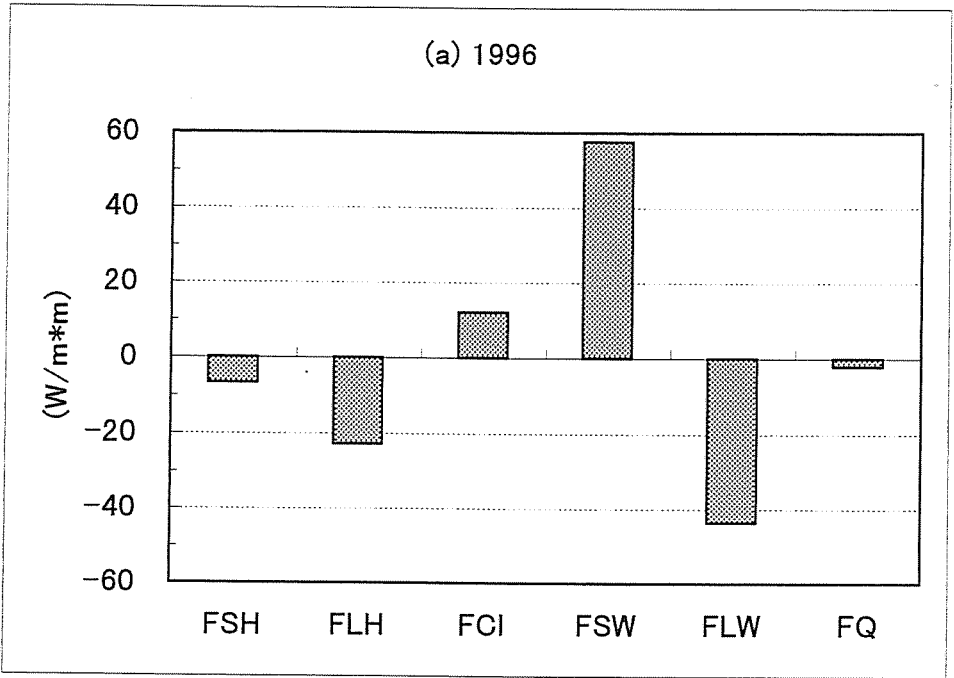


Figure 4.3.1 Heat budgets for daily mean meteorological data.

(a) 1996      (b) 1997

FSH: sensible heat flux

FLH: latent heat flux

FCI: conductive heat flux in ice

FSW: solar radiation

FLW: long wave radiation

FQ: residual

so that the ice growth per day is limited to  $0.49 \pm 0.04\text{cm}$  in 1996 and  $0.25 \pm 0.02\text{cm}$  in 1997. Since ice conditions have a remarkable contrast between two years as mentioned earlier, these values seem to give nearly maximum and minimum under similar meteorological conditions. Consequently, the averaged ice growth rate can be estimated as below  $0.5\text{cm/day}$  and thus thermodynamic growth is limited in this region.

Whereas the turbulent flux of the total area is downward in the polar region because thick ice area is dominant (*Maykut, 1982*), upward flux is estimated in Figure 4.3.1 in both years. This implies that sea ice extent works as a heating source rather than a cooling source. To further examine this characteristics, the non-area-weighted turbulent fluxes are presented in Figure 4.3.2. It is shown that the turbulent flux decreases significantly with ice thickness especially below 50 cm thickness. This decrease is attributed mostly to the change of the sensible heat flux. With the increase of ice thickness, the surface temperature becomes less influenced by the underlying ocean temperature, resulting in the decrease of the upward sensible heat flux, until the turbulent heat flux becomes downward like the polar region for more than 95 cm ice thickness. In this region, however, since relatively thin ice area is dominant, the area weighted turbulent flux becomes upward (see Figure 4.3.3). It is worth mentioning in this figure that more than half of the total upward turbulent heat flux is owed to open water and nilas area in both years. Thus open water and thin ice area characterizes the heat budgets in this region. Figure 4.3.2 also shows that without sea ice the turbulent heat flux would increase to  $57.6\text{W/m}^2$  in 1996 and  $40.6\text{W/m}^2$  in 1997 (refer to open area). These values are twice the area-weighted values. This implies that the turbulent heat flux is restrained by half due to sea ice area.

#### *ECMWF data*

So far we have discussed the heat budgets during our observation period. To examine whether our results hold for other periods, ECMWF twice daily grid data (near hokkaido

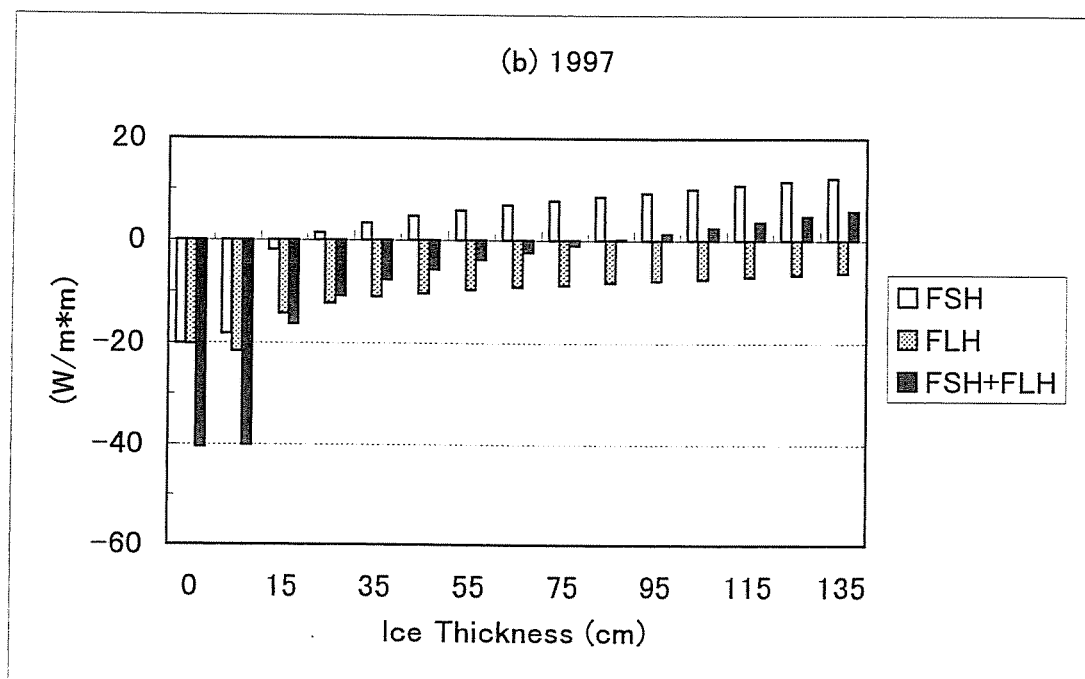
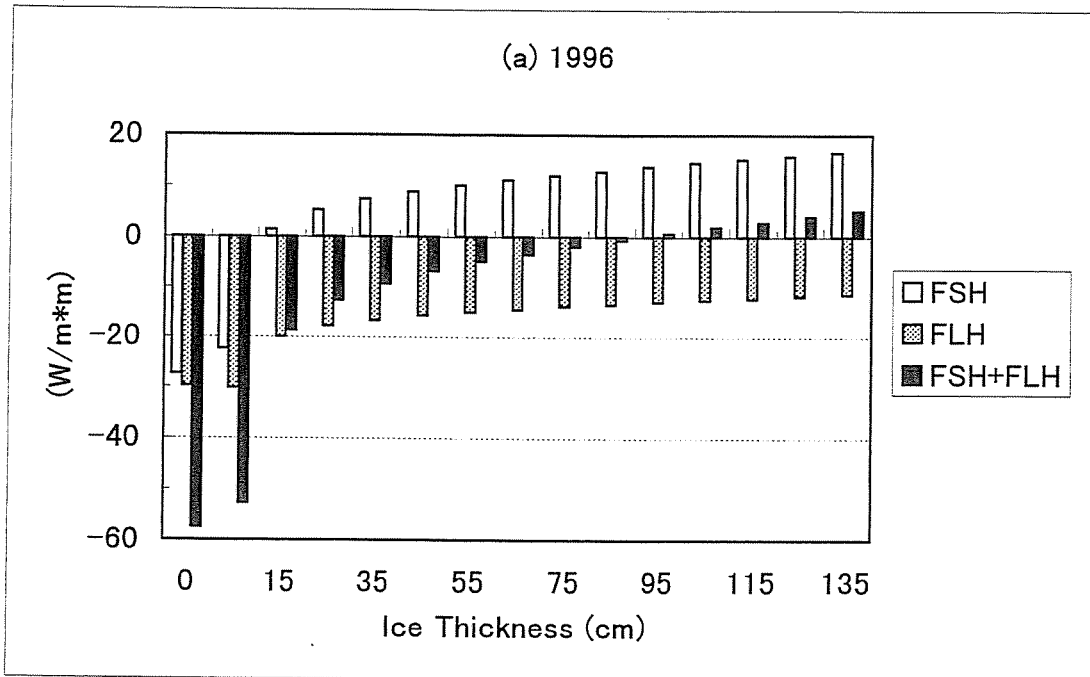


Figure 4.3.2 Turbulent heat flux as a function of ice thickness.

(a) 1996      (b) 1997

FSH: sensible heat flux      FLH: latent heat flux

Positive FSH means that the surface temperature of sea ice is greater than that of air temperature.

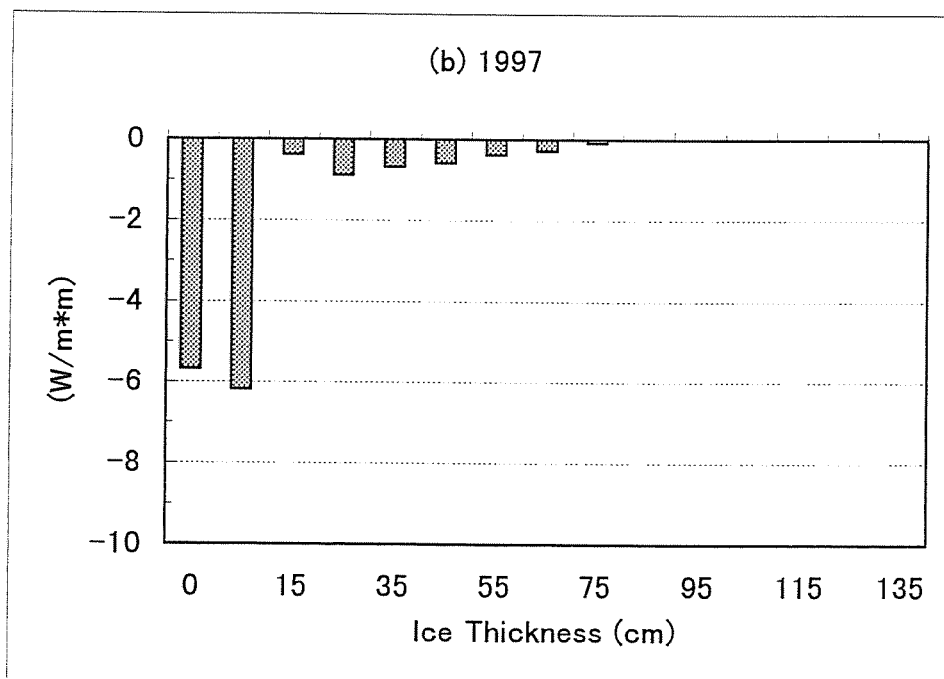
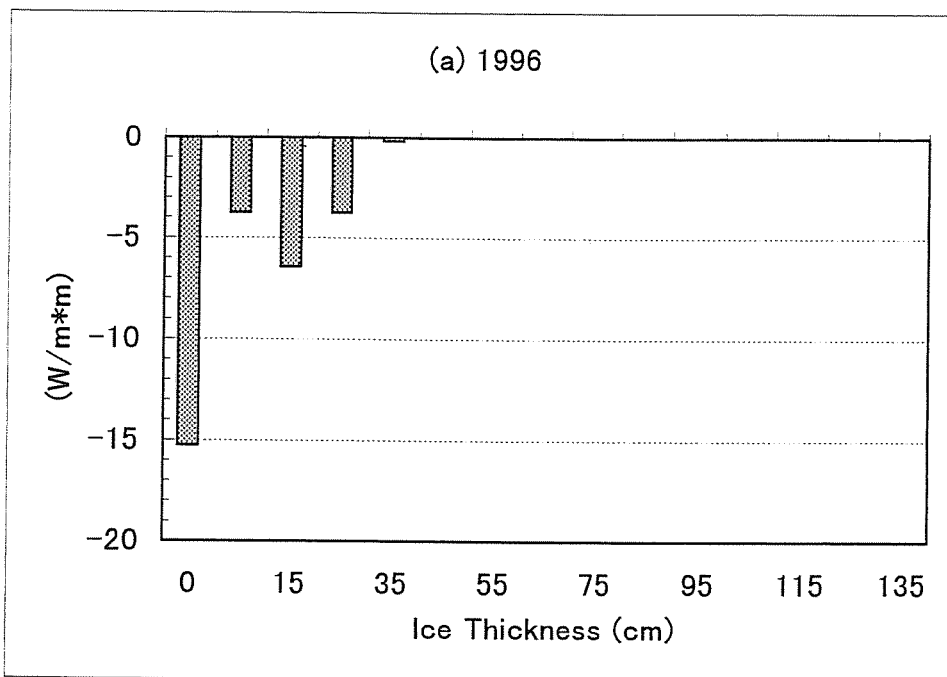


Figure 4.3.3 Area averaged turbulent heat flux (FSH+FLH).

(a) 1996      (b) 1997

coast,  $45.0^{\circ}N, 142.5^{\circ}E$ ) are also examined assuming the same ice conditions. The method of calculation is same as the above except that heat transfer coefficient is taken to be slightly larger values of  $1.40 * 10^{-3}$  (Persson *et al.*, 1997), taking it into account that wind speed height is 10 m in ECMWF data. The daily averaged air temperature, wind speed, and dew point temperature are used. The cloud amount is assumed to be 0.7 here on the basis of our observation. As for daily solar radiation ( $Q_s$ ), the following formula developed for the ocean adjacent to Japan by Kim (1992) is applied here.

$$I_0 = A_0 + A_1 \cos \phi + B_1 \sin \phi + A_2 \cos 2\phi + B_2 \sin 2\phi$$

$$Q_{s0} = I_0(0.865 - 0.5C^2)(1 - \alpha_s)$$

, where  $\phi$  is equal to  $(t-21) * \frac{2\pi}{365}$  (t: Julian Day), C is cloud amount, and  $\alpha$  is albedo at the ocean surface (0.07). In actual calculation,  $[1.325 * Q_{s0} - 7.2697]$  is used as incident solar radiation from the regression between the above formula and the observation at the meteorological observatories of Hokkaido coast (Wakkanai, Kitami-esashi, Abashiri, Nemuro).

The result of ice growth rate is shown in Figure 4.3.4. The mean ice growth rates for our observation period are estimated as 0.13 cm/day in 1996 and -0.09 cm/day in 1997. Although somewhat underestimated compared with those obtained from our observation, it is shown in Figure 4.3.4 that ice growth is as small in February and March of both years as that during observation period. In January, the ice growth rate occasionally becomes somewhat larger due to lower air temperature. However, this region was not covered with sea ice yet at this time. Therefore, it can be said that ice growth is small for almost all the ice covering periods.

The result of the daily turbulent heat flux is shown in Figure 4.3.5. The averaged values for our observation period are estimated as  $-25.1W/m^2$  in 1996 and  $-18.2W/m^2$  in 1997. These values are nearly the same as those estimated from our observational data. Figure 4.3.5 indicates that the turbulent heat flux is upward for almost all the

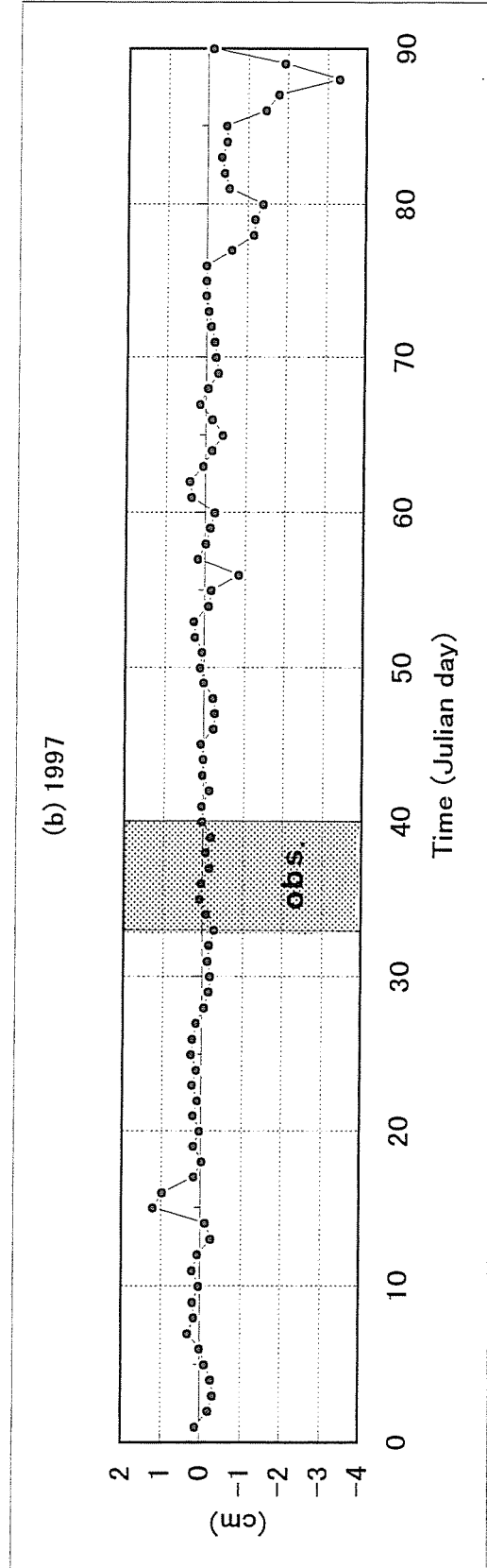
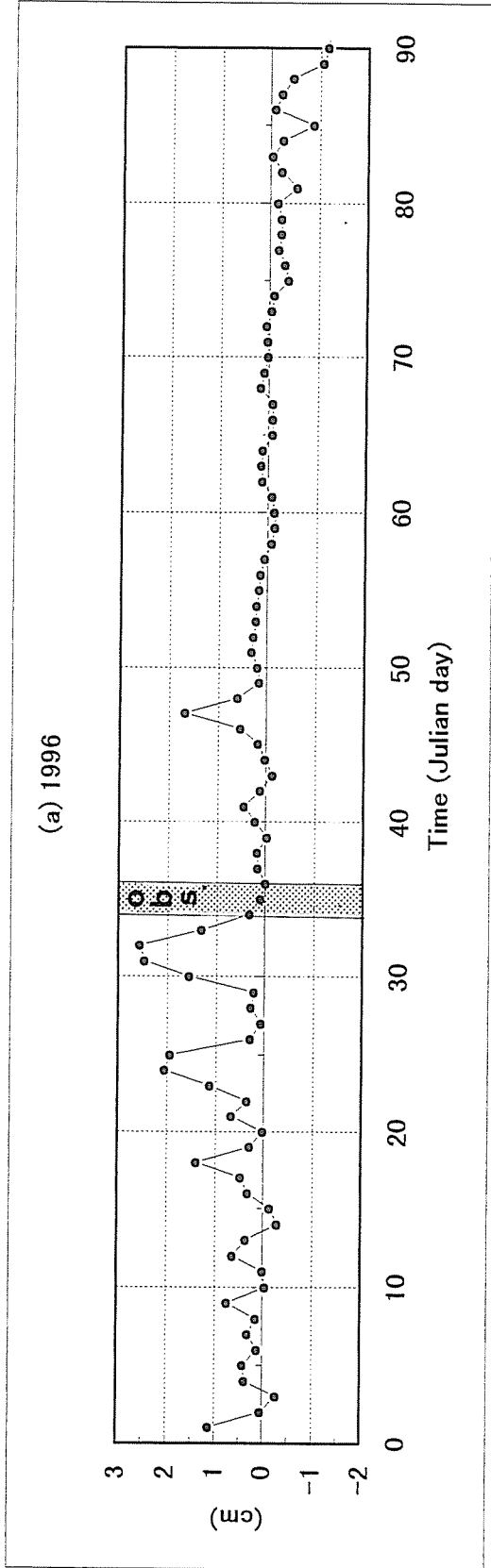


Figure 4.3.4 Ice growth amount per day estimated from ECMWF data.

Grid point:  $45.0^{\circ}N$   $142.5^{\circ}E$

(a) 1996      (b) 1997

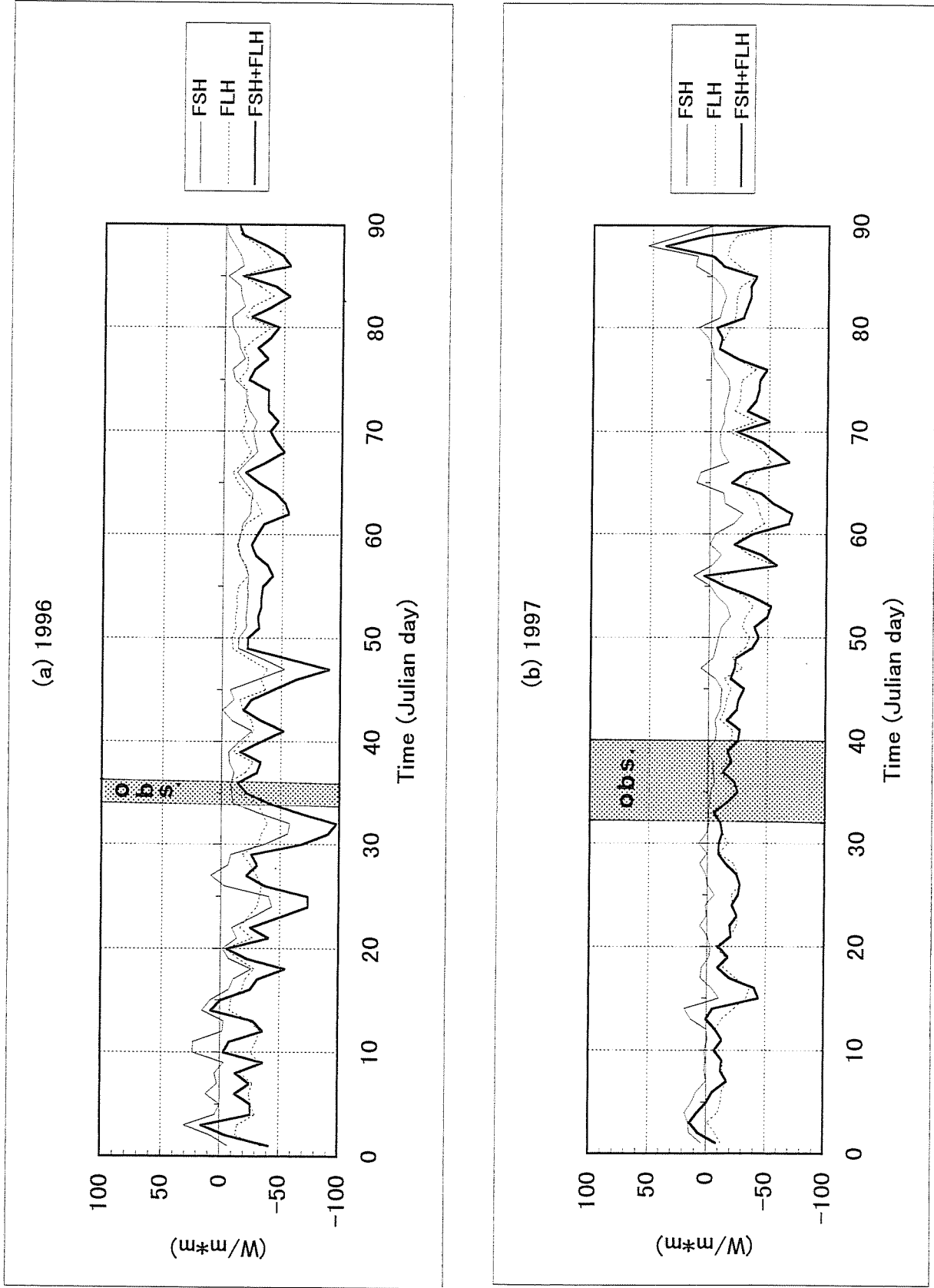


Figure 4.3.5 Turbulent heat flux estimated from ECMWF data.

Grid point: 45.0°N 142.5°E

(a) 1996 (b) 1997



period. The values of flux are eliminated by two thirds to a half compared with those without sea ice (not shown) and hence it is shown that the results obtained from our observational data hold also for other periods. Relatively large fluxes found in early March 1997 is caused by low air temperature ( $-10^{\circ}\text{C}$ ). The reason why larger ice growth is not estimated during this period is attributed to increased solar radiation. After all, it is confirmed that the result estimated from our observational data approximately holds for the entire ice covering periods in this region.

### *Diurnal cycle*

The brief characteristics of heat budget in this region was grasped from the daily-averaged meteorological data. Here we further examine its diurnal cycle from hourly meteorological data in 1997 (see Figure 4.2.1b). The method of calculation is the same as that for the case of *Daily mean*. Again, we assume that the left term of equation (1) ( $\partial T_s/\partial t$ ) is negligible.

First, we pay attention to thin nilas which initially forms over open water because the formation of new ice is particularly important for heat exchange with atmosphere and ocean structure. In calculation, surface albedo is given as the following formula:  $\alpha = -2 * 10^{-6} H_i^3 + 4 * 10^{-4} H_i^2 + 0.0205 H_i + 0.0685$ , which is derived from the observational data of *Allison et al. (1993)*. Melting is supposed to occur when calculated surface temperature exceeds melting point ( $0^{\circ}\text{C}$ ). In that case, melting amount is calculated as  $FQ/(\rho_i * L_f)$ . Ice growth is predicted as a time evolution problem of 1 hour time step using the hourly data (Figure 4.2.1b).

The result is shown in Figure 4.3.6a. This figure shows that sea ice forms at the sunset, grows up to about 1.5 cm until early morning, and then melts away rapidly due to solar radiation. This maximum thickness is in agreement with the observed value during our cruise, and the diurnal cycle of estimated heat budget (not shown) is in good agreement with the detailed observational result over Lake Saroma by *Ishikawa*

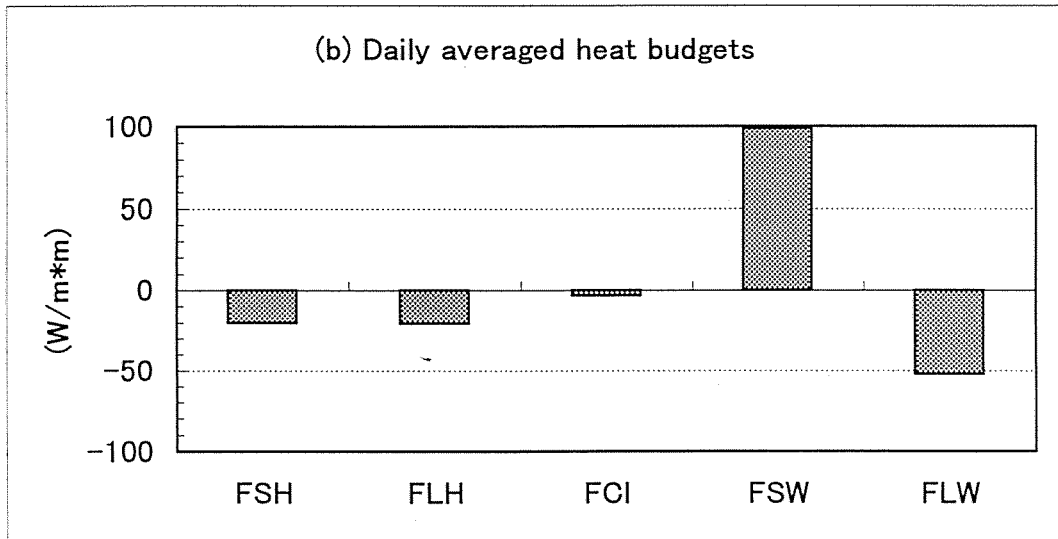
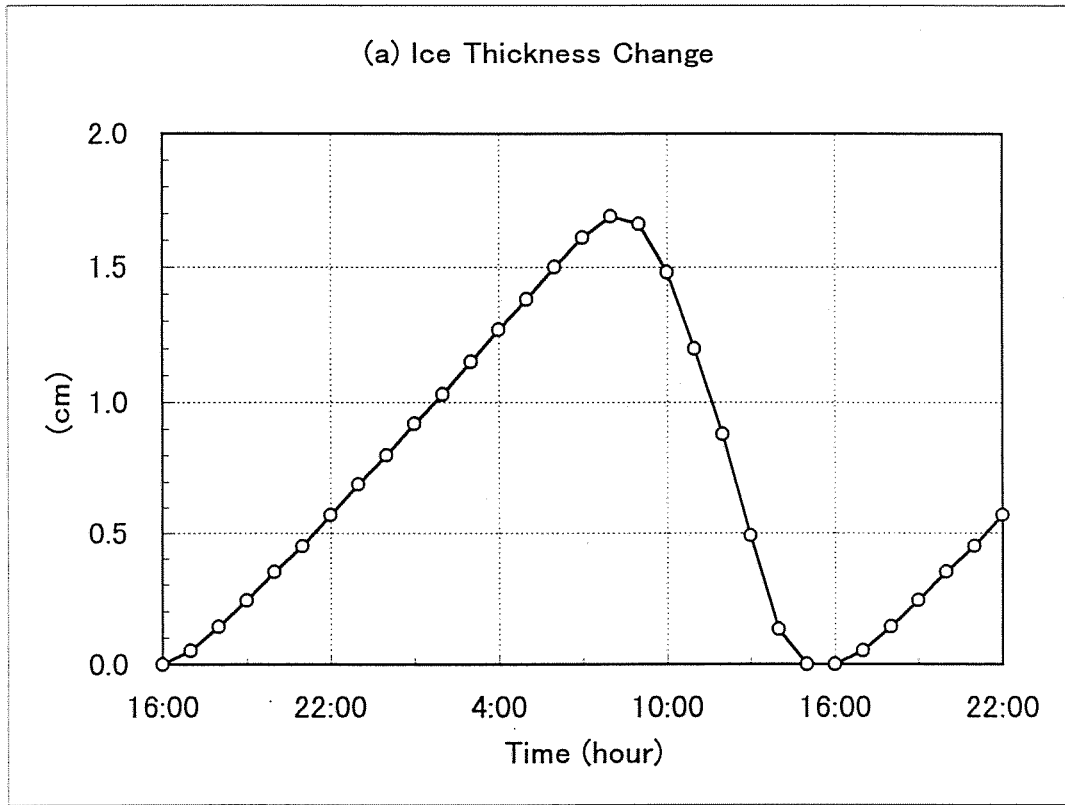


Figure 4.3.6 Results of heat budget for open water calculated from diurnal variation of meteorological data.  
 (a) Ice thickness      (b) Daily averaged heat budget

and Kobayashi (1984). Both results show that freezing occurs at night time when net radiation, sensible and latent heat fluxes are all outgoing sense. This result indicates that solar radiation is a leading factor for ice growth in this region. This fact is also clearly shown by the heat budget components in Figure 4.3.6b, where incident solar radiation is particularly prominent. What draws our interest in Figure 4.3.6a is that the iteration of ice formation and melting may possibly produce less saline water at the surface. In some nilas samples, we could find out the ice structure which may suggest this phenomenon. The details will be discussed in Chapter 5 and 6.

These results also hold when calculation is started from 5cm- and 10cm- thick ice. After one day cycle calculation, 5cm-thick ice grow up to 6.3 cm thick by early morning and decrease to 3.6 cm thick before the sunset. For 10cm-thick ice, it grows up to 11.1 cm thick and decreases to 8.7 cm thick before the sunset. In both cases, incident solar radiation plays a role of the leading factor.

Next we examine heat budget over the entire area. The method of calculation is same as that used for daily mean calculation except that hourly data (Figure 4.2.1b) is used. We did not take the ice thickness change into account here because the treatment of the surface melting process is not easy and the purpose here is to examine the effect of the meteorological diurnal cycle on heat budget. Here heat budget is calculated with the same ice conditions. When the surface temperature ( $T_S$ ) is calculated as more than melting point ( $0^\circ C$ ),  $0^\circ C$  is substituted to  $T_S$  and the residual heat flux ( $FQ = FSH + FLH + FCI + FSW + FLW$ ) is calculated.  $FQ$  is used to melt ice or snow.

The result is presented in Figure 4.3.7a-c. It is shown from Figure 4.3.7a that the emitted long wave radiation is balanced by the sensible heat flux and conductive heat flux at night time, resulting in the ice growth of 1.2 cm/day. The result that the turbulent heat flux is downward implies that sea ice area works as a cooling at night time. On the other hand, Figure 4.3.7b shows that the solar radiation is predominant and causes the surface melting at daytime. When averaged during one day, the effect of solar radiation remains

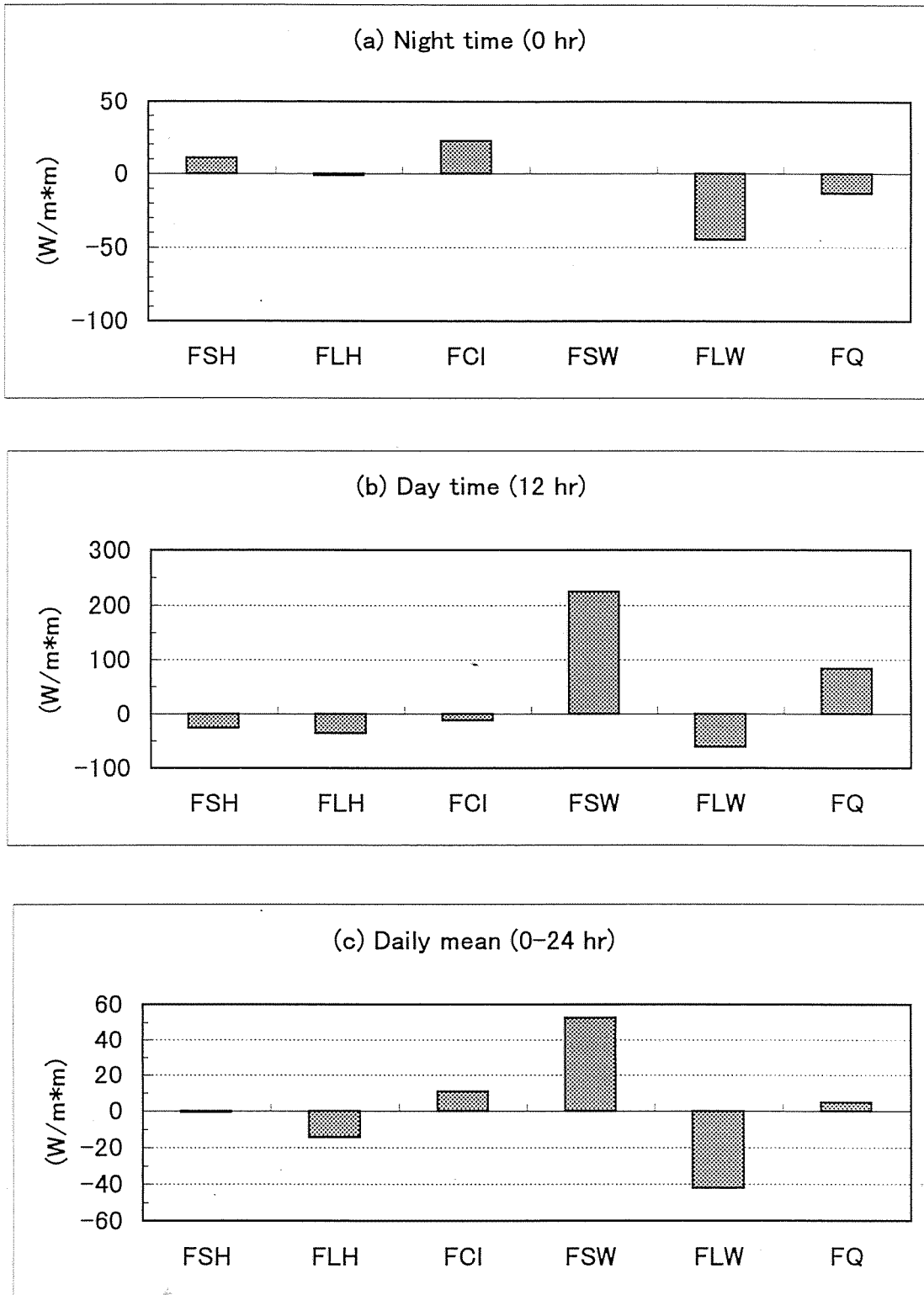


Figure 4.3.7 Diurnal change of heat budget over the entire sea ice area.  
 (a) at nighttime (0 hour) (b) at daytime (noon) (c) daily mean  
 Note that (c) is similar to Fig.4.3.1b.

prominent (see Figure 4.3.7c), so that ice growth rate becomes small (0.4 cm/day) and sea ice area functions as heating source on average. The daily averaged profile (Figure 4.3.7c) is almost same as Figure 4.3.1b.

The additional noticeable thing is that surface melting occurs at daytime. This suggests that flushing events, which mainly promote desalination of ice in the polar regions in spring, may occur in this region. Actually, we could obtain some evidence about this in bulk ice salinity. The ice salinity of our samples showed closer values to that of multi-year ice rather than that of first-year ice in the polar regions. The details will be discussed in Chapter 5.

#### 4.4 Summary and Discussions

In order to examine the thermodynamical characteristics of sea ice in the southern region of the Okhotsk Sea, we estimated the heat budget and the ice growth rate using the bulk method on the basis of our ice and meteorological observation. The results show (1) that the averaged ice growth rate is limited to below 0.5 cm/day due to melting by solar radiation, (2) that sea ice area eliminates the turbulent heat flux about by half, and (3) that more than half of the total turbulent heat flux is owed to open water and nilas area.

In the first result, the actual ice growth rate may be further lower because ocean heat flux was not included in this calculation. *Ishikawa and Kobayashi (1984)* estimated the ocean heat flux in Lake Saroma (salinity is 31 psu) in early February as 10 to 30  $W/m^2$ . *Wettlaufer (1991)* estimated the ice-ocean heat flux in the Fram Strait in a fall season as 0 to 37  $W/m^{-1}$ . If these values are applied to our area, ocean heat flux is balanced by the estimated conductive heat flux and ice growth becomes substantially negligible.

The second result suggests that sea ice area warms the northwesterly cold air gradually. This is a different feature from that of the polar regions where thick ice (*geq* 1 m) is predominant. From the analysis of heat flux over individual ice thickness, it was shown

that thinner ice thickness is responsible for this result. This result is in contradiction to that of *Okubo and Mannoji (1994)*. They showed using the JMA operational model that the sensible heat flux is downward over sea ice extent. We consider that this discrepancy is attributed to the treatment of sea ice area in the model, in which ice concentration is assumed to be 1.0.

On the other hand, the third result is similar to that of the polar regions in that thin ice area has an important role in exchanging heat between ocean and atmosphere. However, the estimated value ( $40 \sim 60W/m^2$ ) is much smaller than that over lead in winter in the polar regions (e.g.  $120W/m^2$  (Allison, 1982),  $130W/m^2$  (Ruffieux et al., 1995),  $189W/m^2$  (Weller, 1980),  $115W/m^2$  (sensible heat flux; Walter et al., 1995)). This much smaller values are considered to be due to relatively higher air temperature than in the polar regions. Thus the heat exchange over thin ice area seems not so drastic as in the polar regions.

From these results, the sea ice in the southern region of the Okhotsk Sea can be characterized as follows:

- (1) Thermodynamical ice growth cannot be expected so much.
- (2) Thin ice and open area contributes much to the turbulent heat flux similarly to the polar regions.
- (3) Since relatively thin ice area is dominant, the area-weighted heat flux becomes upward and sea ice area works as a heating source than a cooling source.

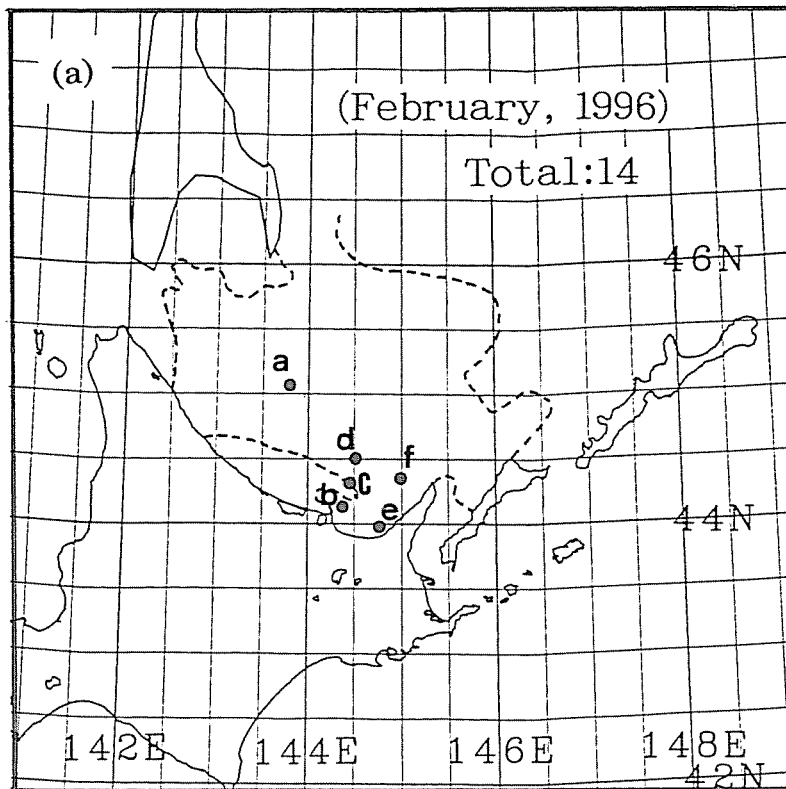
In the next chapter, we will examine how these thermodynamical characteristics influence the ice growth processes through the structural analysis of sea ice samples.

## Chapter 5. Ice Sample Analysis

### 5.1 Introduction

It is still unknown where and how sea ice in the southern region of the Okhotsk Sea forms and grows because of the lack of the analysis of in-situ ice samples. In order to approach this matter, we obtained sea ice samples during the cruises in 1996 and 1997 and investigated their structural characteristics. Since the analysis of in-situ ice samples in marginal ice zones is insufficient not only in the Okhotsk Sea, but also in other polar regions except for the Antarctic Ocean, we believe that our observation serves to understand the characteristics of sea ice in marginal ice zones. Our purpose in this chapter is to show the characteristics of sea ice through the structural analysis of ice samples in connection with the heat budget characteristics in this region which is discussed in the previous chapter. For this purpose, we analyzed thick/thin section, salinity, and density profiles. Here we will present the results of analysis especially from the viewpoint of growth processes.

The total number of ice samples are 14 and 35 in 1996 and 1997, respectively. The 14 ice samples of 1996 consist of one first-year ice, six young ices, three pancake ices, two nilases, and two slushes. The 35 ice samples consist of four first-year ices, nine young ices, seven pancake ices, 10 nilases, two rotten ices, and three brash ices. The sampling locations are shown in Figure 5.1.1a-b. As for the ice samples of 1997, the locations of four types of sea ice are plotted individually in Figure 5.1.2a-d. The brief features of each ice sample are listed in Table 5.1.1. As was shown in Chapter 2, thin ice was predominant in the southern part of the Okhotsk Sea in 1996, while relatively thick ice was remarkable in 1997. Accordingly, the ice samples of 1997 are thicker as a whole than those of 1996. The maximum thickness amounted to 75 cm.



- a: P1
- b: S1
- c: Y1
- d: Y2
- e: Y3-4, F1, N1-2
- f: P2-3, Y5-6

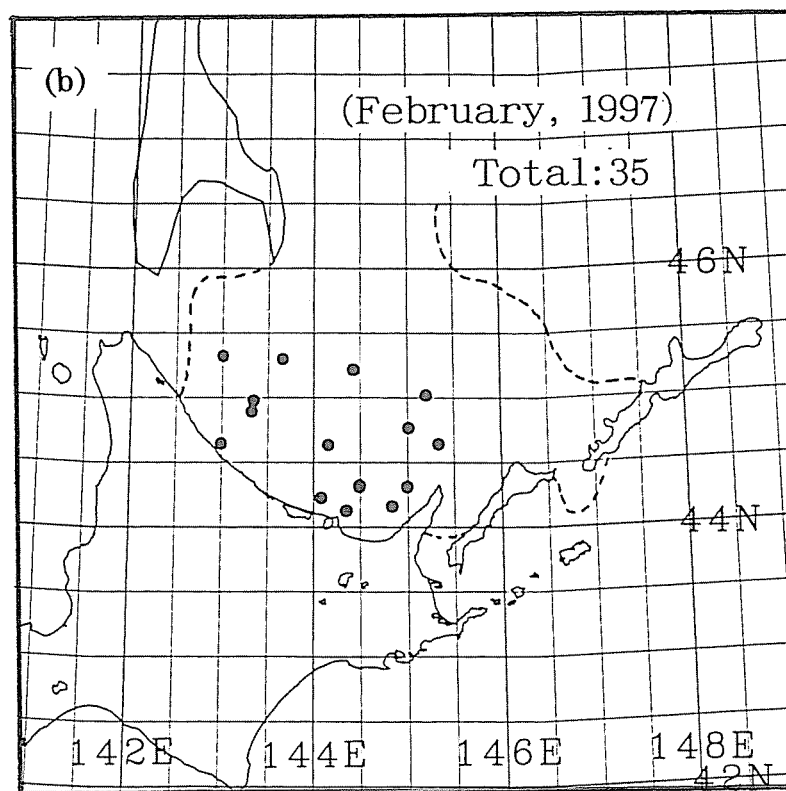


Figure 5.1.1 Sampling locations in (a) 1996 and (b) 1997.

Broken lines denote ice edges.

Notation :

F(first-year ice), Y(young ice), P(pancake ice), N(nilas), S(slush)



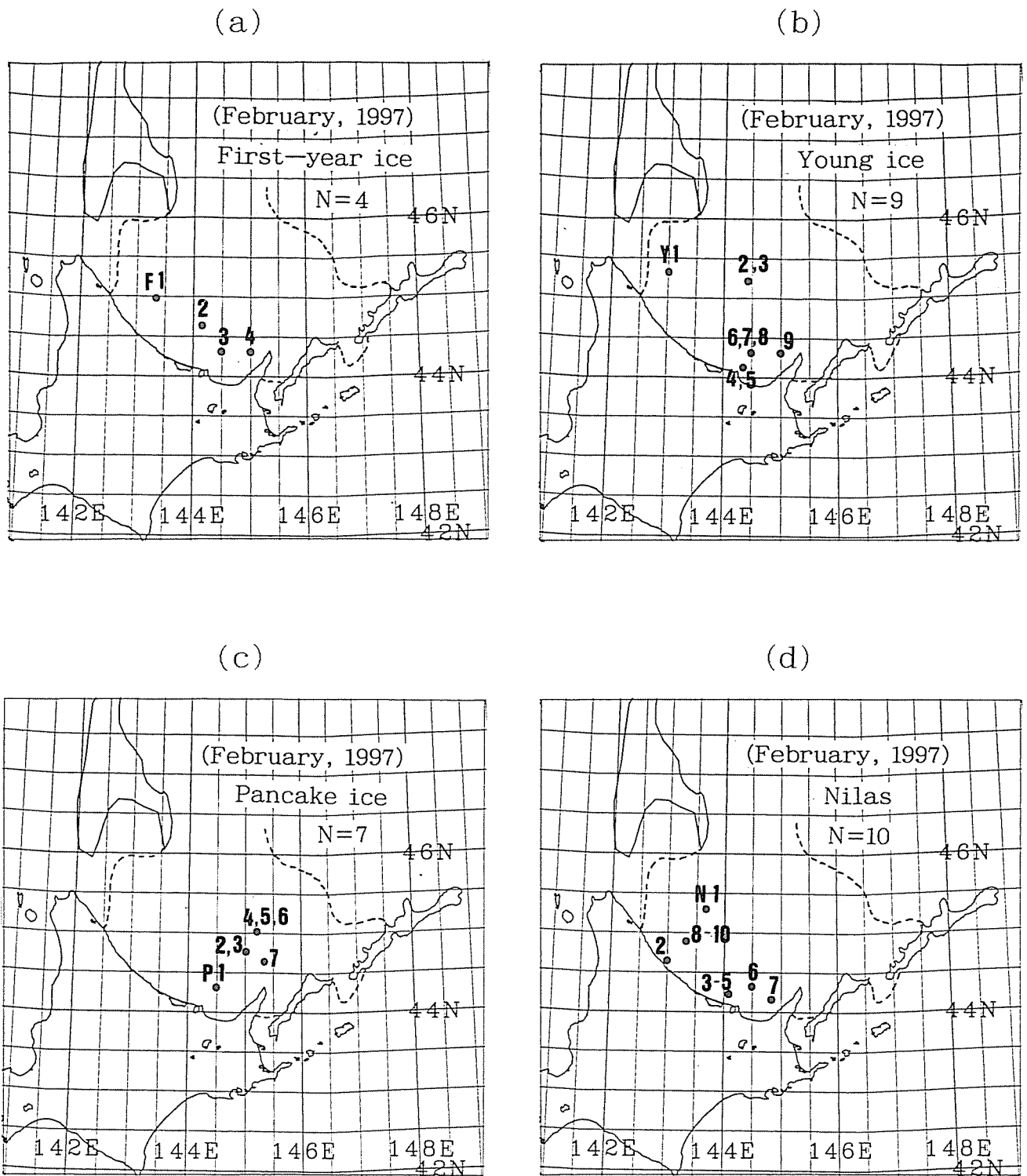


Figure 5.1.2 Sampling locations for

(a) First-year ice, (b) Young ice, (c) Pancake ice, and (d) Nilas.

Broken lines denote ice edges.

**Table 5.1.1 Ice sample data.**

F(First-year ice), Y(Young ice), P(Pancake ice)  
 N(Nilas), S(Slush), B(Brash ice), R(Rotten ice)

1996

sample no.	date	time	Hi(cm)	S(psu)	D(kg/m <sup>3</sup> )
F1	2/5	07:30	32	4.4	813
Y1	2/4	12:00	26	3.3	801
Y2	2/4	16:30	18	4.1	801
Y3	2/4	07:30	21	5.4	865
Y4	2/5	07:30	22	4.4	827
Y5	2/5	14:30	17	2.9	849
Y6	2/5	14:30	15	4.6	843
P1	2/3	09:00	11	8.2	876
P2	2/5	14:30	15	6.2	883
P3	2/5	14:30	13	6.0	821
N1	2/5	09:55	1	12.5	881
N2	2/5	09:55	1	12.5	840
S1	2/4	07:30	5	11.6	688
S2	2/4	12:00	8	2.8	589

Hi: Ice thickness      S: Bulk ice salinity      D: Bulk ice density  
 See Figure 5.1.1 for location.

(definition)

**First-year ice:** Sea ice of not more than one winter's growth, developing from *young ice*; thickness 30cm ~ 2m.

**Young ice:** Ice in the transition stage between *nilas* and *first-year ice*, 10 ~ 30cm in thickness.

**Pancake ice:** Predominantly circular pieces of ice from 30cm ~ 3m in diameter, and up to about 10 cm in thickness, with raised rims due to the pieces striking against one another.

**Rotten ice:** Sea ice which has become honeycombed and which is in an advanced state of disintegration.

**Brash ice:** Accumulations of *floating ice* made up of fragments not more than 2 m across, the wreckage of other forms of ice.

**Slush:** Snow which is saturated and mixed with water on land or ice surface, or as a viscous floating mass in water after a heavy snowfall.

(from WMO, 1970)

**Table 5.1.1** (Continued.)

1997

sample no.	date	time	Hi(cm)	S(psu)	D(kg/m <sup>3</sup> )
F1	2/3	08:00	75	3.4	827
F2	2/5	08:00	55	2.9	885
F3	2/6	15:00	37	3.5	851
F4	2/8	12:45	40	3.0	832
Y1	2/2	13:00	21	4.4	866
Y2	2/4	11:10	26	3.3	833
Y3	2/4	11:10	17	3.6	852
Y4	2/6	12:00	17	4.9	907
Y5	2/6	12:00	12	4.8	905
Y6	2/6	15:00	25	3.4	860
Y7	2/6	15:00	25	3.6	851
Y8	2/6	15:00	21	3.1	842
Y9	2/8	12:45	17	3.5	829
P1	2/6	15:00	6	9.6	834
P2	2/7	07:45	5	8.3	897
P3	2/7	07:45	8	7.8	831
P4	2/7	10:00	2.5	8.1	926
P5	2/7	10:00	1.2	9.1	834
P6	2/7	10:00	2	7.2	865
P7	2/8	08:00	6	7.5	895
N1	2/2	17:00	0.7	7.4	-
N2	2/3	10:50	0.8	7.7	857
N3	2/6	10:15	1.0	8.7	930
N4	2/6	10:15	1.1	9.0	861
N5	2/6	10:15	1.1	8.1	887
N6	2/6	16:10	4	9.1	922
N7	2/8	15:45	1.2	9.7	-
N8	2/9	13:40	3.8	8.3	-
N9	2/9	13:40	2	8.3	-
N10	2/9	13:40	1	9.7	-
R1	2/6	15:00	10	3.1	870
R2	2/6	15:00	8	3.9	916
B1	2/6	12:00	8	5.7	926
B2	2/8	13:00	8	5.0	904
B3	2/8	15:45	11	5.8	894

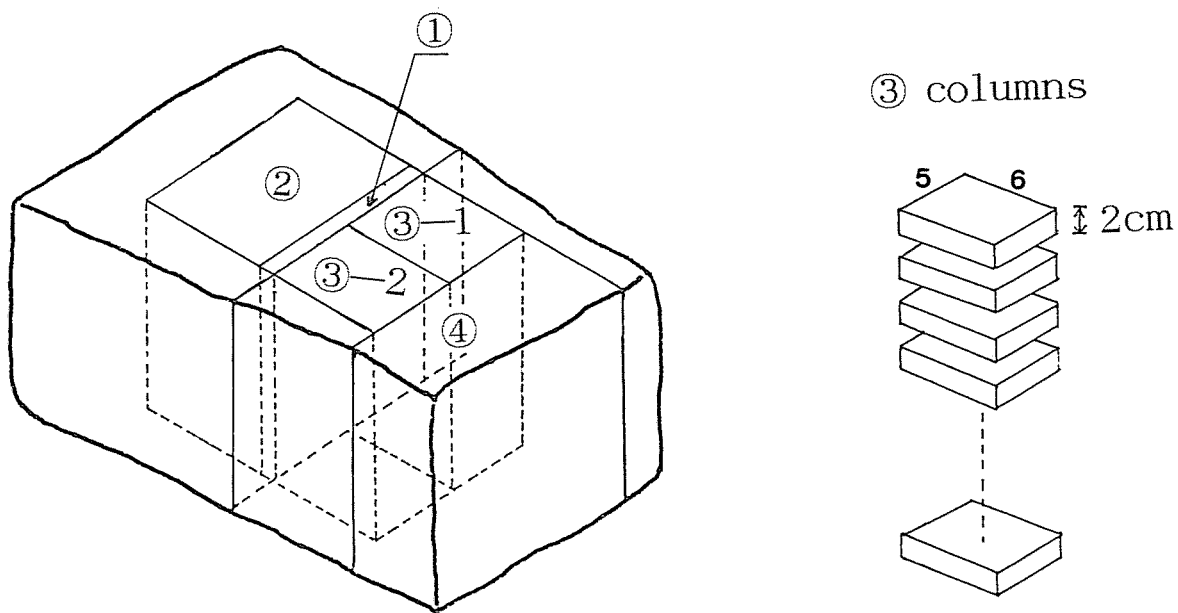
See Figure 5.1.2 for location.

## 5.2 Method of Analysis

The typical procedure of sample analysis is depicted in Figure 5.2.1. First we cut vertically the ice sample in two pieces. One is used for the analysis of salinity and density, while the other is for thin section analysis. Then vertical thin section is made to investigate the vertical structure on the cut face. On the basis of this vertical structure, we made horizontal thin sections of characteristic layers to observe the horizontal distribution of crystal grains. On the other hand, we divided the two columns (Figure 5.2.1) into 2 cm thick pieces to investigate the vertical profiles of salinity and density. The bulk salinity and density were obtained by averaging them vertically.

In thin section analysis, we first sliced off a sheet of about 1 cm thick from an ice sample using a band-saw and planed the surface of one side smooth to stick it on a glass plate. Then we made a thick section of 5 mm thickness by planing off another side of the ice sheet to examine the inclusions like gas and brine pockets in ice samples. For this purpose, we took two kinds of photographs. One is taken for reflected light with the thin section overlaying a piece of a black cloth to examine the light scattered by inclusions (referred to as a scatter photo here). The other is taken for transmitted light with the light source positioned below the thin section to examine opacity of light by inclusions (referred to as a through photo here). After taking these photographs, we again planed off the thin section to about 0.5 mm thick until we can recognize the crystallographic structure of the ice sample. We put this thinly planed section between two polarizing sheets and took a photograph (referred to as a polarized photo here).

From the vertical thin section, we determined the interface between snow and ice, if possible, and cut the columns into pieces of 2 cm thickness from their interface. We planed and polished the facets of each piece carefully so that it took a rectangular shape. Then we calculated the volume by measuring the dimensions (depth, width, and height) of each piece by a caliper with 0.01 mm unit and measured the weight with 0.01 g unit. The density was obtained by dividing weight by volume. After melting each piece at a



- ①: vertical thick/thin section
- ②: horizontal thick/thin section
- ③: columns for salinity and density profile
- ④: archive

Figure 5.2.1 Schematic picture of ice sample analysis.

room temperature (about  $20^{\circ}\text{C}$ ), the salinity was measured with a salt analyzer (TOA Electronics Ltd., SAT-210 type). The remainder of the melted ice is now stocked for the  $\delta^{18}\text{O}$  analysis.

Some pieces were deteriorated and distorted especially at the uppermost and the bottom layers. In such cases, we omitted the data in examining the vertical profiles and bulk salinity and density. In our method of estimating density, even the measuring error by 1 mm would cause as much as 9% error for a piece of standard size (5 cm \* 6 cm \* 2 cm). However, we do not feel that measurement errors are crucial because the estimated ice density shows a systematic vertical profile in many cases.

### **5.3 Results**

#### *5.3.1 General characteristics*

First we will describe the general characteristics concerning salinity and density of sea ice. The bulk salinity is shown as a function of ice thickness (see Figure 5.3.1a). We can find from this figure that ice salinity depends strongly on ice thickness although there is an appreciable amount of scatter at thinner ice thickness. Salinity decreases rapidly from about 10 to about 4 psu with the increase of ice thickness up to 20 cm, while it becomes nearly constant for ice thickness more than 20 cm. This result is in agreement with the observation for first-year ice in the polar regions compiled by *Cox and Weeks(1974)* in that the slope of the salinity decreases significantly at a critical ice thickness. However, this critical ice thickness, which is about 40 cm in the polar regions, is somewhat thinner in our case (20 cm) and the ice salinity is lower by 3 to 4 psu compared with their data as a whole. Considering the fact reported by *Cox and Weeks (1974)* that sea ice salinity decreases much to about 2 psu in melting season, this discrepancy may be attributed to melting conditions in the southern region of the Okhotsk Sea.

Sea ice in this region is subject to melting as indicated by heat budget calculation in the previous chapter. This implies that such a process as flushing caused by surface

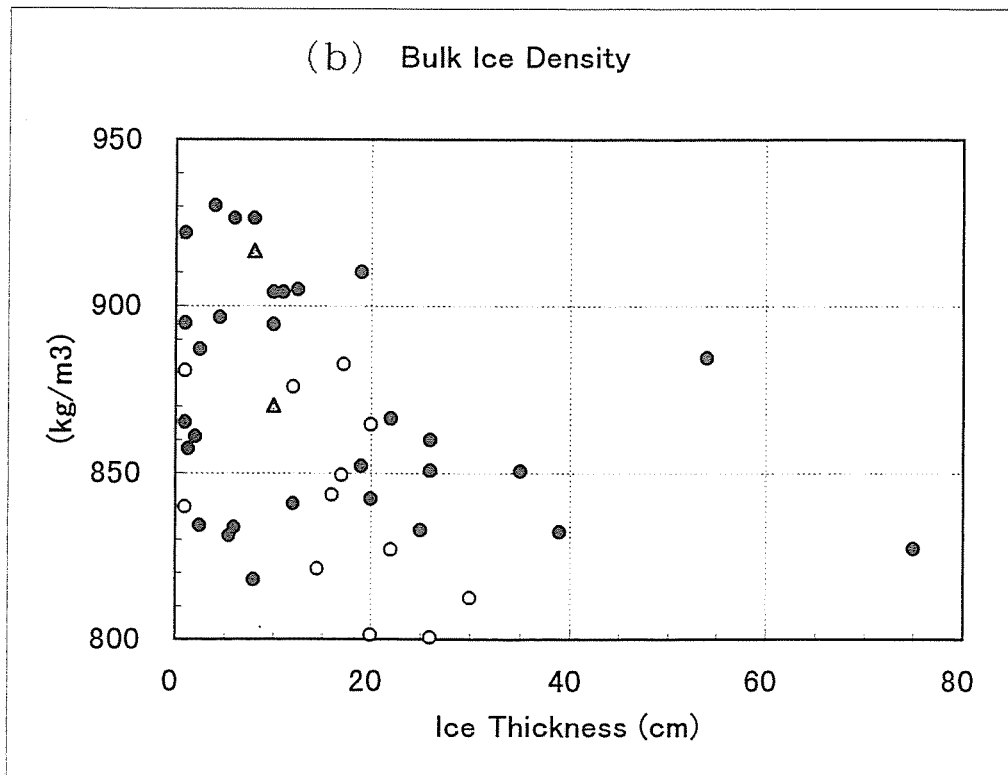
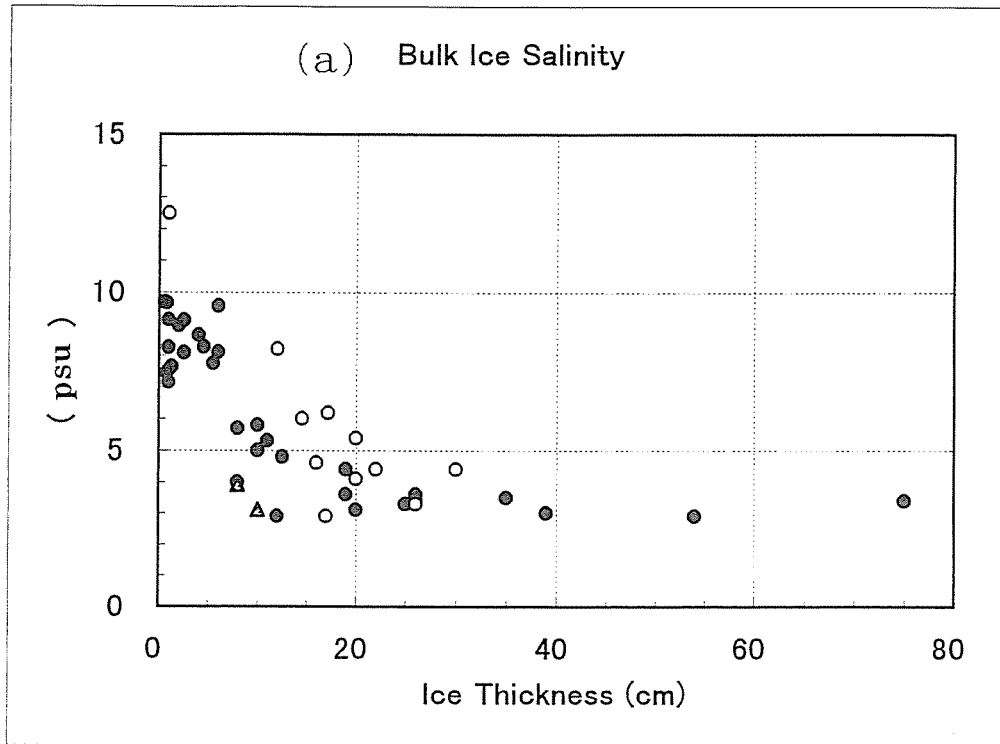


Figure 5.3.1 Bulk features of sampled ice as a function of ice thickness.

(a) Salinity

(b) Density

○ : 1996

● : 1997

△ : rotten ice (1997)

melting, which effectively promotes desalination of sea ice in melting season in the polar regions, can affect sea ice salinity even in mid winter in this region. This melting effect can be recognized in vertical salinity profiles. In many cases, especially young ice, it is found that ice salinity increases with ice depths as a whole. This profile is more similar to that of multi-year ice (*Gow et al., 1987*) than that of first-year ice (*Nakawo and Sinha, 1981*). The typical profiles are shown with polarized photos of vertical thin section in Figure 5.3.2. In Figure 5.3.2(upper), local salinity maximum is found at 5 cm depth near the interface between snow and ice. We consider that this high salinity is attributed to flooding events (percolation of sea water between snow and ice) rather than the effect of the surface brine found in typical first-year ice. Thus these figures show that the structure is rather similar to that of multi-year ice. In addition, the importance of melting effects is suggested by the fact that two rotten ice samples, indicating that melting had clearly occurred, showed lower salinity compared with that of the other ice of same thickness (see Figure 5.3.1a).

Besides, It is suggested by *Crocker and Wadhams (1989)* that relatively high temperature (above about  $-8^{\circ}C$ ) makes brine channels permeable. This suggestion implies that desalination is more promoted for high temperature. In addition, it is known that initial salt entrapment at freezing decreases for slower growth rate (*Wakatsuchi and Ono, 1983*). Considering all these effects, somewhat lower ice salinity even in freezing season may be also one of the features of sea ice in relatively low latitude.

The bulk ice density is also shown as a function of ice thickness as in Figure 5.3.1b. (Here slush samples are excluded because formation process is definitely different from other sea ice.) Bulk ice density ranges from 800 to 930  $kg/m^3$  with remarkable variation. There is no strong correlation between ice thickness and density though weak decreasing trend with ice thickness is detected. The averaged density is  $864 \pm 35 kg/m^3$ , which is somewhat lower than that of typical first-year ice in the polar region. For example, *Tucker et al.(1991)* showed from the observation in the Fram Strait that the density



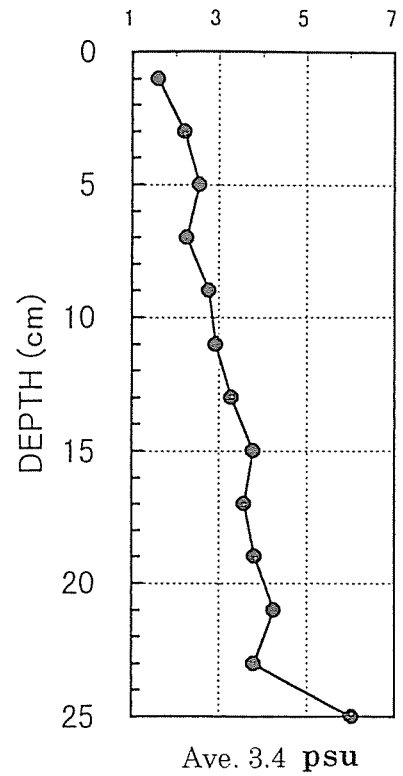
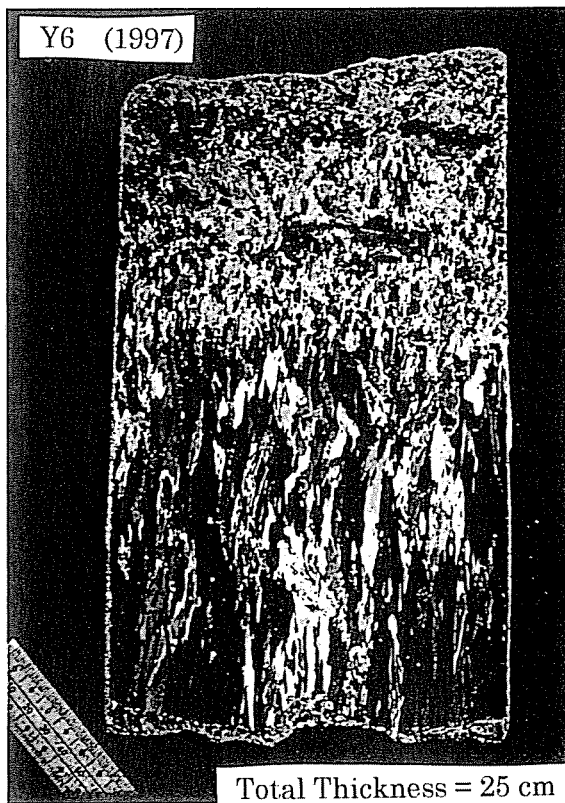
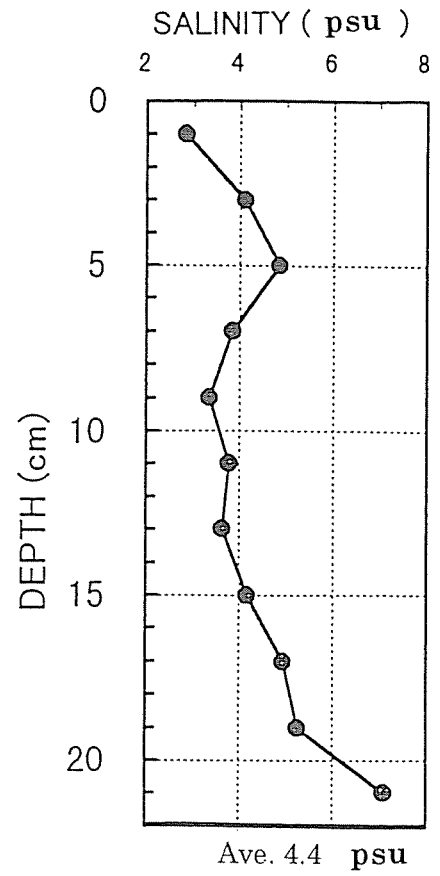
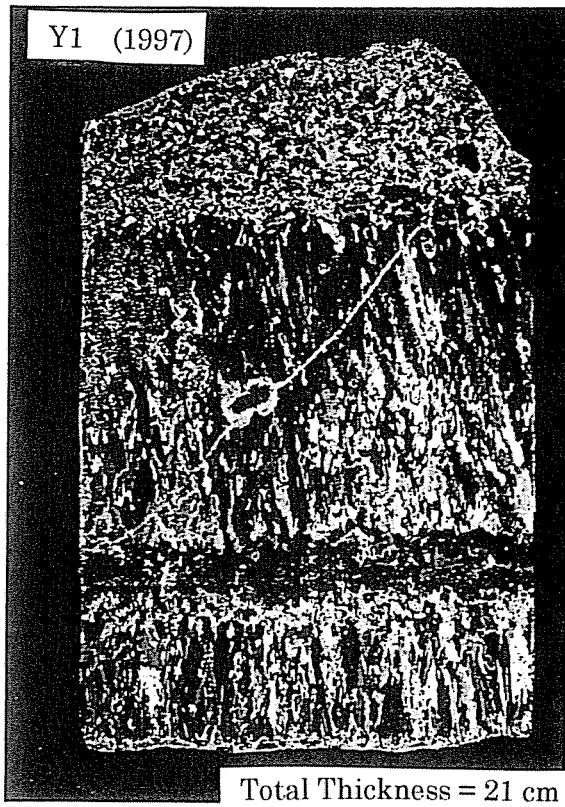


Figure 5.3.2 Salinity and structure profile of young ice.

Note that salinity decreases with ice depth.

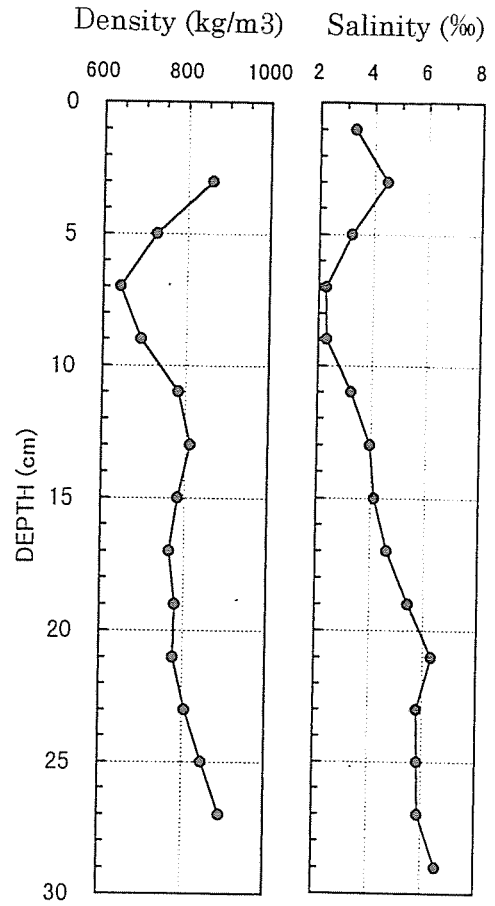
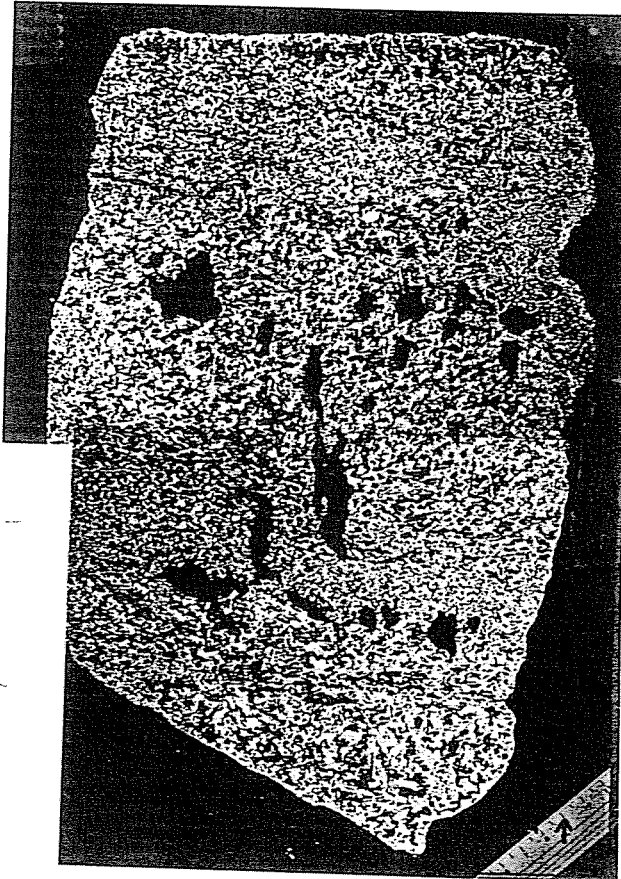
of nilas, pancake ice, and first-year ice is all  $920\text{kg}/\text{m}^3$  and *Perovich and Gow (1996)* showed that the density of first-year ice of the Beaufort Sea is from 900 to  $930\text{ kg}/\text{m}^3$ . Our result is rather closer to that of multi-year ice (e.g.  $887 \pm 20\text{kg}/\text{m}^3$  by *Eicken et al.(1995)*). Somewhat lower density of our ice samples indicates higher gas contents in ice. According to *Tsurikov (1979)*, the main contributions to the gas content of sea ice is the release of gases from the water when freezing and the generation of pores in ice due to melting. Since the first one makes little difference between the Okhotsk Sea and polar regions, the melting effect of the second one seems important. Melted water along brine pockets drains from sea ice and may lower the ice density. We consider that is why the density of our samples are closer to that of multi-year ice which have experienced melting. If it is true, somewhat lower density maybe also one of the sea ice in this region.

In the following section, we will show the results of the detailed analysis of individual ice types, focusing on the structural characteristics.

### 5.3.2 *First-year ice and Young ice*

The vertical structure of first-year ice was varied in each sample, indicating complicated growth processes. The polarized photos of vertical thin sections of all the five first-year ice samples are shown in Figure 5.3.3a-e. It is noticeable in these figures that granular structure is outstanding. Among them, two samples are composed of granular ice in total layers. When we summed up for first-year ice samples in each year, it turned out that the fraction of granular ice amounts to 100% for a 1996 sample and 61% for 1997 samples, while columnar structure occupies 0% for 1996 and 33% for 1997 (Table 5.3.1). Thermodynamical growth is always associated with columnar ice and can be definitely discriminated from dynamic growth. Therefore, it is indicated from this result that dynamic growth process, such as accumulation of frazil ice, is more significant in the southern Okhotsk Sea than thermodynamic growth.

This feature is also found in young ice samples. In the young ice samples of 1996,



Total Thickness = 32 cm

Ave. Density = 813 kg/m<sup>3</sup>

Salinity = 4.4 psu

Figure 5.3.3 Vertical profiles of structure, salinity, and density of first-year ice.

See Figure 5.1.1 and Figure 5.1.2 for each sampling location.

(a) F1 (1996)

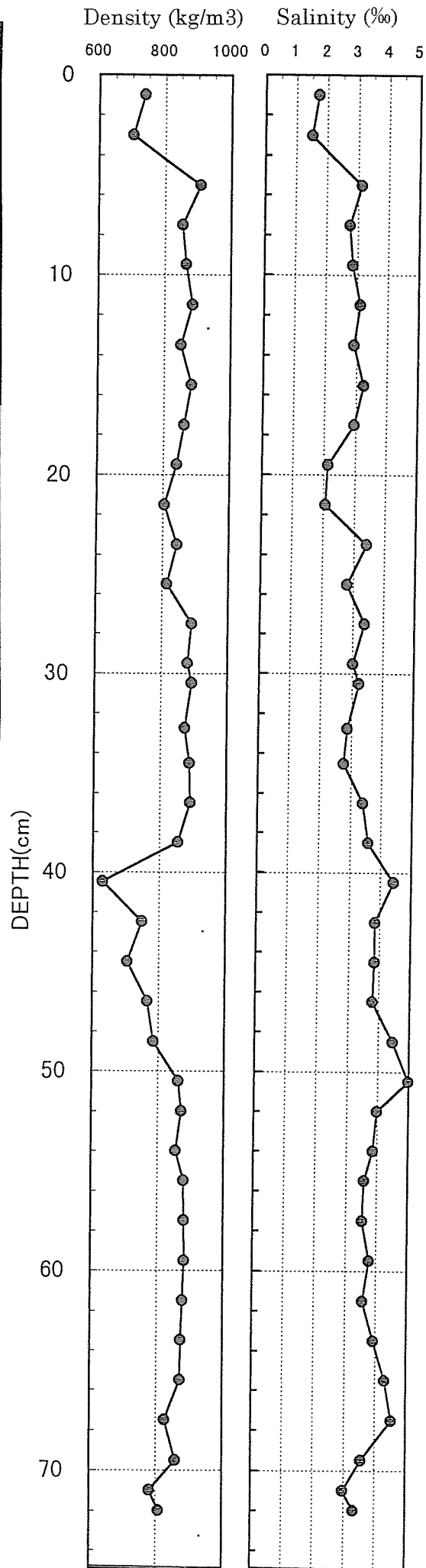
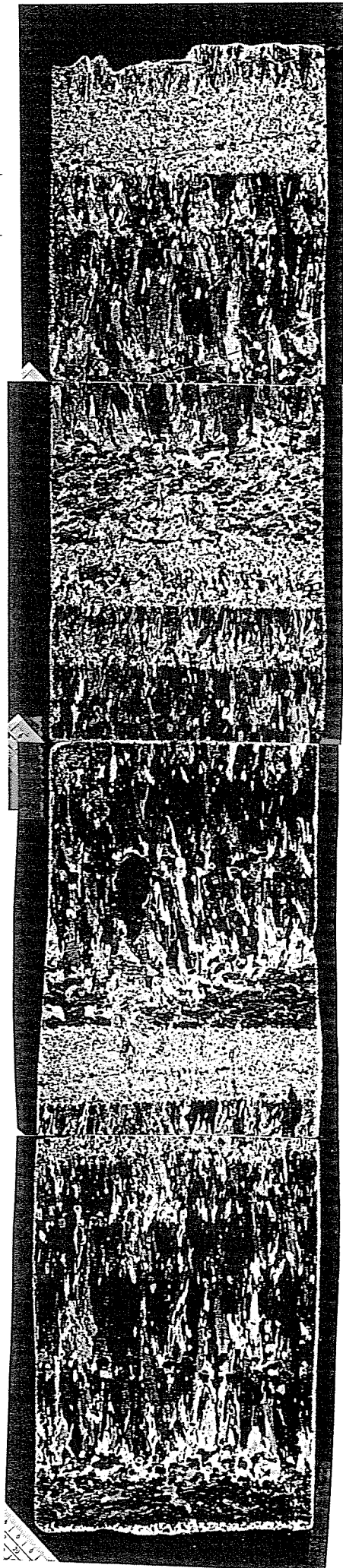
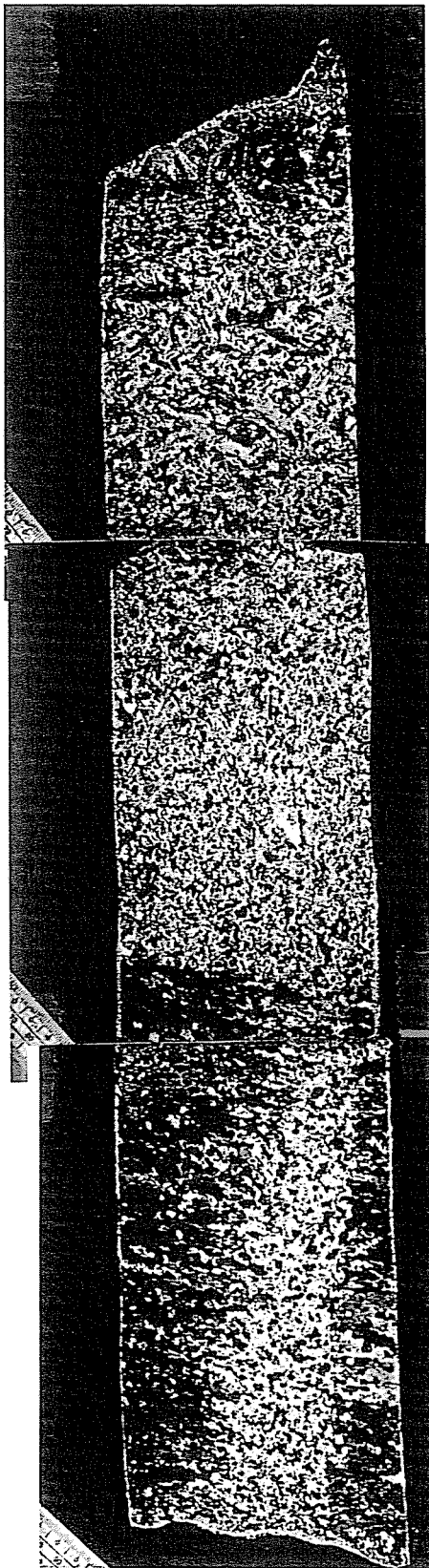
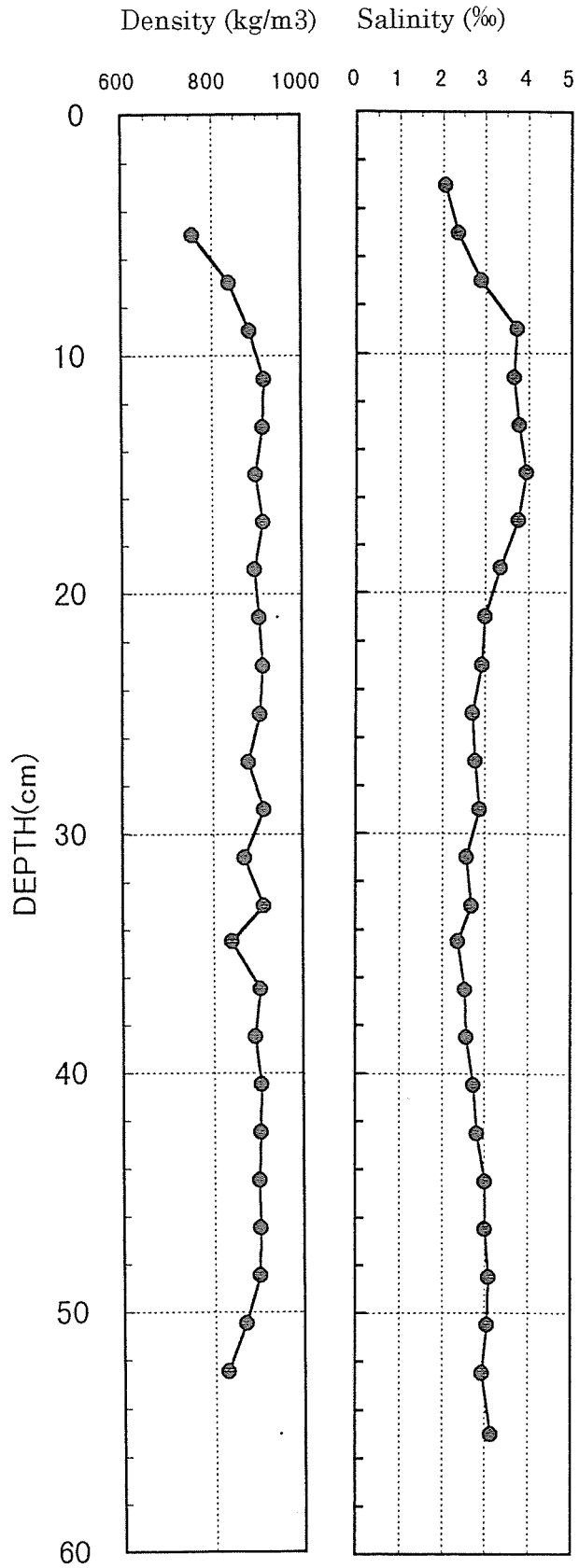


Figure 5.3.3 (Continued.)  
 (b) F1 (1997)



Total Thickness = 55 cm

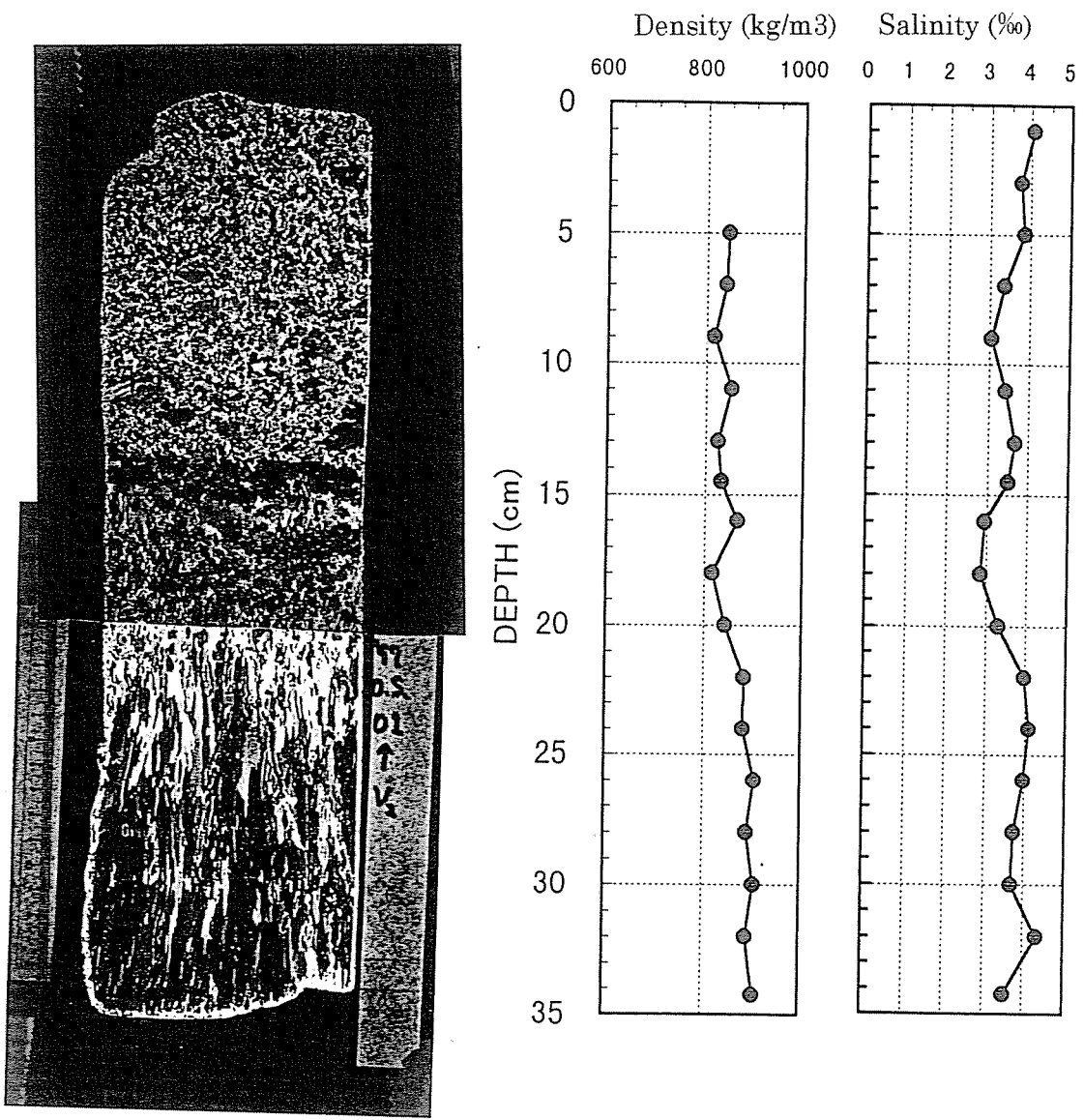


Ave. Density = 885 kg/m<sup>3</sup>

Salinity = 2.9 psu

Figure 5.3.3 (Continued.)

(c) F2 (1997)



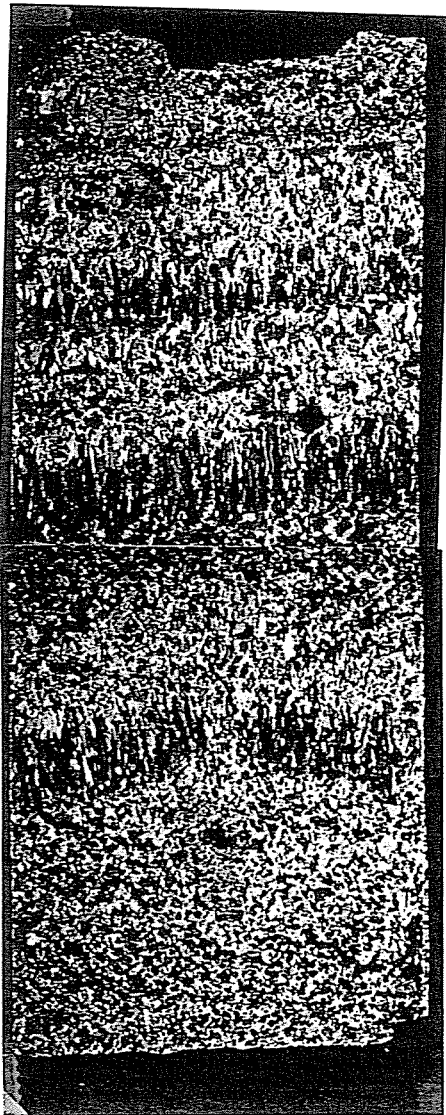
Total Thickness = 37 cm

Ave. Density = 851 kg/m<sup>3</sup>

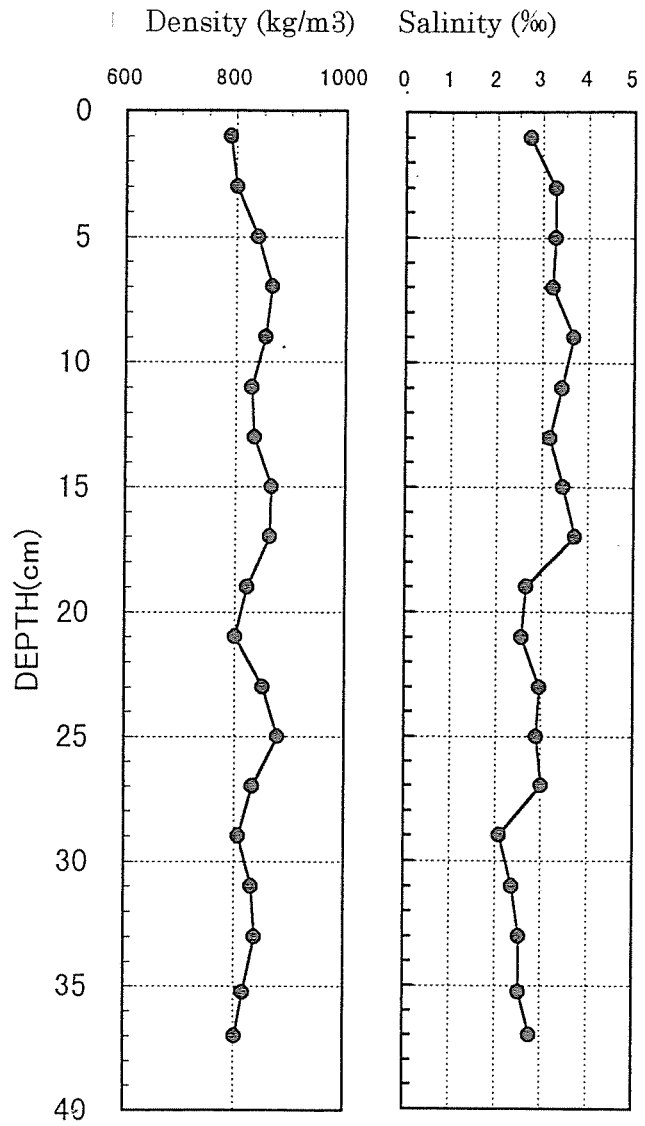
Salinity = 3.5 psu

Figure 5.3.3 (Continued.)

(d) F3 (1997)



Total Thickness = 40 cm



Ave. Density = 832 kg/m<sup>3</sup>

Salinity = 3.0 psu

Figure 5.3.3 (Continued.)

(e) F4 (1997)

**Table 5.3.1  $\bar{F}$  Fractions of ice structure.**

c: columnar ice

g: granular ice

c/g: (mixture of columnar and granular ice)

v: the ice structure where vertically oriented c-axes are predominant.

year	ice types	number	c	g	c/g	v
1996	first-year ice	1	0	100	0	0
	young ice	6	0	100	0	0
	Total	7	0	100	0	0
1997	first-year ice	4	33	61	4	1
	young ice	9	52	36	8	4
	Total	13	42	50	6	3

(unit: %)



almost all the layers were composed of granular ice and columnar ice could be found in a piece of about 2 cm thickness and 5 cm width in only one sample. On the other hand, in 1997 samples, columnar ice is more often observed and sums up to 52%, while granular ice occupies 36% (Table 5.3.1). Considering the satellite observation of sea ice in this region, this structural difference between 1996 and 1997 may be attributed to the growth history. In 1996, sea ice formed mainly by in-situ freezing in 1996, while sea ice in 1997 developed thermodynamically in the northern region off Sakhalin and then flowed southward to this area.

As a whole, granular ice comes up to 50% when we sum up for both first-year ice and young ice of 1997 samples (see Table 5.3.1). This value surpasses columnar ice (42%). Thus it was shown that granular ice is more prominent than columnar ice and dynamic process plays an important role in ice thickening process in this area. This result is consistent with that of heat budget calculation discussed in the previous chapter in that thermodynamic growth is limited even in mid winter in this region. Actually, it is often observed from a helicopter that a number of frazil ice crystals are accumulated around the edge of marginal pack ice probably due to strong wind (Figure 5.3.4a) or gathers together associated with a Langmuir circulation (Figure 5.3.4b) which is suggested by *Martin and Kauffman (1981)*. It can be easily imagined that accumulated frazil ice become solidified as accumulation proceeds. This process of solidification is investigated from laboratory experiments by *Martin and Kauffman (1981)*. We consider that a similar process occurs in a real ocean.

The fraction of columnar and granular ice has been investigated from the analysis of ice samples in both polar regions. For the Arctic regions, *Gow et al.(1987b)* estimated columnar ice as more than 75% for sea ice in the Fram Strait and *Eicken et al.(1995)* estimated columnar/frazil ice as 61/18% for undeformed sea ice in the Eurasian sector of the Arctic Ocean. In the Antarctic regions, it has been reported that granular ice of frazil origin dominates over columnar ice. For example, *Lange and Eicken (1991)* showed that



**Figure 5.3.4** Photographs of accumulated frazil ice from a helicopter.

(a) around the ice pack

taken from 1800 m altitude at 09h39m of February 3, 1997.

(b) associated with Langmuir circulation

taken from 300 m altitude at 13h28m of February 4, 1997.

granular ice of frazil origin occupies 50 to 70% fraction in the Weddell Sea. *Jeffries and Adolphs (1997)* reported that the fraction of columnar ice is only 22% except for coastal regions in the Ross Sea. *Jeffries et al. (1997)* estimated frazil/columnar as 44 / 26% for sea ice in the Bellingshausen and Amundsen Seas. *Allison and Worby (1994)* showed that approximately 50% is composed of small frazil crystals off East Antarctica. This difference between the Arctic and the Antarctic regions can be explained as follows: Open water area between ice floes can appear more easily in the Antarctic regions because wind and swells make ice floes more mobile and consequently numbers of frazil ice is produced in the Antarctic regions. On the other hand, open water area can appear less frequently due to geographical features in the Arctic regions.

The result of our structural analysis is closer to that of the Antarctic regions. It is likely that the formation process of granular ice similar to that of the Antarctic regions takes place also in this region.

Another noticeable feature in Figure 5.3.3a-e is that sea ice is not a single slab but is composed of several layers. For example, three columnar layers are found in Figure 5.3.3e with granular layers sandwiched between them. Since columnar structure is never changed to granular structure during the thermodynamical growth process, it seems that several ice sheets piled on each other to form this ice sample. Granular structure can further be divided from the difference of grain sizes. Consequently, this ice sample (Figure 5.3.3e) appears to be composed of seven layers.

In similar ways, we analyzed the layer structure of all the first-year and young ice samples of 1996 and 1997 using the polarized photos and the scatter and through photos. The results are shown in Figure 5.3.5a-c. In analysis, if we can recognize that one columnar layer originated from its adjacent granular layer, we regarded them as one layer. As a result, the averaged thickness of one layer was 5.8 cm and 9.4 cm for ice samples of 1996 and 1997, respectively. This implies that ice floes of 5 to 10 cm thickness on average pile up on each other to form sea ice in this region. It is suggested from this

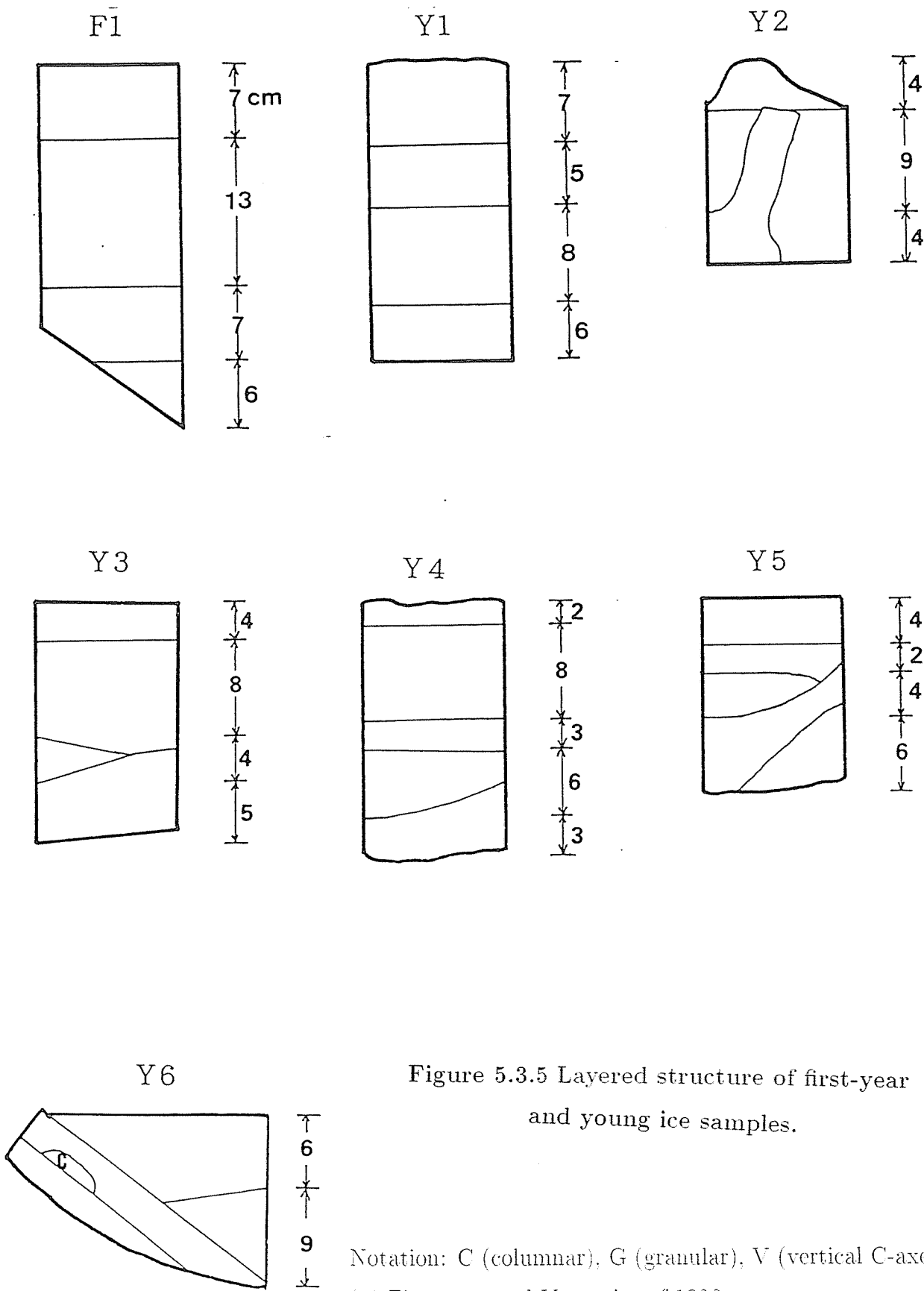


Figure 5.3.5 Layered structure of first-year and young ice samples.

Notation: C (columnar), G (granular), V (vertical C-axes)  
 (a) First-year and Young ice of 1996.

Without one exception (columnar), all the structure is granular.

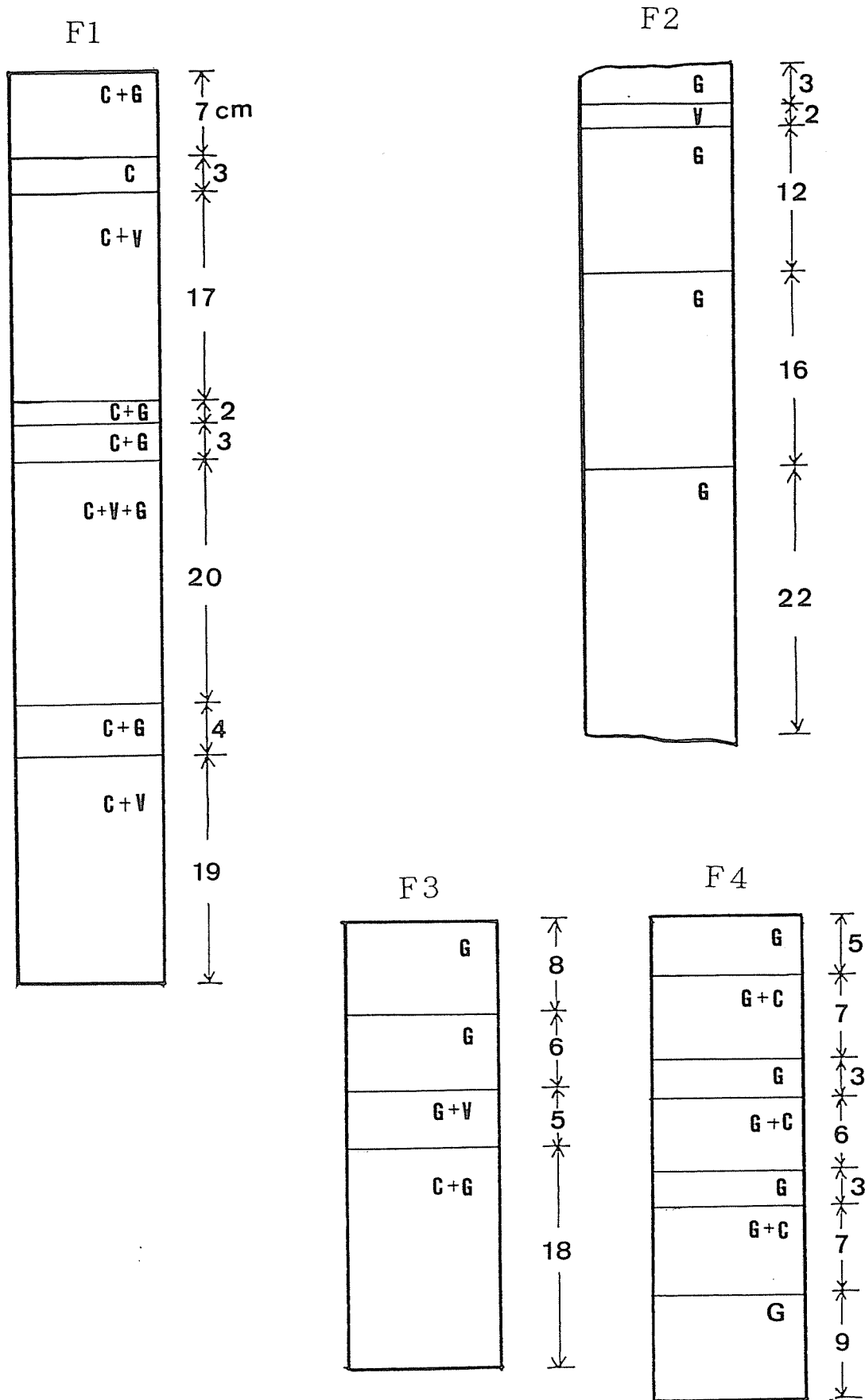


Figure 5.3.5 (Continued.)

(b) First-year ice of 1997.

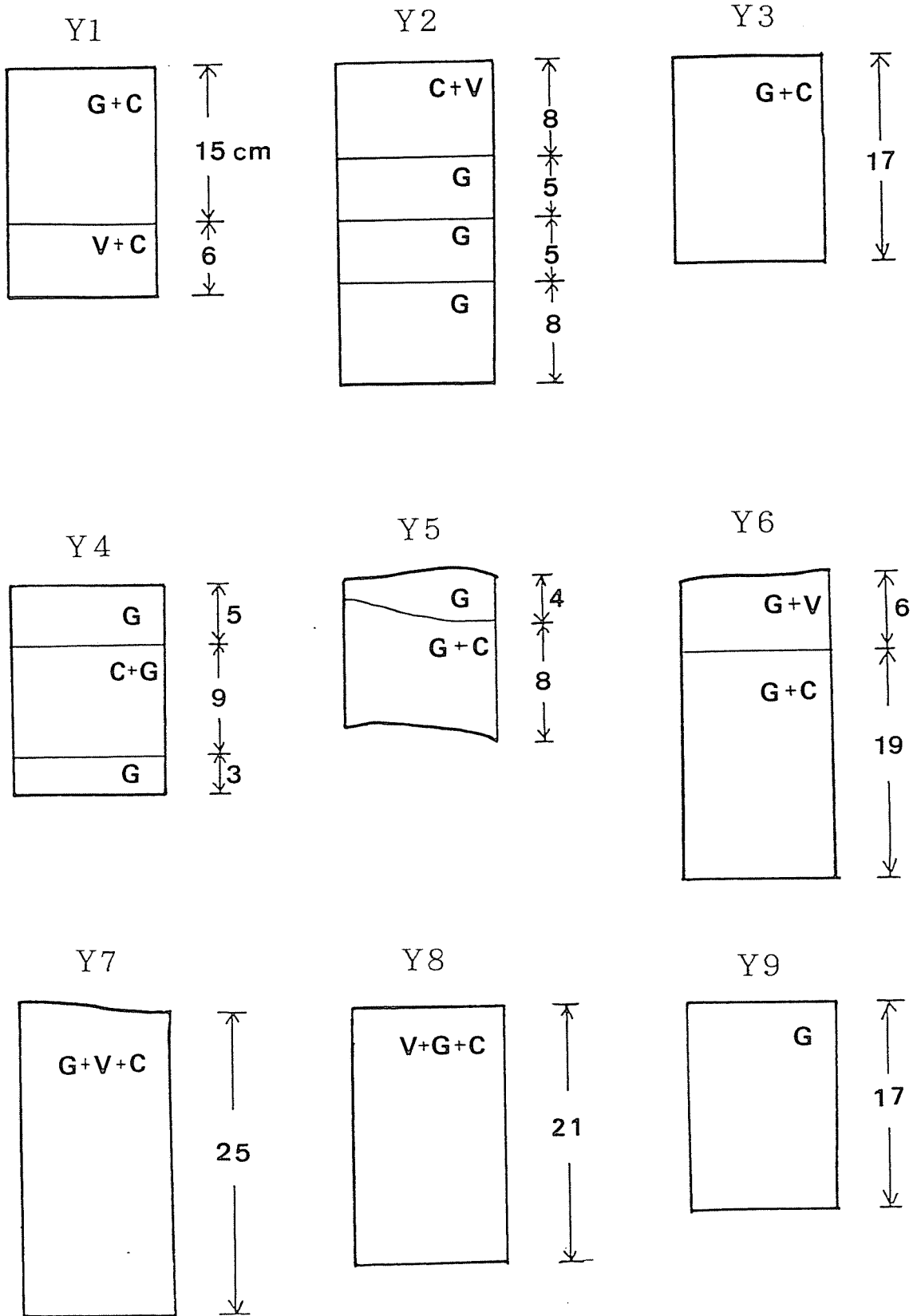


Figure 5.3.5 (Continued.)  
(c) Young ice of 1997.

result that a rafting process, which is one of dynamic growth processes, plays a significant role in the growth of sea ice in this region.

The importance of a rafting process has been pointed out also in the Antarctic region. It has been shown that sea ice floes in the Antarctic region are composed of several ice sheets unlike those in the Arctic region. For example, *Worby et al.(1996)* have estimated the averaged thickness of one layer to be only 12 cm. From observational results, *Lange et al.(1989)* proposed a conceptional model named '*pancake cycle*' as a growth process by rafting (Figure 5.3.6). Their model is explained as follows: Sea ice initially forms in the open ocean. Second this ice is piled up on each other by the effects of strong wind and swells and open area is created. Again sea ice is formed in this open area and piled up. This process is repeated and sea ice grows. Considering that the averaged thickness per layer is the same order as ours and that strong wind and swells prevail in winter in the Okhotsk Sea, it is likely that the same process occurs also in the Okhotsk Sea.

Finally, we would like to point out a unique ice crystallographic structure. In some samples, the layer where c-axis of ice crystal is almost vertical is found (referred to as a CAV layer here). The thickness of this layer is one to a few centimeters. One polarized photo of the typical case is shown in Figure 5.3.7. In this layer, vertical structure is seen almost uniform and grain sizes appears to be somewhat larger compared with those of other granular ice (about one millimeters). To our knowledge, this kind of ice layer has not been noticed from the observation in the polar ocean. It seems impossible that this layer is created beneath ice bottom during thermodynamical growth process. One of the possibilities is that nilas of 2 cm thick was piles up on another ice floe. However, we wonder if such a kind of nilas as has 2 cm thick CAV layer can form from sea water. It is known that the CAV layer is only limited to a few millimeters at the freezing surface (*Weeks and Ackley, 1986*). Therefore, it is more likely that a large number of round thin ice crystal discs, which are produced in sea water below a sea ice floe under supercooled conditions, are lifted slowly by buoyancy forcing keeping the disc facets horizontal and

「Pancake cycle」

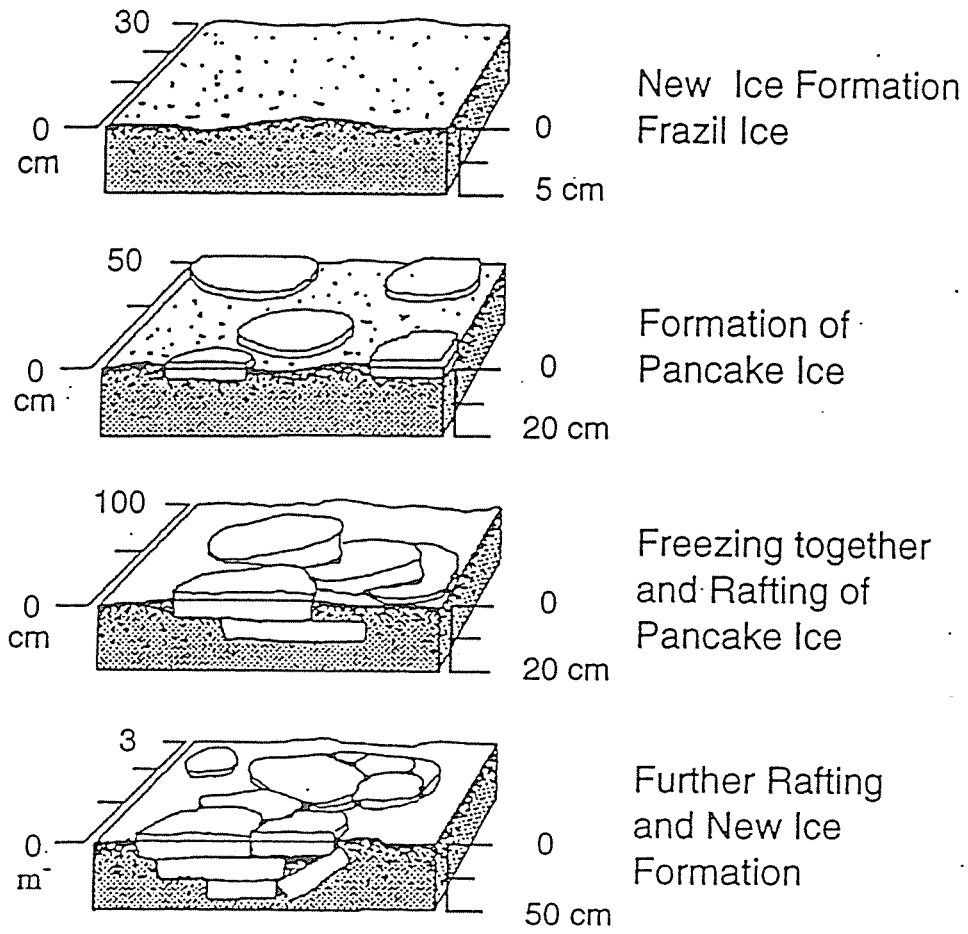


Figure 5.3.6 'Pancake cycle' cited from *Lange et al.(1989)*.



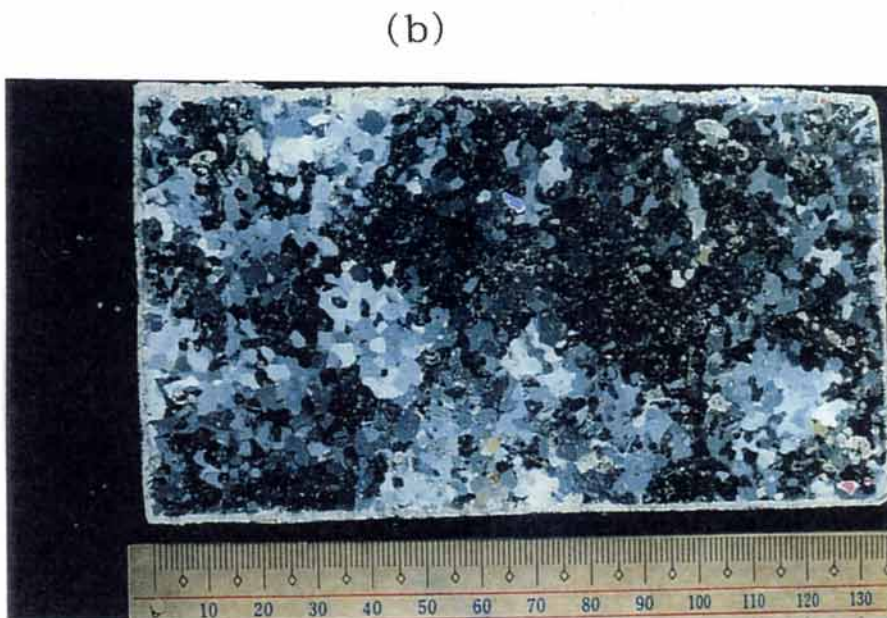
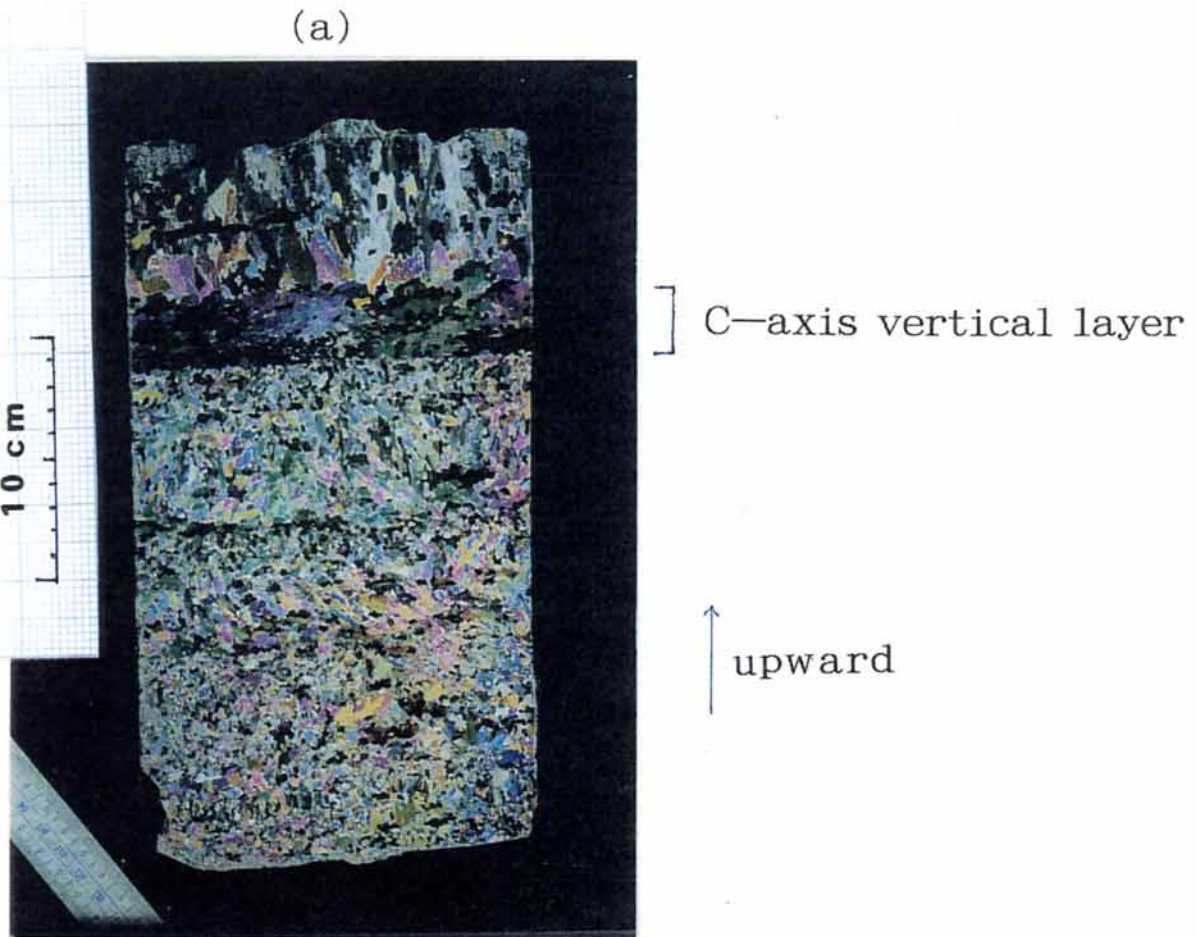


Figure 5.3.7 Polarized photos of C-axes vertical layer found in young ice (Y2, 1997).

(a) vertical section (b) horizontal thin section.

The thickness of CAV layer reaches 2 cm.

Black area in horizontal thin section corresponds to C-axes vertical layer.

accumulated beneath a sea ice floe. This process is suggested by the laboratory experiment of *Ushio and Wakatsuchi (1993)* (see Fig.8b in their paper). If this is the case, this type of ice structure should appear also in the polar regions. We are not sure why it has not been reported before, but it is an interesting structure. Further observation will be desired.

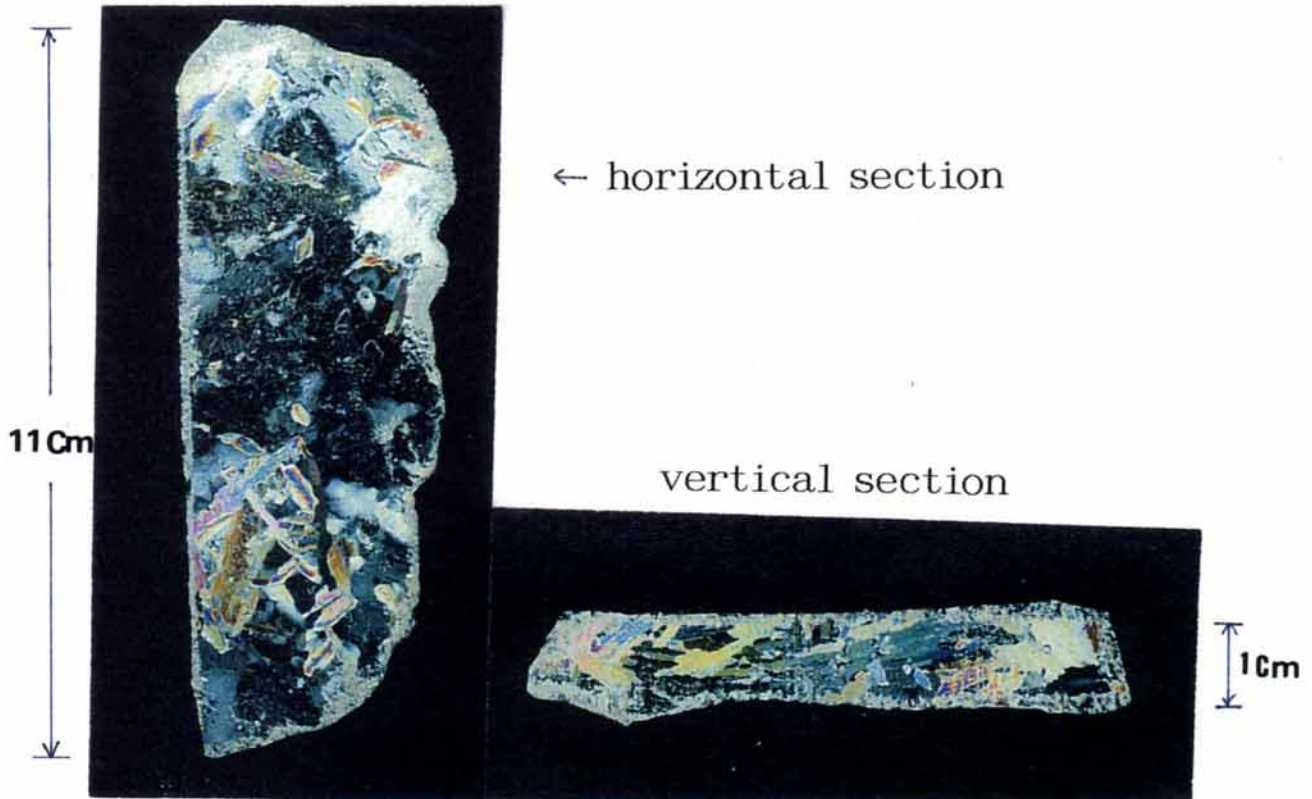
### 5.3.3 Nilas

During the cruise in 1996, we took two samples of 1-cm thick nilas near Shiretoko Peninsula in the morning. Thin section analysis showed that both samples had vertically uniform-layered structure and large-sized grains (up to a few centimeters) (Figure 5.3.8). These structural features are quite different from those of the first-year and young ice samples in 1996 and, moreover, those of nilas in the Fram Strait which is reported by *Tucker et al.(1991)*. The salinity was both 12.5 psu which is somewhat lower than that observed by *Tucker et al.(1991)* (15.3‰ for 3cm thick nilas). The values of density were 881 and 840  $kg/m^3$ , which are also somewhat lower than 920  $kg/m^3$  reported by them.

In order to further examine this structure, we divided grain area in the horizontal thin section and measured the c-axis direction of each grain area using a universal stage. The distributions of c-axes zenith angle are depicted in Figure 5.3.9a and b. It is shown that the areas which have almost vertical c-axes are prominent and that their sizes are much larger than those of the grain areas with less vertically-oriented c-axes. This feature is clearly shown by Figure 5.3.10 in which areal fraction is depicted as a function of the c-axes zenith angle.

*Weeks and Ackley (1986)* have shown that c-axes are roughly perpendicular to the freezing surface at the very thin surface of the ice skim. However, it has not been known that the sea ice can have vertically oriented c-axes layer of as thick as 1 cm. The reason why such layer cannot develop much in sea ice can be explained as follows: In the case of fresh water, a static state is maintained while freezing because the temperature of

(a)



(b)

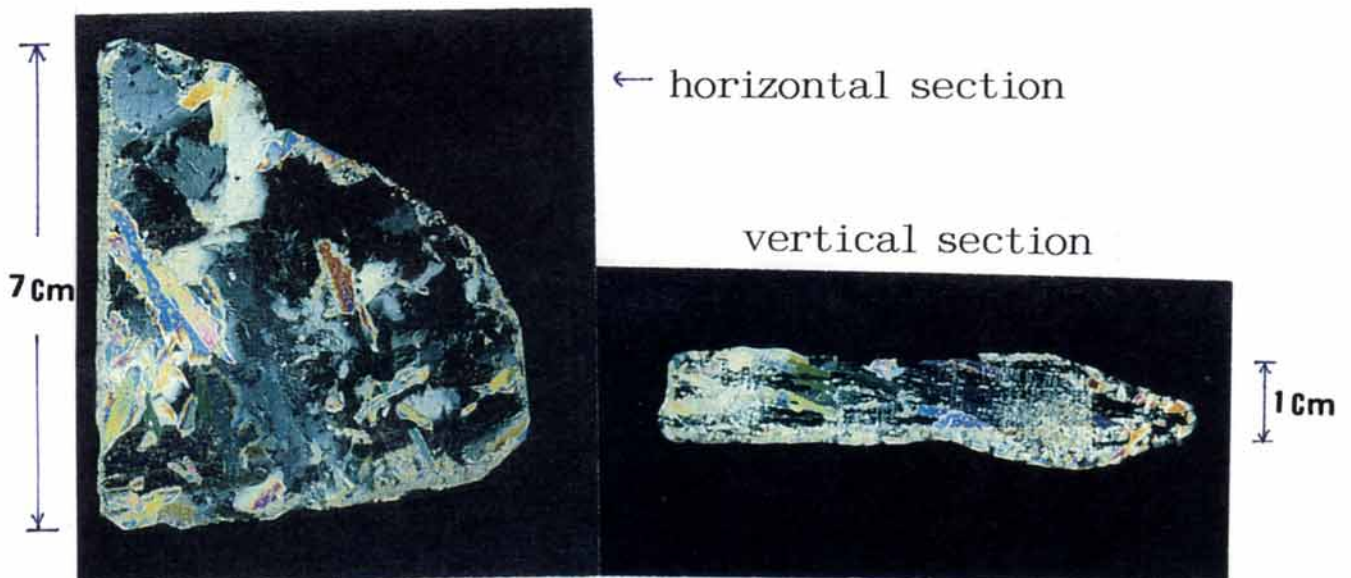
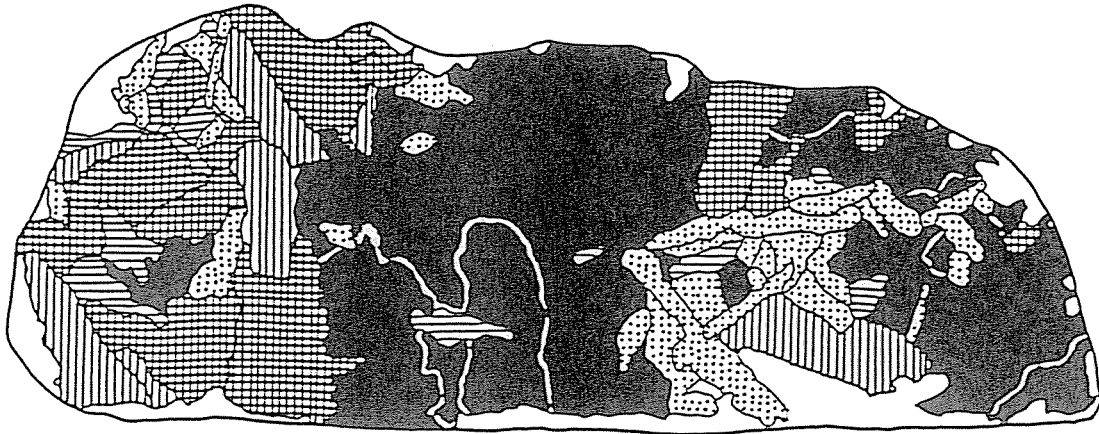


Figure 5.3.8 Polarized photographs of nilas.

(a) N1 (1996)      (b) N2 (1996).

(a)



(b)

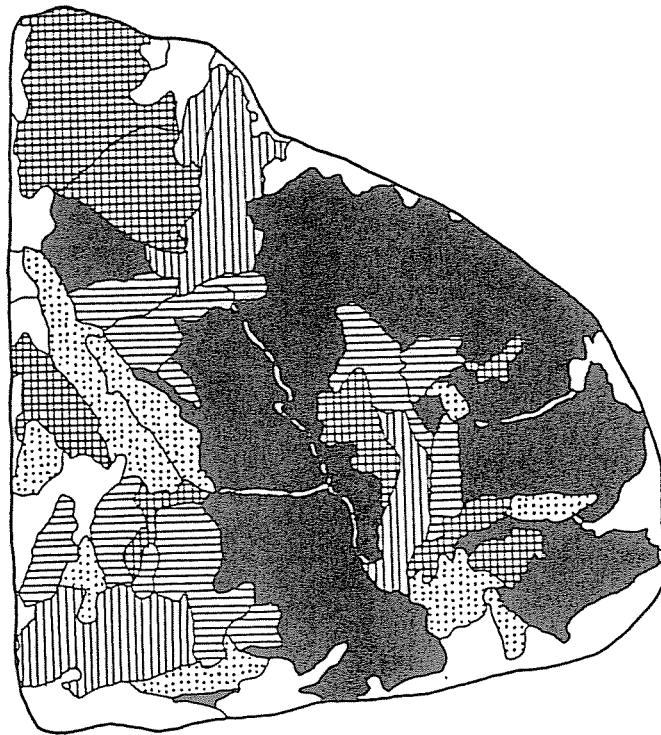


Figure 5.3.9 Zenith angle distribution of C-axes for two samples of nilas taken off the Shiretoko Peninsula during the cruise in 1996.

(a) N1 (1996)

(b) N2 (1996)

■ : 0 ~ 15 deg.

▣ : 15 ~ 30

▤ : 30 ~ 45

▥ : 45 ~ 60 deg.

▦ : 60 ~ 90

□ : excluded from analysis.



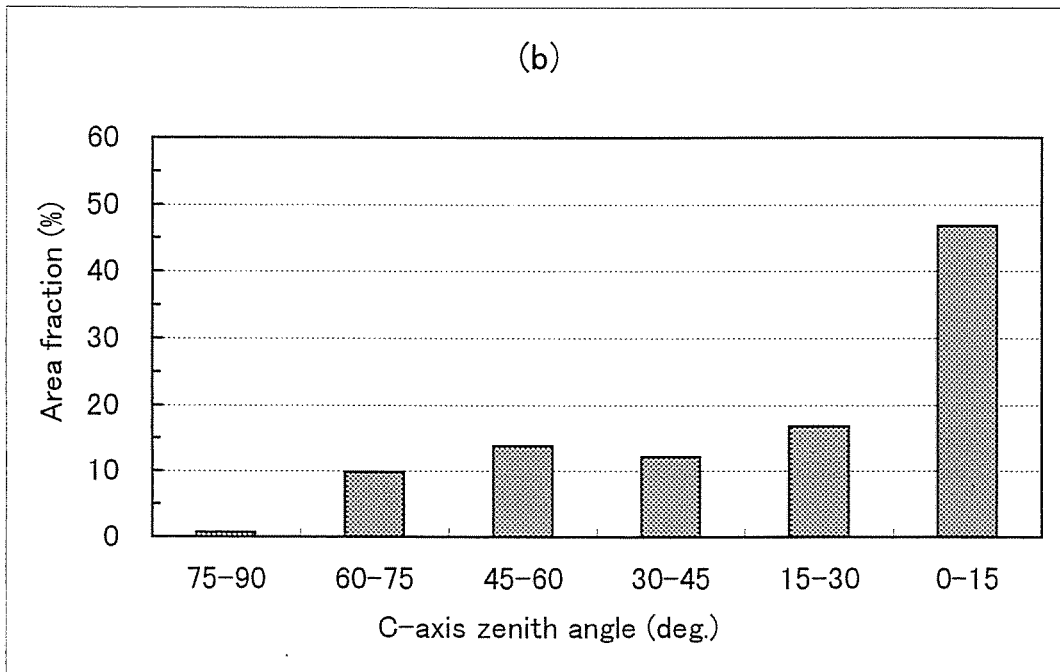
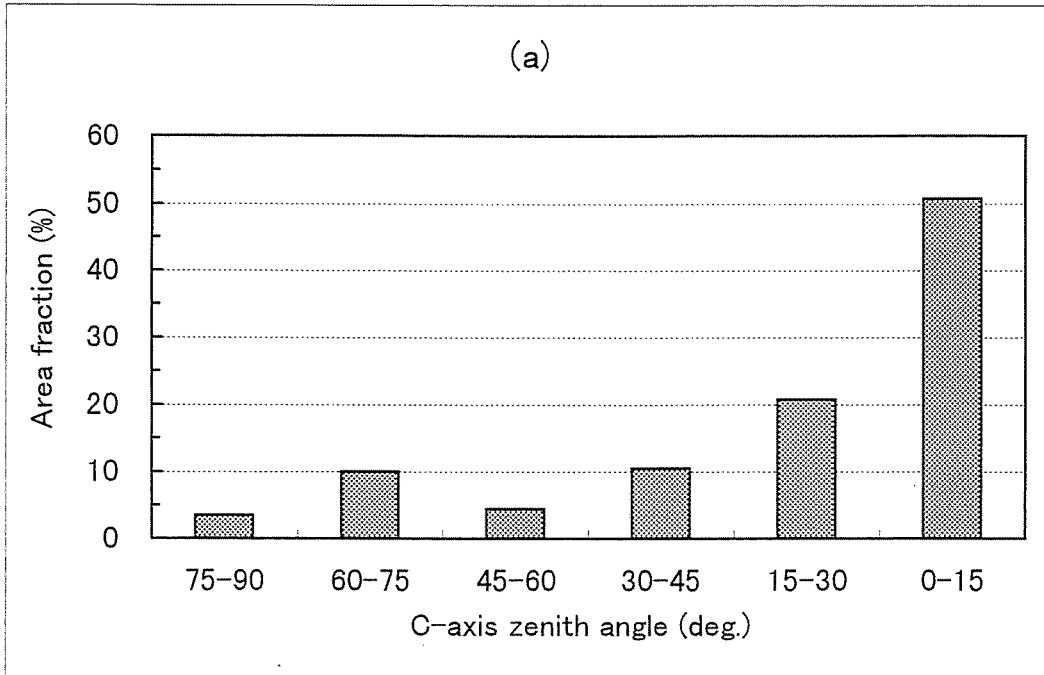


Figure 5.3.10 Histograms of the area fractions of horizontal section as a function of C-axis zenith angle.

(a) N1 (1996)      (b) N2 (1996)

maximum density is above freezing point. Thus fresh ice develops statically with the c-axis orientation being kept vertical. On the other hand, in the case of sea ice, convective motion easily occurs while freezing because of the following reasons. First, since the temperature of maximum density is below freezing point for salinity of more than 25 psu, the water cooled at the surface induces convection. Second, dense brine water expelled from sea ice causes instability under the ice. Therefore, a static state can hardly be realized during the freezing of sea water, which leads to the inclination of the c-axis. For this reason, we consider that special conditions are required for the CAV layer to develop.

In order to further examine the structure of nilas, we took 10 samples at different areas during the cruise in 1997 (see Figure 5.1.2d for location). Although the CAV layer can be found at the ice skim in all the samples, its thickness ranges from 3 to 9 mm and the inclined c-axes layers appear under the CAV layer in many samples. Among them, the nilas of similar structure to 1996 samples can be found out (see Figure 5.3.11). The vertical thin section (Figure 5.3.11b) shows that the structure is vertically uniform and it is shown from the horizontal thin section (Figure 5.3.11c) that all the area is occupied by the vertically oriented c-axes. The structure is further closer to that of fresh water ice compared with two samples of 1996.

From these results, it is shown that nilas has the CAV layer at the skim in many cases and its thickness ranges from 3 to 10 mm and that some nilas samples among them are occupied by this layer in all the layer (8 to 10 mm). Here we put the following questions: what causes the difference of the layer thickness? Are any special conditions required for this layer to develop to 10 mm? To the author's knowledge, little attention seems to have been paid to this matter. Therefore, we tried to approach this matter through laboratory experiments. As for the factors which may affect the thickness of CAV layers, ice growth rate and water salinity are taken into account. The results will be shown and discussed in the next chapter.

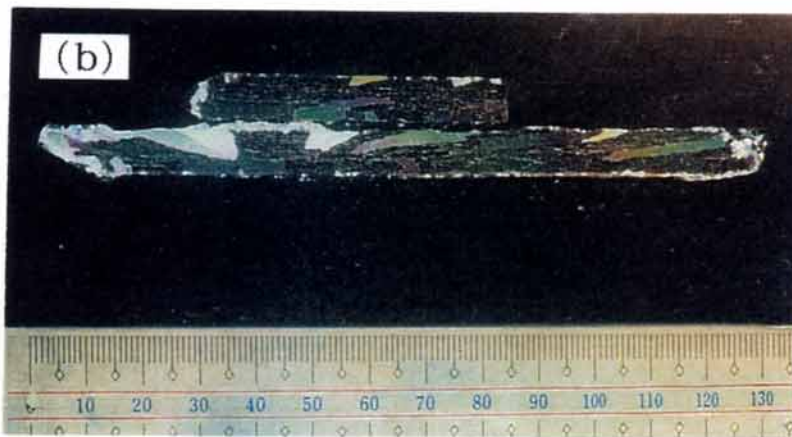
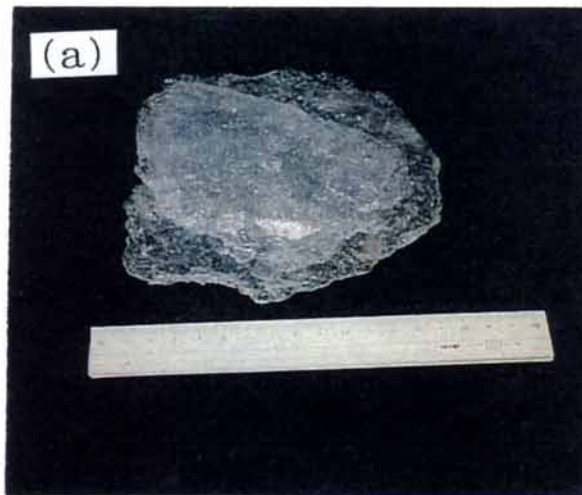


Figure 5.3.11 Polarized photographs of thin section of nilas N2 (1997) taken off the northeastern Hokkaido coast (see Figure 5.1.2c).  
(a) Full scale sample (b) Vertical section  
(c) Horizontal section (Black area represents vertical C-axis.)

#### 5.3.4 Pancake ice

Structural analyses of pancake ice have been relatively limited so far (e.g. *Tucker et al. (1991)*, *Wadhams et al. (1996)*). Given that pancake ice occupies a significant area and is one of the typical ice types at the seasonal and marginal ice zone, it is important to analyze the structure for the understanding of the formation process. We took three and seven samples in 1996 and 1997, respectively. The individual samples of 1996 ranged in size from 70 to 100 cm in diameter and ranged in thickness from 11 to 15 cm. Those of 1997 ranged in size from 6 to 100 cm in diameter and ranged in thickness from 1 to 8 cm. The bulk salinity ranged from 6 to 8 psu in 1996 and from 7 to 10 psu in 1997. These values are somewhat lower than those of the pancakes observed in the Fram Strait by *Tucker et al. (1991)* (9 to 12 psu). The bulk ice density ranged from 821 to 926  $kg/m^3$  and also showed somewhat lower values compared with their values (920  $kg/m^3$ ). Both these lower values may be caused by the melting effect described in section 5.3.1.

In the ice samples of 1996, all the layers were composed of granular structure whose diameter is less than 1 mm. This indicates that this pancake ice formed through the accumulation process of frazil ice due to wind and swells. On the other hand, different structure of pancake ice was found out in the samples of 1997 (Figure 5.3.12). This pancake existed in closely packed form at this site (Figure 5.3.12a). Thick/thin section (Figure 5.3.12bc) indicates that a few ice sheets were piling up, bended, and overlaid with granular ice. The elonged shape of each grain is somewhat similar to that of the pancake reported by *Tucker et al. (1991)*. However, its alignment is rather random in their case and quite different between ours and theirs. In our pancake, each grain is well aligned and its c-axis is almost vertical. This type of structure has not been reported before. The structure of this ice is similar to that of the previously described nilas. Similar structure was found also in the other samples near this area. This result indicates that these samples of pancake ice were formed from the piling of nilas which had initially covered the wide ocean area.





Figure 5.3.12 Vertical structure of pancake ice P3 (1997)

taken near the marginal ice zone.

(a) View around the sampling area from the ship.

(b) Scatter photo (5 mm thick) of vertical section.

(c) Polarized photo (0.5 mm thick) of vertical section.

#### 5.4 Summary and Discussion

In order to investigate the characteristics of sea ice in the southern region of the Okhotsk Sea, we took ice samples during the cruises in early February of 1996 and 1997 and examined their structure especially from the viewpoint of ice growth processes.

Through thick/thin section analysis, it was found for first-year and young ice that granular ice occupies greater part than columnar one and that many ice samples are composed of several ice sheets with average thickness of 5 to 10 cm. These results show that a dynamic process plays a significant role in ice growth processes in this region. The latter result indicates the importance of a rafting process and that a phenomenon similar to 'Pancake cycle' (Lange *et al.*, 1989) in the Antarctic region occurs also in this region. A rafting process is recognized also in some pancake ice. These results are consistent with those of heat budget analysis discussed in the previous chapter in that we showed that a thermodynamic process is not dominant in ice growth processes in this region.

For thin ice, the nilas samples of about 1 cm thickness with vertically oriented c-axes in all the layers were found out. This type of structure has not been reported in other sea ice regions so far. Further investigation is performed through laboratory experiments. The details will be shown in the next chapter.

We also measured salinity and density of our ice samples. The result shows that bulk ice salinity is lower by about 3 psu than the salinity of sea ice taken at the freezing season in the polar regions and that bulk ice density is lower by about  $40 \text{ kg/m}^3$  than that of first-year ice in the polar regions with widely varied range. Low salinity may be attributed to desalination due to melting and somewhat lower density may be attributed to increased porosity due to melting. Considering that the melting is caused by abundant solar radiation and relatively high temperature, these results may be also one of the characteristics of sea ice in this region. Further data accumulation will be desired in the future.

## Chapter 6. Laboratory Experiments

### 6.1 Introduction

In the previous chapter, we showed that a kind of nilas, in which crystal grains of almost vertical c-axes are predominant in all the layer of about 1 cm thickness, was found out in the southern region of the Okhotsk Sea. This structure is rather similar to that of fresh water ice and is discriminated from the other structures of sea ice. It has been known that crystal grains with vertical c-axes are dominant in the very thin layer of sea ice as well as fresh water ice when ice initially forms from sea water under calm conditions (*Weeks and Ackley, 1986*). As the ice growth proceeds, the crystals with inclined c-axes become prominent because the expelled dense brine induces convection under ice surface. In the meanwhile, crystals with almost horizontally oriented c-axis occupies most part of the area by the time ice thickness reaches about 5 cm (*Kawamura, 1982; Weeks and Ackley, 1986*). Thus the layer composed of the crystals with vertically oriented c-axes is supposed to be limited to very thin layer near the surface, even if it exists.

Our matter here is to what thickness this thin layer can develop. That is, can it be as thick as 1 cm as we observed, when ice forms from normal sea water (32 ~ 34 psu)? *Kawamura(1982)* showed from the analysis of 5cm-thick ice frozen in the Saroma Lake that numbers of c-axes of crystals are already inclined at 1 cm-depth. According to the analysis of sea ice frozen at Thule, Greenland by *Weeks and Ackley (1986)*, crystals with vertically oriented c-axes occupy significant part but their frequency is below 30% at 0.5 cm-depth. In the light of these previous studies, special conditions may be required for this layer to develop up to 1 cm thickness. Since little attention have been paid to the thickness of ice skim layer so far, we examined it through laboratory experiments.

Regarding required conditions, we considered two kinds of factors here. One is low salinity of sea water. This factor possibly affects the thickness of the skim layer, consid-

ering that *c*-axes become mostly vertical in all the layer of ice frozen from fresh water. It was shown from the heat budget analysis in Chapter 4 that surface less saline layer can be produced due to ice melting at daytime in this region. The other one is ice growth rate, which affects the salt flux of the brine excluded from ice (*Wakatsuchi and Ono, 1983*). Since the difference of the salt flux causes the change of salinity beneath ice, it is considered that ice growth rate also affects the result.

The purpose of our laboratory experiments is to freeze sea ice under calm conditions, and to examine to what thickness the skim layer can develop and how this thickness changes with these growth conditions. For this purpose, we prepared four thermally insulated tanks, put water of different salinities (8, 17, 25, 34 psu in principle) into each tank, and froze water at the same time in a cold room until ice thicknesses reach about 5 cm. The room temperature was set at  $-10, -15, -20^{\circ}\text{C}$ . We measured the thickness of the ice skim through thick/thin section analysis. We consider that this work is related to the physical process concerning the change of *c*-axes orientation during ice growth, which is one of the interesting problems of sea ice.

In this chapter, the details of apparatus will be described in the next section. We will show the results in section 6.3, and discuss them in section 6.4.

## 6.2 Apparatus and Experimental procedures

In order to examine the ice structure of initial growth stages, we prepared four thermally insulated square tanks with inner dimensions of 0.3 m length, 0.3 m width, and 0.65 m high (see Figure 6.2.1). These tanks are made of 1-cm-thick transparent acrylic boards and are covered with 10-cm-thick styrofoam except at the upper surfaces to avoid the freezing at the side walls. We made six holes on a side wall of the tanks at the depths of 10, 20, 30, 40, 50, 60 cm from the top and stuffed them with rubber stoppers to sample water for salinity measurement (see Figure 6.2.1 and Figure 6.2.2). To enable this measurement, we hollowed part of the styrofoam board and took it away only when we

<Side View>

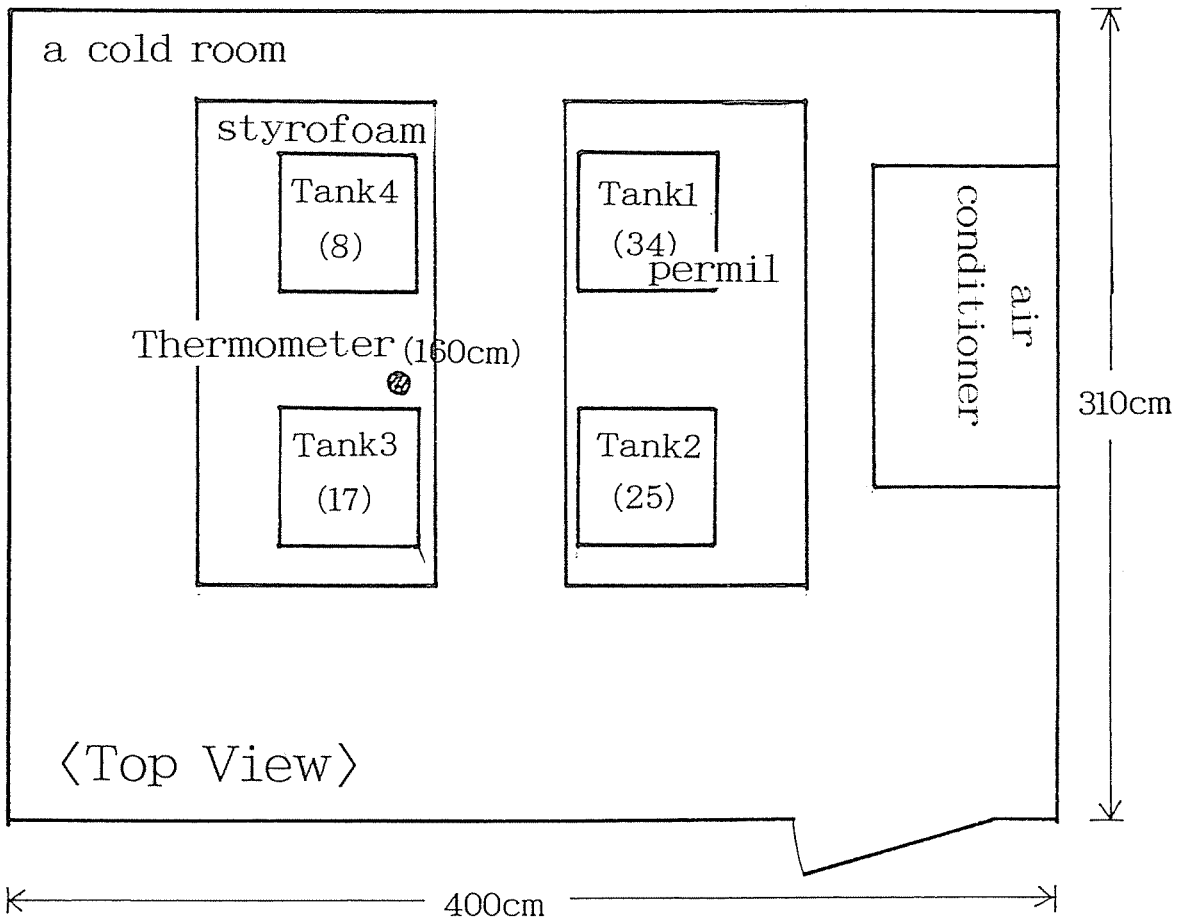
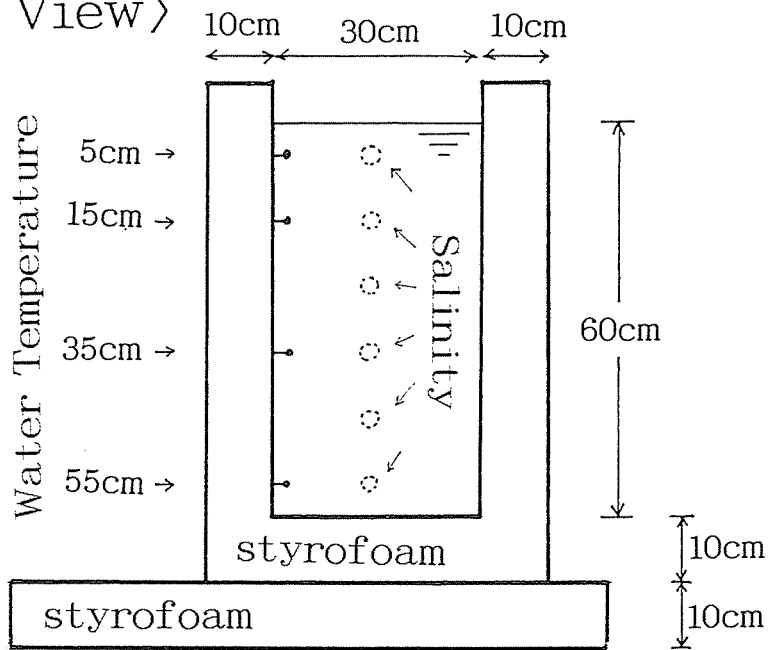


Figure 6.2.1 Schematic pictures of a experimental tank and deployments in a cold room.



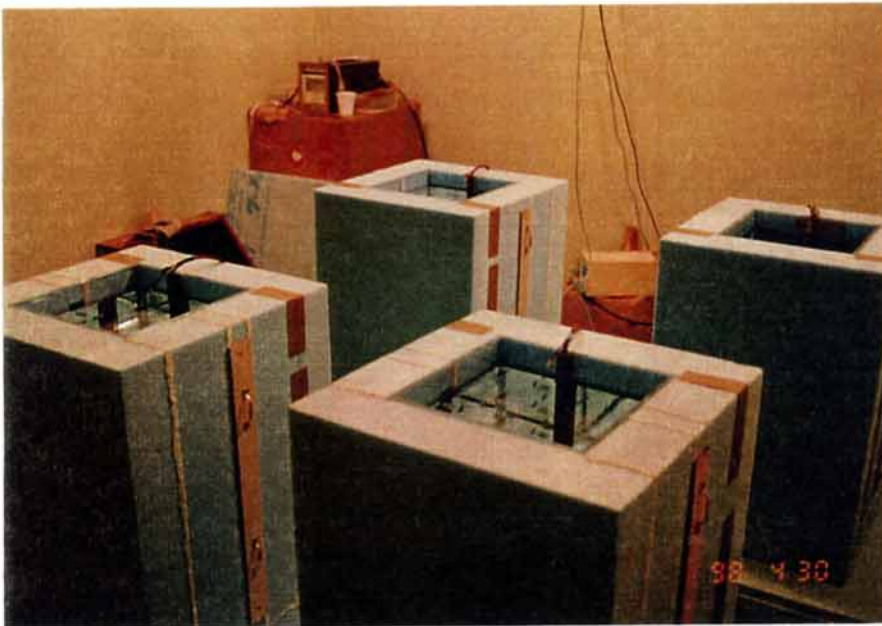
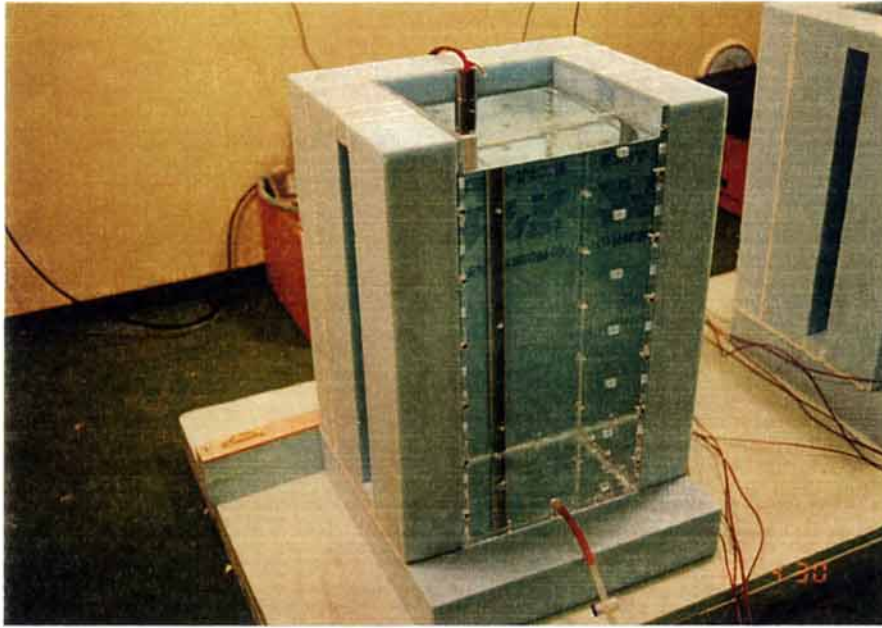


Figure 6.2.2 Photographs of experimental tanks.

took water samples. Water samples were taken carefully from these rubber stoppers with an injector at six hours' intervals. We kept them in a room at ordinary temperature for a few days and then measured their salinity. As for ice thickness, we also put a measuring scale on the side wall and measured it visually. In order to monitor water temperature at depths, we prepared copper-constantan thermocouples, and mounted them at the depths of 5, 15, 35, 55 cm from the water surface (see Figure 6.2.1 and Figure 6.2.2). The room temperature was monitored at the height of 1.6 m with a thermo-/hydro-meter. These temperature data were recorded on loggers at one minute's intervals.

These tanks were put on 10-cm-thick styrofoam to minimize the cooling at the bottom, and were filled with water of different salinities (34(Tank 1), 25(Tank 2), 17(Tank 3), 8(Tank 4) in principle) up to 60-cm-depth. These different salinity waters were made by adding fresh water to sea water (34 psu).

Before starting this experiment, these tanks were cooled enough in a cold room at the temperature of  $0^{\circ}\text{C}$ . The water was sometimes stirred so that all the layer of the water was uniformly cooled. After the water temperature settled down to  $0^{\circ}\text{C}$ , the room temperature was set down to  $-10$  (Case 1),  $-15$  (Case 2), and  $-20^{\circ}\text{C}$  (Case 3). The room temperature decreased to the set values in an hour for Case 1 and Case 2 before freezing started. However, it took longer time for the room temperature to settle down for Case 3. To avoid freezing before the set value, a lid of styrofoam was put on each tank until the temperature decreased to  $-20^{\circ}\text{C}$  in this case. In order to realize freezing under quite calm conditions, it would be desirable to cool water down to the freezing point of each tank. However, it was impossible because the freezing points were different in each tank. We do not consider that this alters the results substantially because the dependence of CAV layer thickness on temperature was relatively small as shown later. When the ice thickness reached about 5 cm, we cut out a square ice piece of 16 cm across from each tank, and kept it in another cold room of  $-16^{\circ}\text{C}$  until ready for thin section analysis.

### 6.3 Results

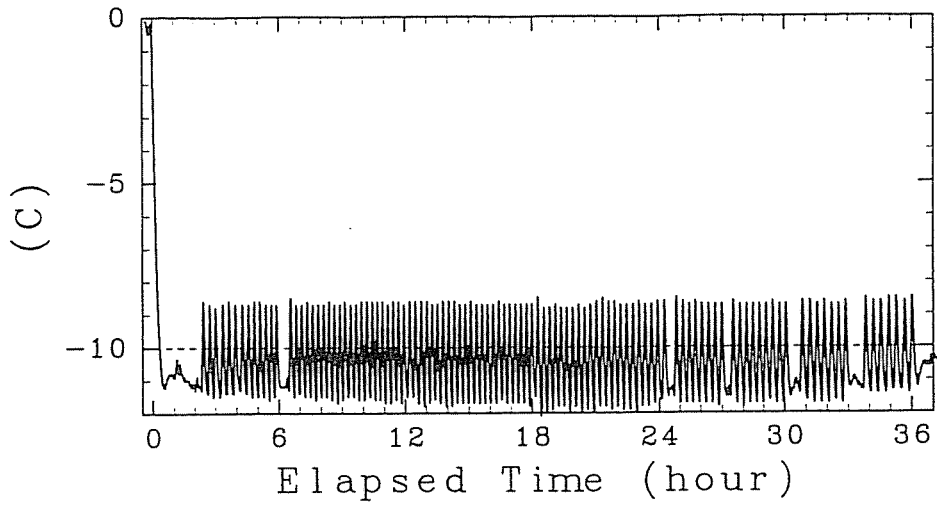
It took 36, 24, and 18 hours for Case 1, Case 2, and Case 3, respectively, until ice thickness grew up to about 5 cm. Figure 6.3.1a-c show the time series of the room temperature monitored by a thermo-/hydro-meter. It is seen from these figures that temperature was kept almost constant for Case 2 and Case 3 during the experiments. Appreciable fluctuation with the amplitude of  $1.5^{\circ}\text{C}$  and the period of 20 min. is found for Case 1. This was caused by the mechanism of the air conditioning system. Even so, the observed water temperature changed much more slowly (see Figure 6.3.3a) and it is unlikely that this fluctuation had a significant effect on the ice structure.

Figure 6.3.2a-c show the growth of ice thicknesses. It is shown from these figures that although ice growth rate is a function of air temperature and water salinity, the dependence on air temperature is much higher and we can regard temperature as a leading factor of growth rate. We show the dependence of ice growth rate on air temperature in Figure 6.3.2d by picking up the data of Tank-1(sea water). It is seen that the growth rate is 1.5, 2.5, and 3.0 cm/12hour for Case 1, Case 2, and Case 3, respectively. From the ice growth calculation in Chapter 4, 1.5 cm/12hour is approximately same as that in the Okhotsk Sea, while 3.0 cm/12hour corresponds to that in the polar regions. Therefore, we consider that the result of Tank-1 for Case 1 is a model case of the nilas which forms in the southern region of the Okhotsk Sea.

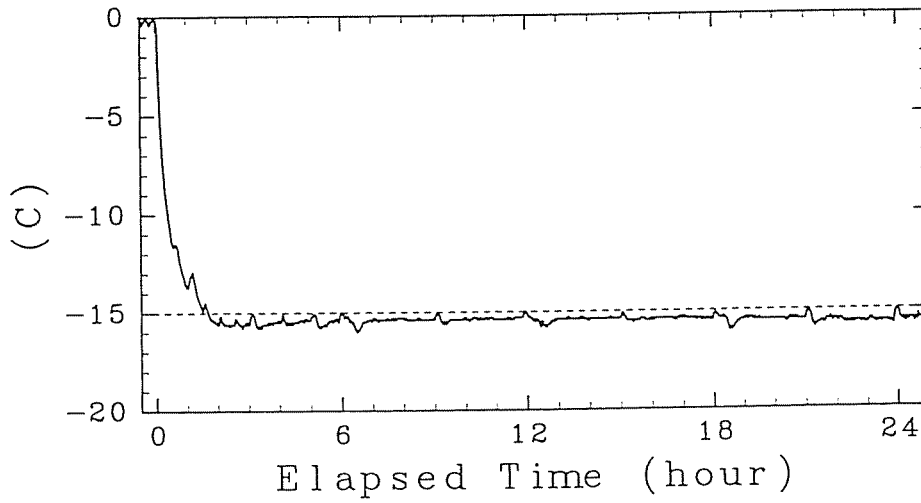
The time series of the water temperature monitored by thermocouples during the experiments were shown in Figure 6.3.3a-c. Broken lines represent the freezing temperatures which were calculated from measured water salinity at each depth. It is shown from these figures that water temperature at each depth changed almost uniformly in each tank except the bottom layers of Tank-2 and -3 and that super-coolings were kept during the ice growth. The changes of salinities are depicted in Figure 6.3.4a-c. Their vertical profiles are almost uniform as well except the upper most layer which is sub-



(a) Case-1



(b) Case-2



(c) Case-3

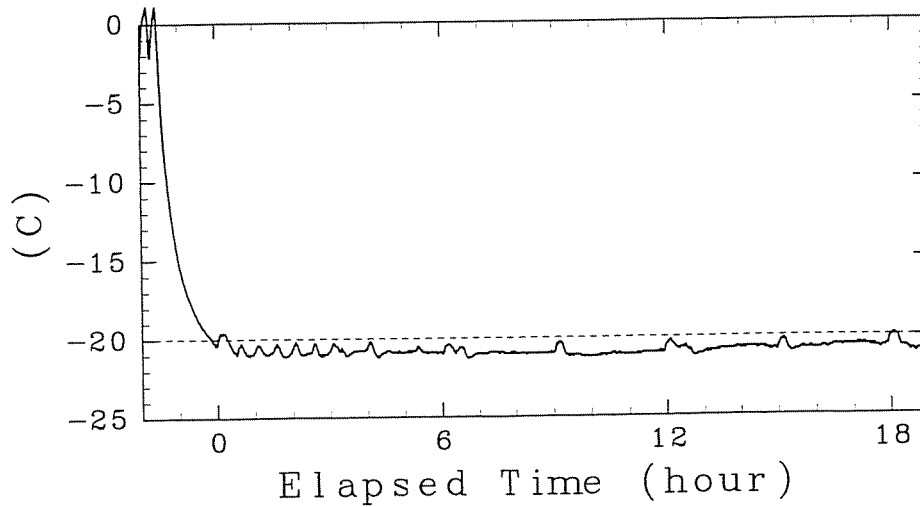


Figure 6.3.1 Time series of the room air temperature.

(a) Case 1      (b) Case 2      (c) Case 3

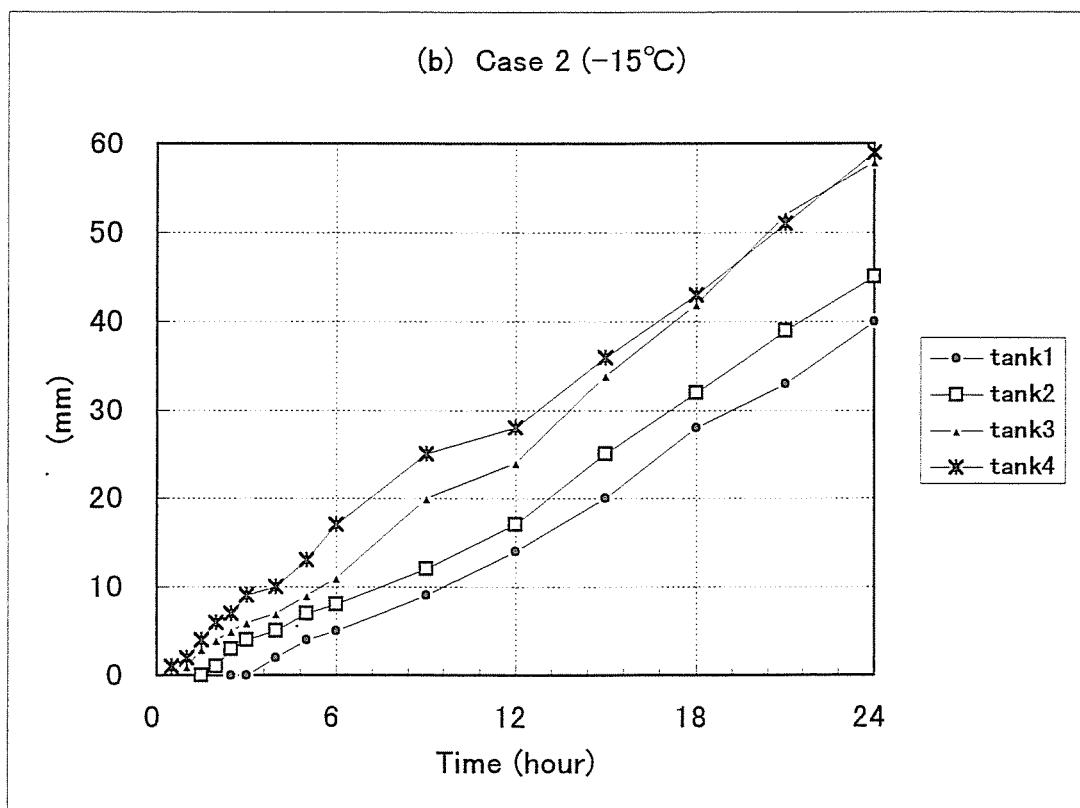
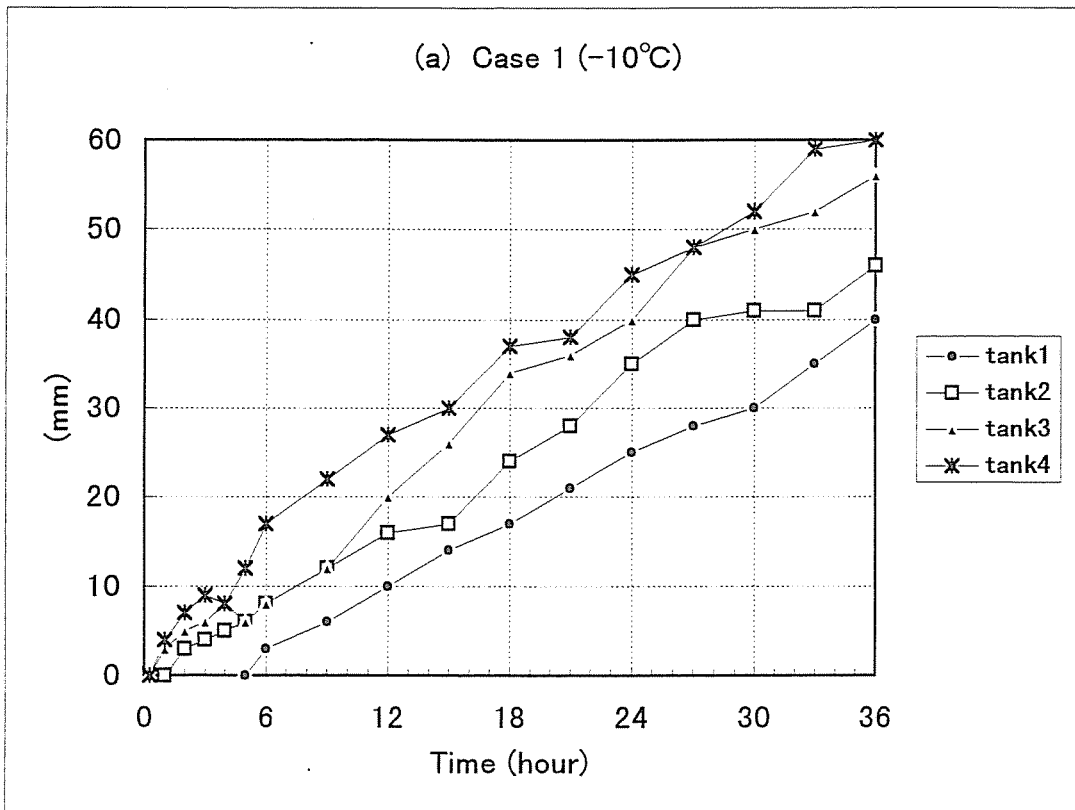


Figure 6.3.2 Growth of ice thickness.  
 (a) Case 1      (b) Case 2

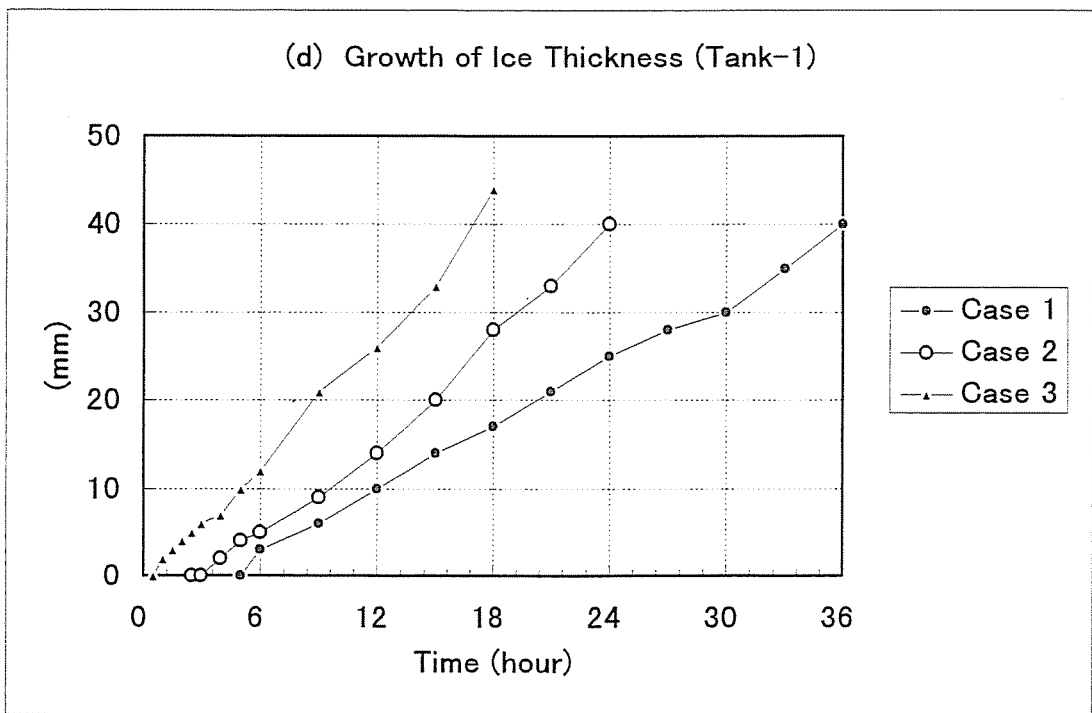
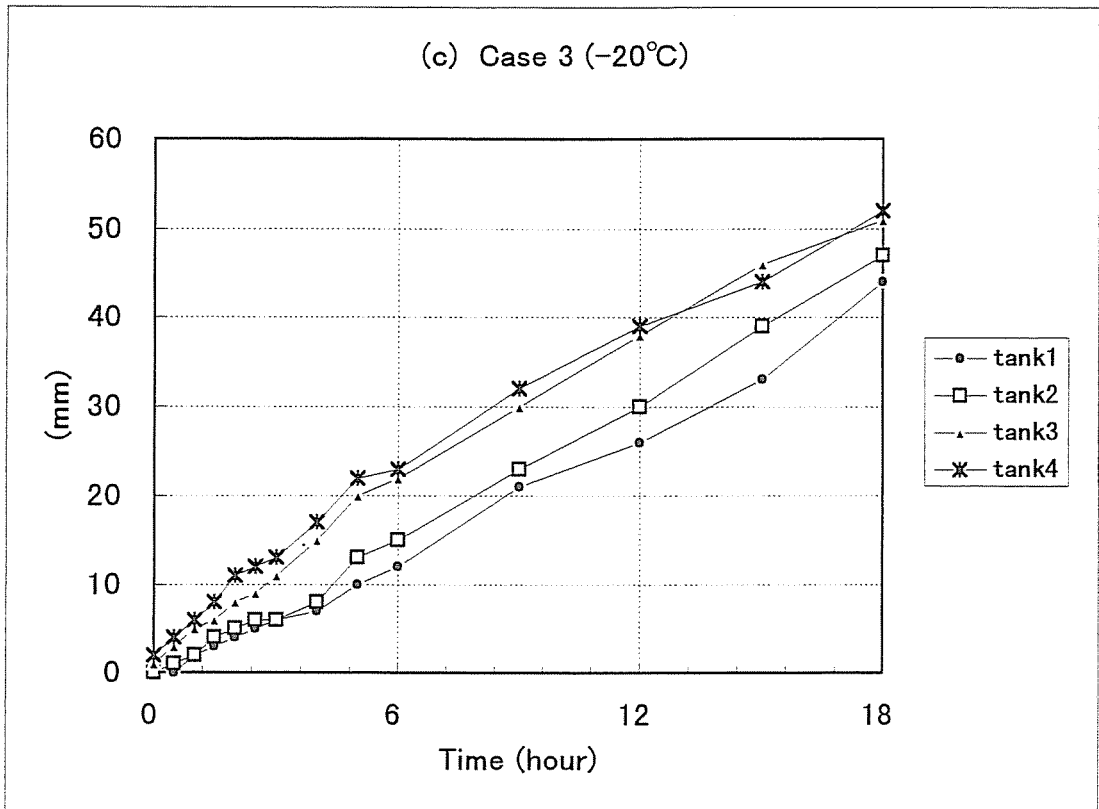


Figure 6.3.2 (Continued.)

(c) Case 3

(d) Tank-1

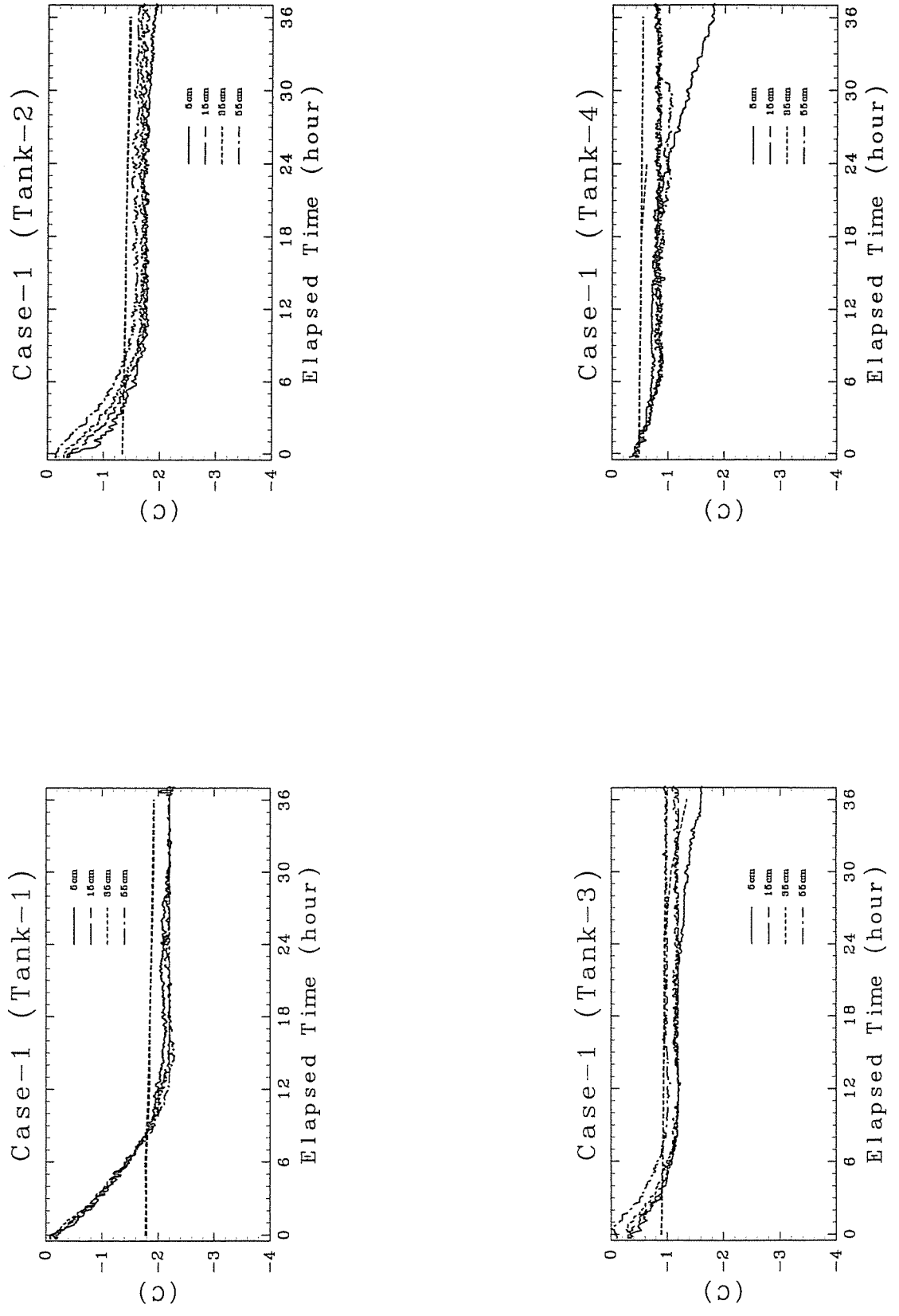


Figure 6.3.3 Time series of water temperature.  
(a) Case 1

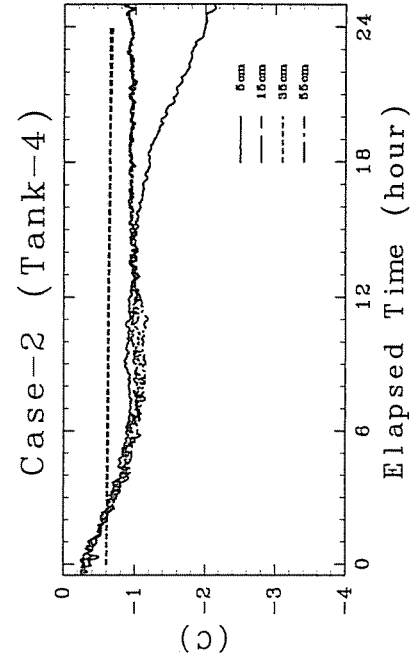
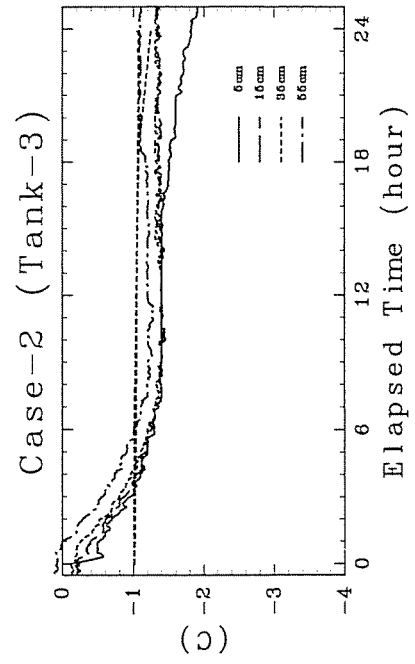
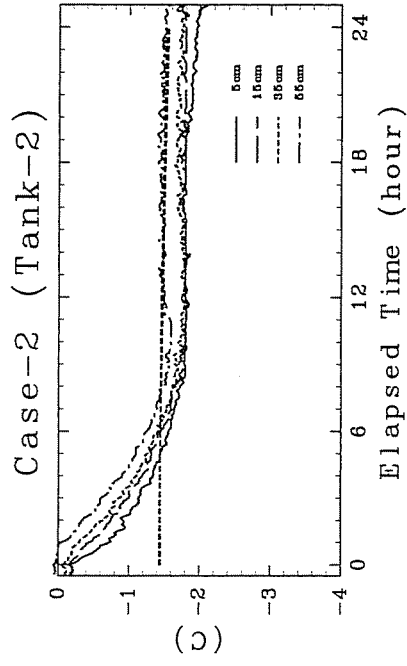
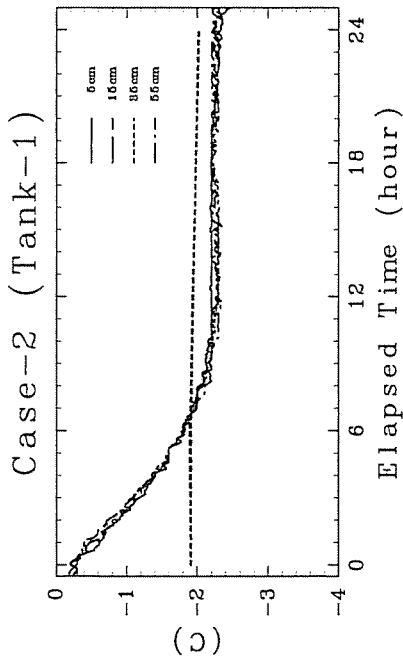


Figure 6.3.3 (Continued.)  
 (b) Case 2

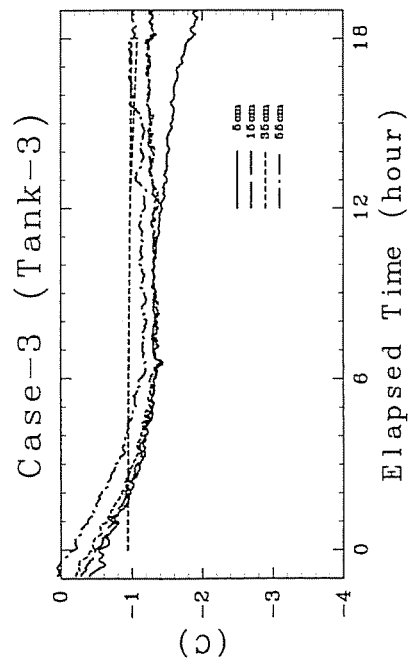
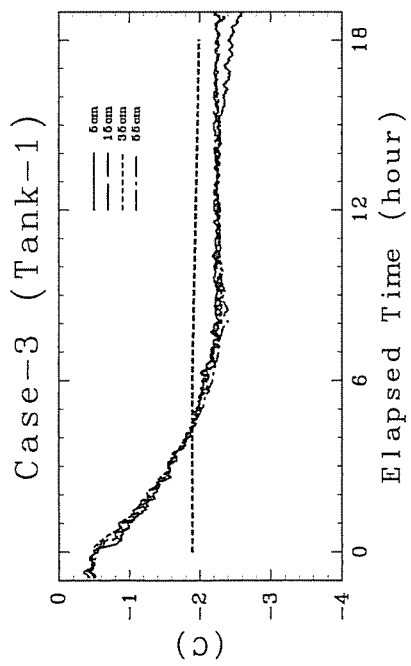
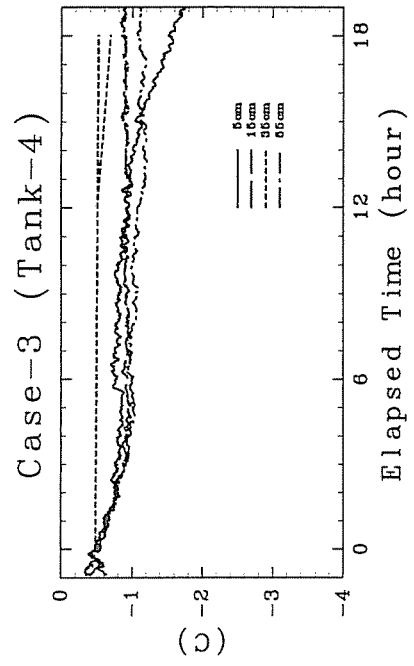
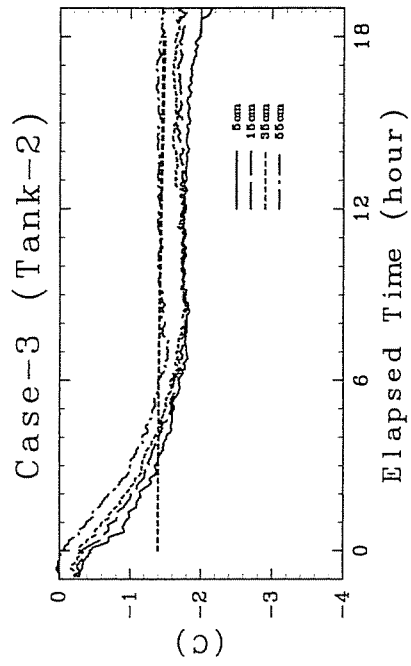


Figure 6.3.3 (Continued.)

(c) Case 3

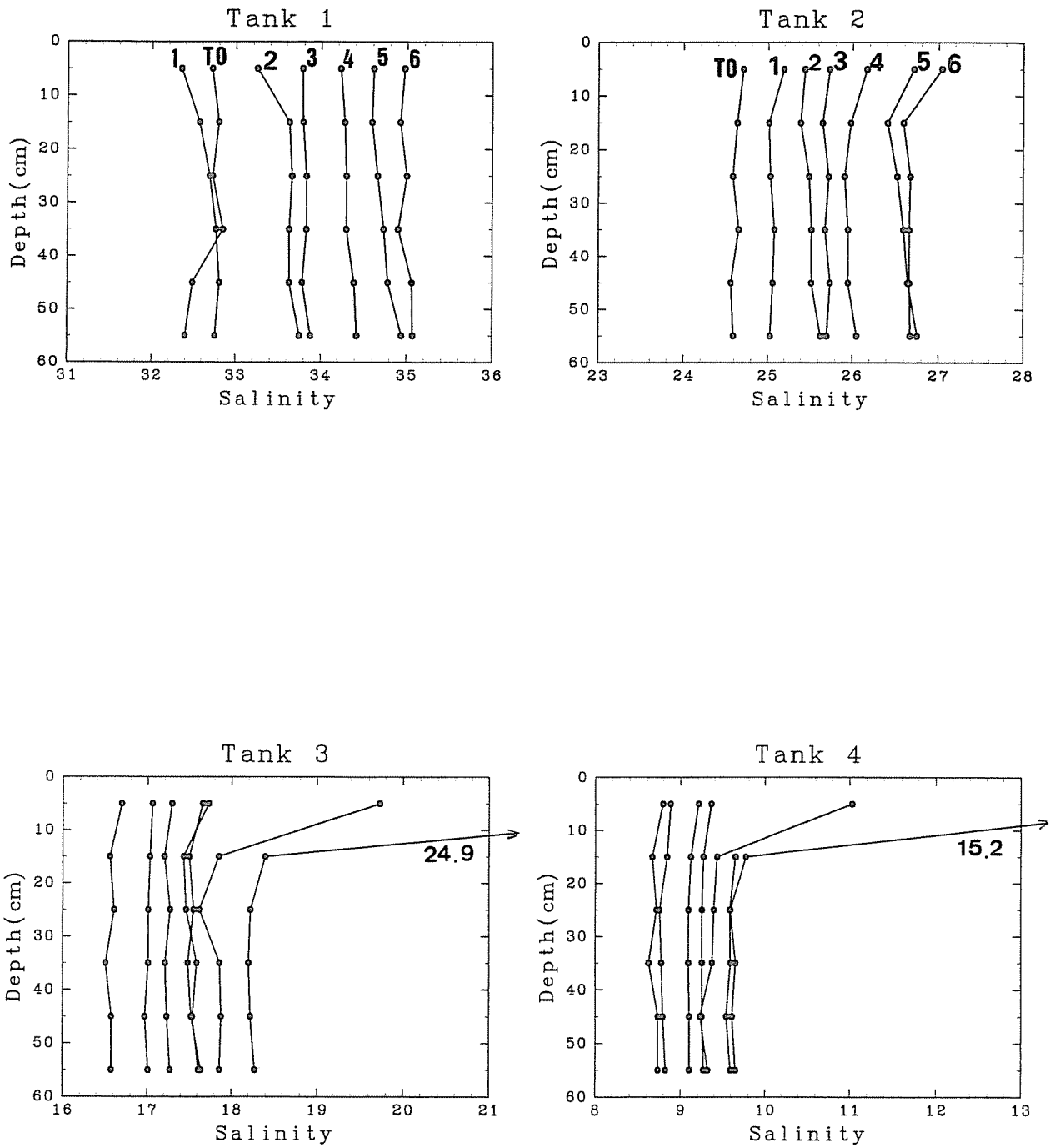


Figure 6.3.4 Time series of the vertical profile of water salinity at 6 hours' intervals.

T0,1,2, means initial, 6hours, 12hours, respectively.

(a) Case 1

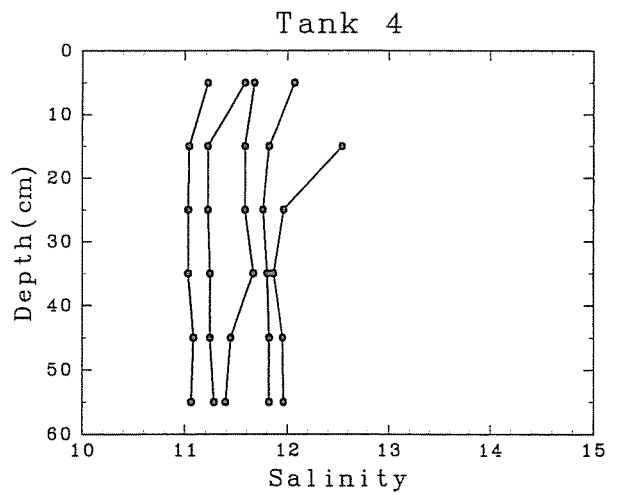
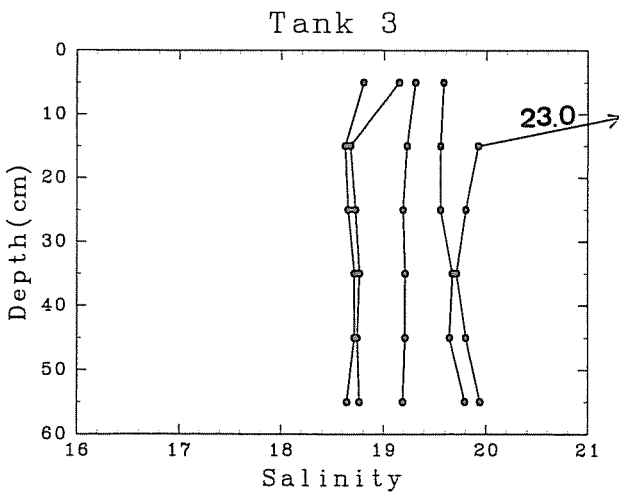
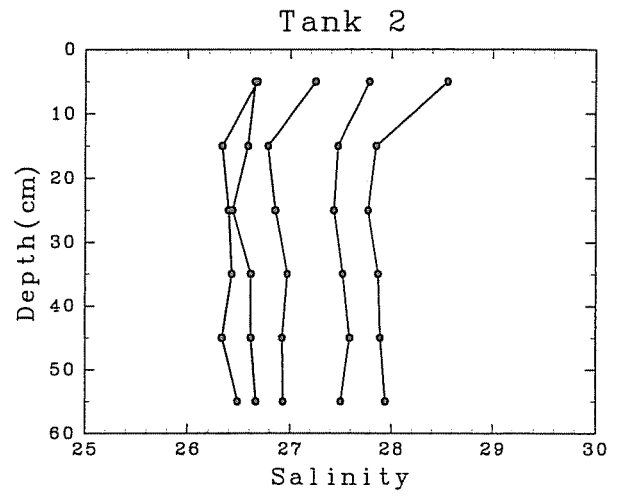
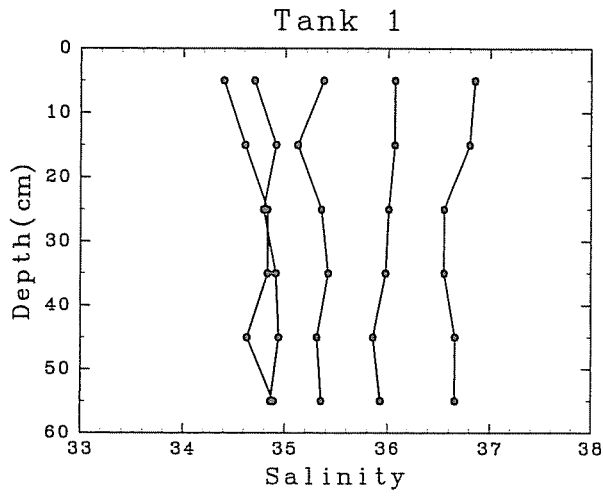


Figure 6.3.4 (Continued.)

(b) Case 2



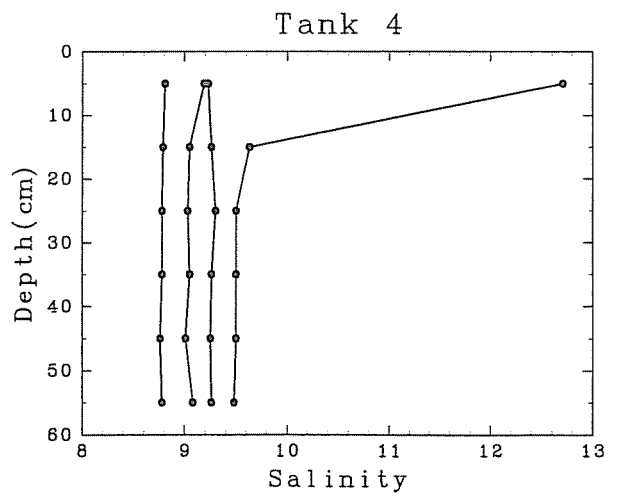
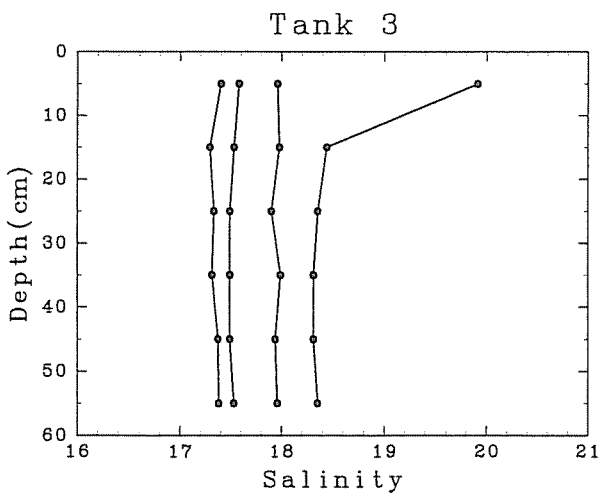
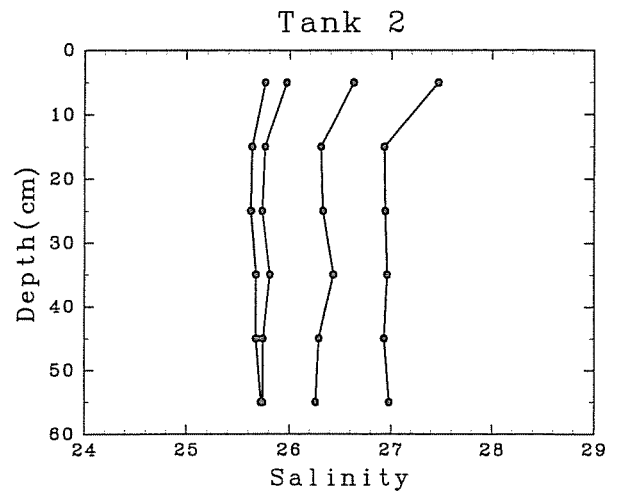
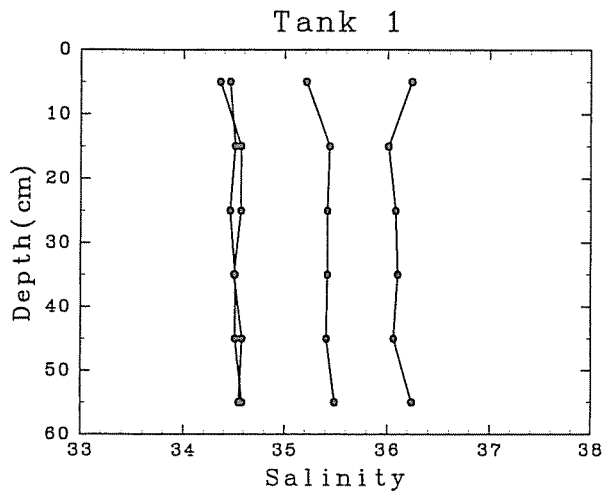


Figure 6.3.4 (Continued.)

(c) Case 3

ject to expelled brine. Because highly saline water is expelled as ice grows, salinity was found to increase by 2 to 3 psu as a whole. However, since the salinity just below the ice under-surface was remarkably high compared with the water salinity at middle depth as shown in Tank-3 and -4 of Figure 6.3.4, this slight increase in salinity did not seem to affect the local activity of the ice growth beneath ice under-surface. The decrease of freezing temperature associated with the salinity increase was almost negligible as shown in Figure 6.3.3.

When the experiments were finished, the ice thickness of each tank was almost uniform (Figure 6.3.5a) and hence the effect of the freezing on the side walls appeared to be only a little. We cut out a square ice sample with dimensions of about 16cm \* 16cm using a hand-saw. It was found that a number of ice plates were developed beneath the ice under-surface, which is one of the characteristics of ice formed from super-cooled sea water (Figure 6.3.5b). Since this type of ice appears after the crystal c-axes becomes nearly horizontal, it does not seem to be relevant to the structure of ice skim which is the matter in this chapter.

We cut a square sample into four pieces and examined their vertical structure through thin section analysis. The method of thin section analysis is same as that described in the previous chapter. One example is shown in Figure 6.3.6. It is shown that the upper most skim layer of a few millimeters thickness is much more transparent in the scatter photo, and should be discriminated from the lower layer. In fact, these horizontal structures were definitely different. In the upper layer, the crystal c-axes were almost all vertical (Figure 6.3.7a), while they were much inclined in the lower layer (Figure 6.3.7b). We measured the thickness of the upper layer at 1-cm interval for all the samples and examined the representative thickness of this c-axis vertical layer (referred to as CAV here). Individual polarized photographs are shown in Figure 6.3.8.

The result of measurement is shown in Figure 6.3.9a-d. Error bars represent the standard deviation. We can see from Figure 6.3.9ab that the thickness of CAV in Tank-1

(a)



(b)



Figure 6.3.5 Photograph of formed ice

(a) Formed ice just after the experiment.

(b) Cut-out ice (upside down).

(a)



(b)

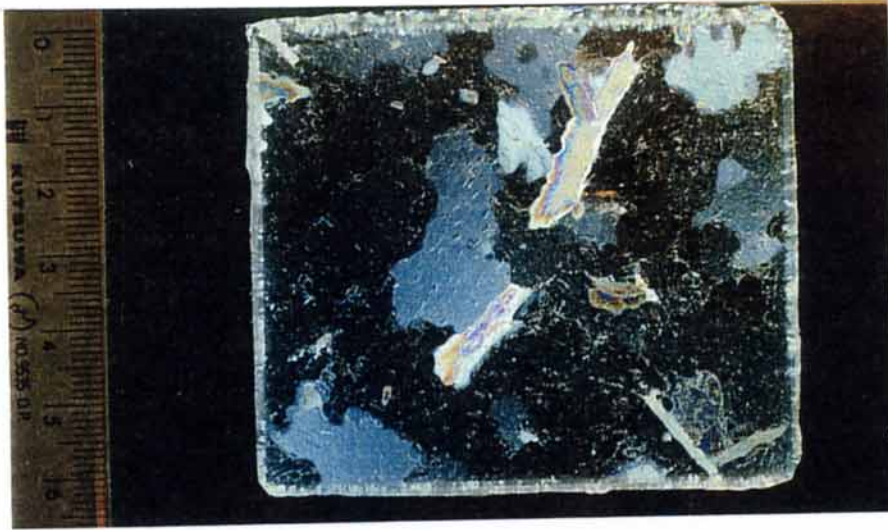


Figure 6.3.6 Vertical thin section.

(a) Scatter photo (5mm thick).

(b) Polarized photo (0.5mm thick).

(a)



(b)



Figure 6.3.7 Polarized photos of horizontal thin section.

(a) Upper most layer

(b) Mid layer



Tank 1



Tank 2



Tank 3



Tank 4

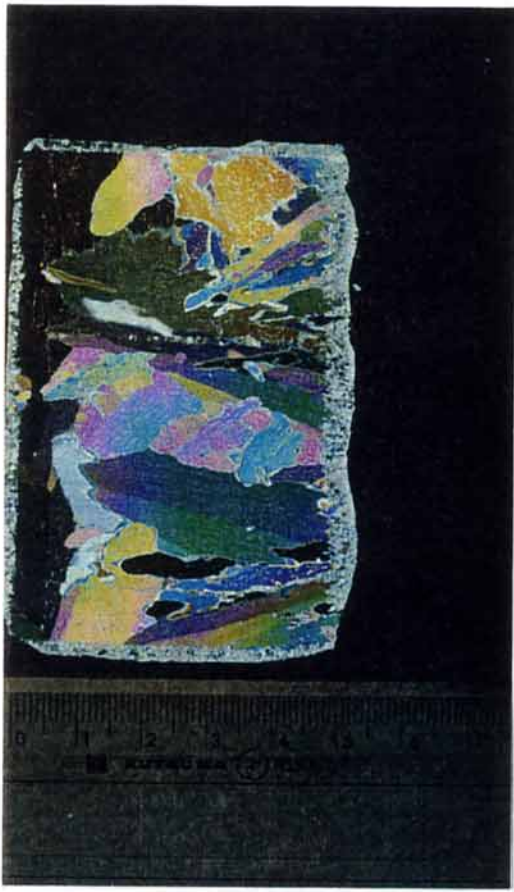


Figure 6.3.8 Polarized photos of vertical thin section.

(a) Case 1



Tank 2



Tank 4



Tank 1



Tank 3



Figure 6.3.8 (Continued.)  
(b) Case 2

Tank 1



Tank 2



Tank 3



Tank 4



Figure 6.3.8 (Continued.)  
(c) Case 3



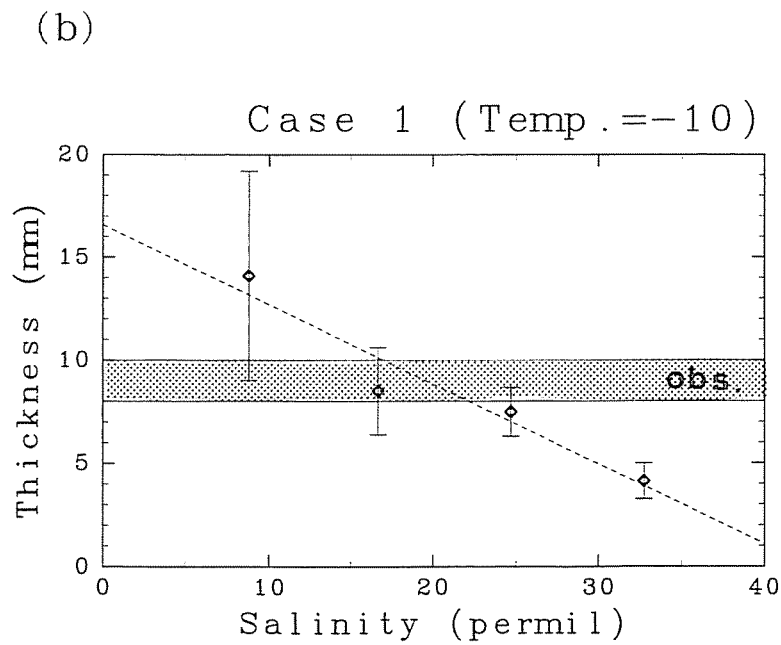
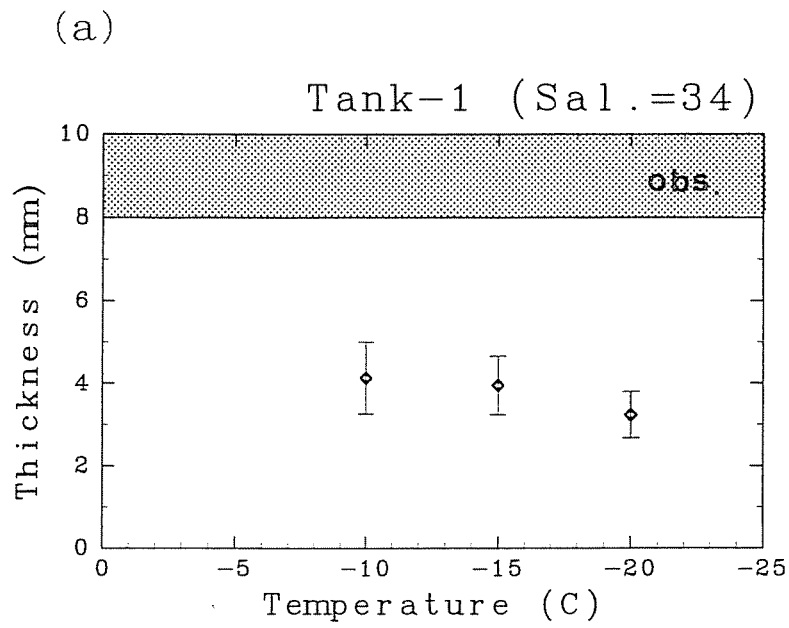
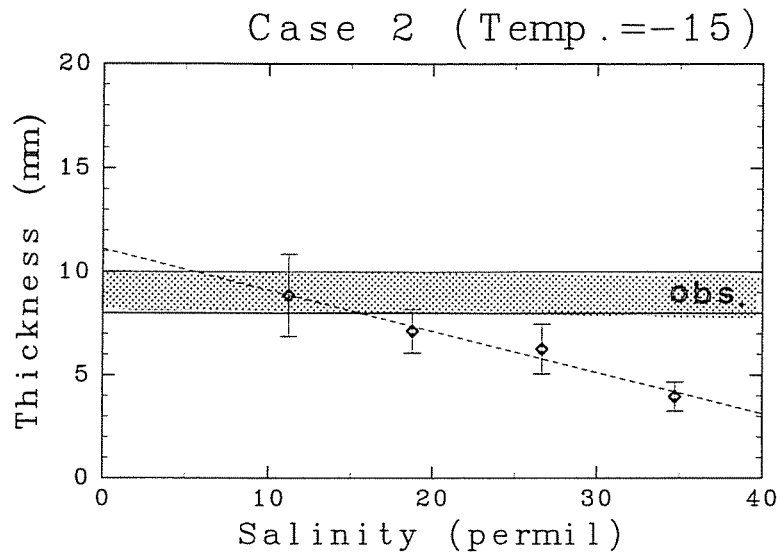


Figure 6.3.9 Thickness of c-axis vertical layers.

(a) Tank-1 (34 permil)

(b) Case 1

(c)



(d)

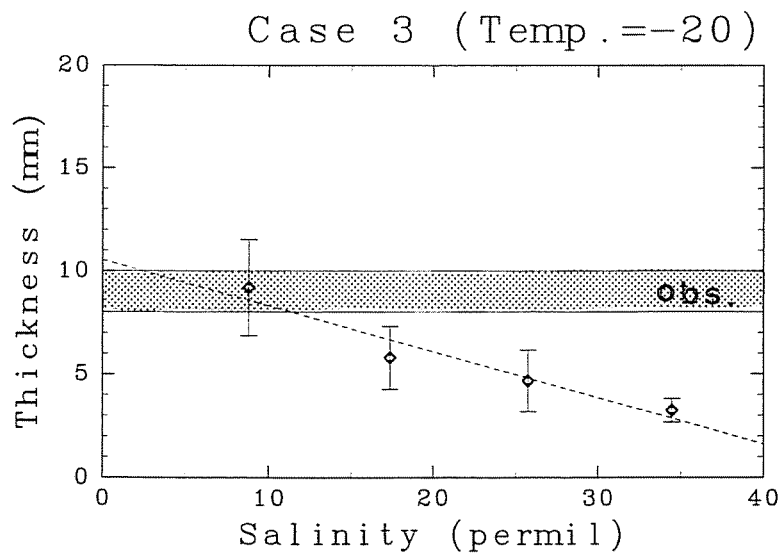


Figure 6.3.9 (Continued.)

(a) Case 2

(b) Case 3

(Okhotsk model case) is about half of the observed value and its variation is also small. This means that the CAV thickness cannot develop up to the observed value even if quite calm conditions are realized in the observed area. This thickness and its variation depend much on salinity. They both increase rapidly with the decrease of salinity. For example, when water salinity is below 25 psu, it is sufficiently possible for CAV to develop to 8-10 mm thickness, which was observed in the southern region of the Okhotsk Sea. It is true also for Case 2 and Case 3 (Figure 6.3.8cd). On the other hand, the dependence of the CAV thickness on temperature is relatively small, although slight increase can be detected with the decrease of temperature (Figure 6.3.9a). This implies that growth rate is less important than salinity to the thickness.

From these results, it is shown that less saline water plays an important role in the developing of the CAV layer to develop to the observed thickness in the southern region of the Okhotsk Sea. According to the ice growth calculation in Chapter 4, less saline water at the sea surface can possibly be produced due to the ice melting at daytime. If this is the case, this type of nilas may be one of the characteristics of the sea ice existing in the Okhotsk Sea.

#### 6.4 Summary and Discussion

In order to examine the thickness of the c-axis vertical layer, which appears at the ice skim when ice forms under calm conditions, we conducted laboratory experiments. Four tanks filled with waters of different salinities were prepared for this experiments and were cooled under the same conditions. The experiments were carried out for the room temperatures of  $-10^{\circ}C$ ,  $-15^{\circ}C$ ,  $-20^{\circ}C$ . The thicknesses of the upper most layer of each artificially formed ice sample were measured at 1-cm-intervals through thin section analysis. The results show that the c-axis vertical layer does not develop up to the observed thickness of 8-10 mm, and that its thickness depends more strongly on water salinity than on temperature conditions. Considering that less saline water can possibly

be produced due to ice melting at daytime in the southern region of the Okhotsk Sea, it is considered that less saline water was responsible for the observed nilas structure.

Here, we discuss what kind of process causes the c-axis to be inclined during the ice growth process. Since it is suggested from the above results that water salinity is a leading factor, we here focus on the effect of salinity. Because averaged bulk ice salinities were 8.2 (Tank-1), 5.9 (Tank-2), 3.9 (Tank-3), and 2.1 (Tank-4) for Case 1, and ice thicknesses were 4.0, 4.6, 5.6, 6.0 cm, respectively, the expected increase of salinity was 2.4 (Tank-1), 1.6 (Tank-2), 1.3 (Tank-3), and 0.7 (Tank-4) in psu if we assume that increased salinity is well mixed. The observed increase was 2.3, 2.0, 1.6, and 0.9, respectively, and thus prediction and observation almost match well. This implies that most of the expelled brine from ice was mixed well with the underlying whole water and that the extremely high values salinity, which were observed at the upper most layer in Tank-3 and Tank-4, were only limited to thin layer beneath ice under-surface. This local high salinity just below growing ice is also found in the experiments by *Wakatsuchi (1977)*, and can be explained by the balance of salinity diffusion and advection (*Weeks and Ackley, 1986*). From these results, we assumed the following c-axis inclination process:

- (1) While greater part of the expelled brine fall down and is well mixed with underlying water, some part of the expelled brine is stocked at the thin layer beneath ice under-surface.
- (2) The salinity at this thin layer increases as ice grows and brine is expelled.
- (3) When it reaches a critical value, convective activity becomes vigorous rapidly.
- (4) This activity causes c-axis to be much inclined from vertical.

Here we try to estimate the critical salinity value from calculation. We assume that part of the expelled brine is stocked at the fixed thin layer ( $x - mm$ ) beneath ice. Then the salinities at this layer when CAV layer reaches its maximum thickness are described as

follows:

$$\text{Tank - 1 : } \quad (S_{W01} - S_{I1}) * \frac{H_1}{x} + S_{W01} \quad (\text{psu}) \quad (1)$$

$$\text{Tank - 2 : } \quad (S_{W02} - S_{I2}) * \frac{H_2}{x} + S_{W02} \quad (\text{psu}) \quad (2)$$

$$\text{Tank - 3 : } \quad (S_{W03} - S_{I3}) * \frac{H_3}{x} + S_{W03} \quad (\text{psu}) \quad (3)$$

$$\text{Tank - 4 : } \quad (S_{W04} - S_{I4}) * \frac{H_4}{x} + S_{W04} \quad (\text{psu}) \quad (4)$$

, where  $S_{W0i}$  is initial water salinity (32.72, 24.70, 16.69, and 8.79 psu, for  $i=1,4$ ),  $S_{Ii}$  is the ice salinity of CAV layer (7.24, 3.93, 2.16, and 1.91 psu), and  $H_i$  is the thickness of CAV layer (4.13, 7.48, 8.50, 14.10 mm). If we assume that the critical salinity is independent of water salinity, the above salinities are considered to be same. When we take the data of Tank-1 and Tank-2, in which the variation of CAV thickness is relatively small, we get  $x = 6.3$  mm by resolving the equation of (1)=(2). This  $x$  value gives the critical salinity of 49.4 psu. On the other hand, from the regression shown in Figure 6.3.9b, the salinity above which CAV layer cannot exist is estimated as 42.9 psu. This value is nearly consistent with the estimated critical salinity. The similar calculation was also done for Case 2. The result showed that the critical salinity was 51.0 psu and that the salinity calculated from the regression (Figure 6.3.8c) was 55.7. Again, both salinity matched well for this case. These results imply that CAV layer can hardly exist above about 50 psu, and support our assumption that crystal c-axes tend to be slanted at a fixed critical value. In addition, our results of temperature dependence are consistent with that of *Wakatsuchi and Ono (1983)*. According to their results, salt flux increases with the increase of ice growth rate. That is, CAV thickness is expected to be thinner for higher growth rate because the critical salinity would be more quickly reached with the increase of salt flux. Our result is in agreement with this expectation (see Figure 6.3.9a).

Next we consider what the critical salinity means. One of the possible explanations is suggested by *Wettlaufer et al. (1997)*. It is known that the solid growing from a liquid mixture (such as sea water) usually forms a porous layer. Through laboratory experi-

ments, they presented the idea that the brine expelled by growing sea ice initially remains trapped by this porous layer and drains into the underlying water by dynamically breaking when it exceeds a critical density. If the similar process occurred in our experiments, it is likely that convective activity becomes vigorous when salinity beneath ice reaches a critical value, causing the c-axes to be inclined. To understand the real mechanism, further investigation will be required.

Finally, we discuss the applicability of the experimental results to the real ocean. It was shown through laboratory experiments that somewhat less saline water can cause as thick as 1-cm CAV layer under very calm conditions in the southern region of the Okhotsk Sea. But can such calm conditions be realized in the real ocean? In general, turbulence is dominant in the ocean due to wind and swells. Turbulence causes mixture of water and low salinity water at the surface is difficult to be maintained. Within the sea ice area, however, it is known that sea ice floes works as buffers which damp turbulent wave motions (e.g. *Keller, 1998*). Actually, extremely flat ocean surfaces were sometimes observed within sea ice area during the cruise. Besides, once thin ice is formed, it protects sea water from being disturbed by wind. Therefore, we consider that such calm conditions as the laboratory circumstances, under which we conducted the experiments, can possibly occur in the real ocean. From in-situ observation, such low salinity at the ocean surface has not been proved yet. To present an actual evidence, very careful sampling will be required. We would like to try in the future.

## Chapter 7. Conclusions

In order to investigate the characteristics of the sea ice, particularly its growth processes, in the southern region of the Okhotsk Sea, we conducted ice observations in connection with meteorological and hydrographical observation from 3 to 5 February of 1996 and from 2 to 9 February of 1997. The results of the analytical study is summarized as follows:

### Albedo

From the analysis focusing on the horizontal scale of a few kilometers, it was found that the surface albedo was highly correlated with the ice concentration with the *RMS* of 0.062. It had a statistically significant correlation with solar zenith angle, and the daily integrated sea ice albedo was estimated as  $0.63 \pm 0.03$  from the linear regression. This value is somewhat lower than that of snow covered land-fast ice before melting in the polar regions. The characteristics of the snow grains, which develop rapidly due to the effect of sea water and/or solar radiation, may be responsible for this lower value.

Sea ice albedo had also a weak but significant correlation with ice thickness. If we take ice concentration, thickness, and solar zenith angle as the parameters of the regression, the *RMS* between observation and prediction was reduced to 0.050. The data which still deviated considerably from regression seemed to be caused by surface conditions rather than by cloud cover. From examination of video images, it was found that albedo of less snow covered ice floes is lowered, whereas for remarkably large ice floes albedo is heightened. The degree of surface roughness did not seem to be substantial. The daily integrated sea ice albedo for individual ice thickness, which is obtained from the regression, is used for heat budget calculation.

### Heat budget

On the basis of meteorological observation and the estimated sea ice albedo, the heat budget over this region was calculated with a one dimensional thermodynamical model.

From the result of calculation, the sea ice extent over this region can be characterized as follows:

- (1) Thermodynamical ice growth cannot be expected so much (below 0.5cm/day) mainly due to abundant solar radiation.
- (2) Thin ice and open area contributes by more than half to the turbulent heat flux, which is a similar feature to the polar regions.
- (3) Since relatively thin ice area is dominant, the area-weighted heat flux becomes upward and sea ice area works as a heating source than a cooling source, which is different characteristics from the polar thick ice regions.

#### Sample analysis

We took ice samples of 14 in 1996 and 35 in 1997 and analyzed them to examine their structure. It was found through thick/thin section analysis of thick ice that granular structure occupies greater part of the ice sample than columnar one and that many ice samples are composed of several ice sheets of 5 to 10 cm thickness/layer on average. These results show that dynamic processes play a significant role in ice growth processes in this region. These features are similar to those of the Antarctic sea ice. Particularly, the latter result indicates the importance of a rafting process and it is considered that a phenomenon similar to 'Pancake cycle' (Lange *et al.*, 1989) in the Antarctic region occurs also in this region. These results are consistent with those of heat budget analysis in that thermodynamical process cannot be dominant in the ice growth processes in this region.

For thin ice, the samples of nilas of about 1 cm thickness with almost vertically aligned c-axes is dominant in all the layer were found out. From the result of laboratory experiments, it is shown that less saline water than normal sea water is required for this c-axis vertical layer to develop up to the observed values of 8-10 mm. On the other hand, it is shown from heat budget analysis that such less saline water can possibly be produced due to ice melting by solar radiation at daytime. Thus, this kind of nilas may be one of



the characteristics of sea ice at a low latitude.

From the analysis of bulk ice salinity, it is shown that bulk ice salinity is by 3 to 4 permil lower than the salinity of sea ice taken at the freezing season in the polar regions. Considering that desalination can occur more quickly due to ice melting by relatively high temperature and abundant solar radiation in this region, this result may indicate the characteristics of the sea ice in this region. Vertical salinity profiles also support this idea.

Finally, we would like to conclude this paper by presenting the answers to the questions which we put in the introduction.

(1) How does sea ice in the southern region of the Okhotsk Sea develop ?

Thermodynamical growth cannot be expected so much, and such dynamical growth as rafting of ice floes plays an important role in growth processes.

(2) How much effect does the existence of sea ice have on the heat exchange between the atmosphere and the ocean in this region ?

Heat exchange with atmosphere is eliminated by about half compared with the values without sea ice and thin ice and open area are responsible for more than the heat exchange.

(3) Does sea ice of relatively low latitude have different features from that of the polar regions ?

Sea ice albedo is somewhat lower than that of the polar land-fast ice regions, which is attributed to the characteristics of snow on sea ice. Sea ice area works as a heating source due to relatively thin ice thickness distribution. Further the nilas samples which had the c-axis vertical layer of as thick as 8-10 mm were found out.

Although some characteristics of sea ice in the southern Okhotsk Sea could be obtained, the in-situ ice observations over this region have just started a few years before. Further data accumulation will be desired to clarify the ice growth processes in this region.

## References

- Allison, I., C.M. Tivendale, G.J. Akerman, J.M. Tann, and R.H. Wills, 1982:  
Seasonal variations in the surface energy exchanges  
over Antarctic sea ice and coastal waters. *Ann. Glaciol.*, 3, 12-16.
- Allison, I., R.E. Brandt, and S.G. Warren, 1993: East Antarctic sea ice:  
albedo, thickness distribution, and snow cover.  
*J. Geophys. Res.*, 98, 12417-12429.
- Allison, I., A.P. Worby, 1994: Seasonal changes in sea ice characteristics  
off east Antarctica. *Ann. Glaciol.*, 20, 195-201.
- Andreas, E.L. and A.P. Makshtas, 1985: Energy exchange over Antarctic sea  
ice in the spring. *J. Geophys. Res.*, 90, 7199-7212.
- Aota, M., M. Ishikawa, and E. Uematsu, 1988: Variation in ice concentration off Hokkaido  
island. *Low Temp. Sci., Ser. A*, 47, 161-175. (in Japanese with English summary)
- Aota, M., K. Shirasawa, T. Takatsuka, 1989: Measurements of an atmospheric  
boundary layer around the air-sea-ice observation tower: 1989 winter experiments.  
*Low Temp. Sci., Ser. A*, 48, 79-89. (in Japanese with English summary)
- Chen, S.-J., Y.-H. Kuo, P.-Z. Zhang, and Q.-F. Bai, 1991: Synoptic climatology  
of cyclogenesis over east Asia, 1958-1987. *Mon. Wea. Rev.*, 119, 1407-1418.
- Crocker, G.B., and P. Wadhams, 1989: Modelling Antarctic fast-ice growth.  
*J. Glaciol.*, 35, 3-8.
- Cox, G.F.N., and W.F. Weeks, 1974: Salinity variations in sea ice.  
*J. Glaciol.*, 13, 109-120.
- Eicken, H., M. Lensu, M. Lepparanta, W.B. Tucker III, A.J. Gow, and O. Salmela, 1995:  
Thickness, structure, and properties of level summer multiyear ice  
in the Eurasian sector of the Arctic Ocean.  
*J. Geophys. Res.*, 100, 22697-22710.

- Fukuzawa,T., and E.Akitaya, 1993: Depth-hoar crystal growth in the surface layer under high temperature gradient. *Ann.Glaciol.*,18,39-45.
- Grenfell,T.C. and G.A.Maykut, 1977: The optical properties of ice and snow in the Arctic Basin. *J.Glaciol.*,18,445-463.
- Grenfell,T.C. and D.K.Perovich, 1984: Spectral albedos of sea ice and incident solar irradiance in the southern Beaufort Sea. *J.Geophys.Res.*,89,3573-3580.
- Gow,A.J., S.F.Ackley, K.R.Buch, and K.M.Golden, 1987a: Physical and structural characteristics of Weddell Sea pack ice. *CRREL Report*,87-14,75pp.
- Gow,A.J., W.B.Tucker III, and W.F.Weeks, 1987b: Physical properties of summer sea ice in the Fram Strait, June-July, 1984. *CRREL Report*.87-16,81pp.
- Honda,M., K.Yamazaki, Y.Tachibana, and K.Takeuchi, 1996: Influence of Okhotsk sea-ice extent on atmospheric circulation. *Geophys.Res.Let.*,23,3595-3598.
- Ingram,W.J., C.A.Wilson and J.F.B.Mitchell, 1989 Modeling climate change: an assessment of sea ice and surface albedo feedbacks. *J.Geophys.Res.*,94,8609-8622.
- Ishikawa,N. and S.Kobayashi, 1984: Experimental studies of heat budget of very thin sea ice. *Seppyo*,46,109-119 (*in Japanese*).
- Japan Meteorological Agency, 1996: The results of sea ice observation,14 (*in Japanese*).
- Japan Meteorological Agency, 1997: The results of sea ice observation,15 (*in Japanese*).
- Jeffries,M.O., and U.Adolphs, 1997: Early winter ice and snow thickness distribution, ice structure and development of the western Ross Sea pack ice between the ice edge and the Ross Ice shelf. *Antarctic Sci.*,9,188-200.

- Jeffries, M.O., A.P. Worby, K. Morris, W.F. Weeks, 1997:  
 Seasonal variations in the properties and structural composition of sea ice  
 and snow cover in the Bellingshausen and Amundsen Seas, Antarctica.  
*J. Glaciol.*, 43, 138-151.
- Kawamura, T., 1982: Measurements of crystallographic orientations of sea ice.  
*Low Temp. Sci., Ser. A41*, 173-178. (in Japanese with English summary)
- Kawamura, T., M. Aota, and T. Tabata, 1975: On the divergence and rotation of ice field  
 off Okhotsk Sea coast of Hokkaido. *Low Temp. Sci., Ser. AA*, 33, 179-190.  
 (in Japanese with English summary)
- Keller, J.B., 1998: Gravity waves on ice-covered water.  
*J. Geophys. Res.*, 103, 7663-7669.
- Kim, Y.-S., 1992: Estimate of heat transport across the sea surface  
 near Japan with bulk methods. *D. Sci., Univ. of Tokyo*, 124pp.
- Kondo, J. 1967: Analysis of solar radiation and downward longwave radiation data  
 in Japan. *Science Report Tohoku University*, 5, 91-124.
- Lange, M.A., S.F. Ackley, and P. Wadhams, 1989: Development of sea ice  
 in the Weddell Sea. *Ann. Glaciol.*, 12, 92-96.
- Lange, M.A., and H. Eicken, 1991: Textural characteristics of sea ice and  
 the major mechanism of ice growth in the Weddell Sea. *Ann. Glaciol.*, 15, 210-215.
- Maykut, G.A., 1978: Energy exchange over young sea ice in the central Arctic.  
*J. Geophys. Res.*, 83, 3646-3658.
- Maykut, G.A., 1982: Large-scale heat exchange and ice production in the Central Arctic.  
*J. Geophys. Res.*, 87, 7971-7984.
- Maykut, G.A., and P.E. Church, 1973: Radiation Climate of Barrow, Alaska, 1962-66.  
*J. Appl. Met.*, 12, 620-680.
- Martin, S., and P. Kauffman, 1981: A field and laboratory study of wave damping  
 by grease ice. *J. Glaciol.*, 27, 283-313.

- Mellor, M., 1977: Engineering properties of snow. *J.Glaciol.*,19,15-66.
- Muramoto,K., K.Matsuura and T.Endoh, 1993:  
 Measuring sea-ice concentration and floe-size distribution  
 by image processing. *Ann. Glaciol.*,18,33-38.
- Nakamura,H., T.Toyota, and M.Ohbayashi, 1986: Geographical distribution of the ratio  
 of lengths of warm fronts to cold fronts in the northern hemisphere  
 during 1978-1979 winter. *J.Meteor.Soc.Japan*,64,519-529.
- Nakawo,M. and N.K.Sinha, 1981: Growth rate and salinity profile of  
 first-year sea ice in the high Arctic. *J.Glaciol.*,27,315-330.
- Okubo,H. and N.Mannoji, 1994: The influence of the sea ice distribution on the  
 surface wind forecast by Japan Spectral Model. *Tenki*,41,847-851 (in Japanese).
- Ono,N., 1965: Thermal properties of sea ice. I  
 Measurements of the thermal conductivity of young winter ice.  
*Low Temp.Sci.,Ser.A*.23,167-176. (in Japanese with English summary)
- Ono,N., 1967: Specific heat and heat of fusion of sea ice.  
*Physics of snow and ice*, International conference on low temperature science,  
*proceeding, Vol.1*,edited by H.Oura, 599-610.
- Overland,J.E. and C.H.Pease, 1982: Cyclone Climatology of the Bering Sea  
 and its relation to sea ice extent. *Mon.Wea.Rev.*,110,5-13.
- Perovich,D.K., 1994: Light reflection from sea ice during the onset of melt.  
*J.Geophys.Res.*,99,3351-3359.
- Perovich,D.K., and A.J.Gow, 1996: A quantitative description of sea ice inclusions.  
*J.Geophys.Res.*,101,18327-18343.
- Persson,P.O.G., D.Ruffieux, and C.W.Fairall, 1997: Recalculations of pack ice  
 and lead surface energy budgets during the Arctic Leads Experiment  
 (LEADDEX) 1992. *J.Geophys.Res.*,102,25085-25089.

- Ruffieux,D., P.O.G.Persson, C.W.Fairall, and D.E.Wolfe, 1995:  
Ice pack and lead surface energy budgets during LEADDEX 1992.  
*J.Geophys.Res.*,100,4593-4612.
- Sasaki,H. and S.Deguchi, 1988: Numerical experiments of the convergent band  
off the western coast of Hokkaido in winter. *Tenki*,35,723-729 (in Japanese).
- Schlosser,E. ,1988: Optical studies of Antarctic sea ice.  
*Cold Reg. Sci. and Technol.*,15,289-293.
- Shimoda,H., T.Endo, K.Muramoto, N.Ono, T.Takizawa, S.Ushio,  
T.Kawamura, K.Ohshima,1997:  
Observations of sea-ice conditions in the Antarctic coastal region  
using ship-board video cameras. *Antarctic Record*,41,355-365 (in Japanese).
- Shine K.P. and A.Henderson-Sellers ,1985:  
The sensitivity of a thermodynamic sea ice model to changes  
in surfaces albedo parameterization. *J.Geophys.Res.*,90,2243-2250.
- Tabata,T., 1966: Studies of the mechanical properties of sea ice.IX  
Measurement of flexural strength in situ (3). *Low Temp.Sci.,Ser.A*,24,259-268.  
(in Japanese with English summary)
- Tabata,T., M.Aota, M.Ohi, and M.Ishikawa, 1969: Observations on the movement  
of drift ice with the sea ice radar. *Low Temp.Sci.,Ser.A*,27,295-315.  
(in Japanese with English summary)
- Tachibana,Y., M.Honda, and K.Takeuchi, 1996: The abrupt decrease of the sea ice  
over the southern part of the Sea of Okhotsk in 1989 and its relation  
to the recent weakening of the Aleutian low. *J.Meteor.Soc.Japan*,74,579-584.
- Thorndike,A.S., D.A.Rothrock, G.A.Maykut, and R.Colony, 1975:  
The thickness distribution of sea ice. *J.Geophys.Res.*,80,4501-4513.
- Tsurikov,V.L., 1979: The formation and composition of the gas content of sea ice.  
*J.Glaciol.*,22,67-81.

- Tucker III, W.B., T.C. Grenfell, R.G. Onstott, D.K. Perovich, A.J. Gow, R.A. Shuchman, and L.L. Sutherland, 1991: Microwave and physical properties of sea ice in the winter marginal ice zone. *J. Geophys. Res.*, 96, 4573-4587.
- Untersteiner, N., 1961: On the mass and heat budget of arctic sea ice. *Arch. Met. Geophys. Bioklim.*, A(12):151-182.
- Ushio, S., and M. Wakatsuchi, 1993: A laboratory study on supercooling and frazil ice production processes in winter coastal polynyas. *J. Geophys. Res.*, 98, 20321-20328.
- Wadhams, P., J.C. Comiso, E. Prussen, S. Wells, M. Brandon, E. Aldworth, T. Viehoff, R. Allegrino, and D.R. Crane, 1996: The development of the Odden ice tongue in the Greenland Sea during winter 1993 from remote sensing and field observations. *J. Geophys. Res.*, 101, 18213-18235.
- Wakatsuchi, M., 1977: Experiments on haline convection occurring under growing sea ice. *Low Temp. Sci., Ser. A* 35, 249-258. (in Japanese with English summary)
- Wakatsuchi, M., and N. Ono, 1983: Measurements of salinity and volume of brine excluded from growing sea ice. *J. Geophys. Res.*, 88, 2943-2951.
- Walsh, J.E., and C.M. Johnson, 1979: An analysis of Arctic sea ice fluctuation, 1953-77. *J. Phys. Oceanogr.*, 9, 580-591.
- Walter, B.A., J.E. Overland, and P. Turet, 1995: A comparison of satellite-derived and aircraft-measured regional surface sensible heat fluxes over the Beaufort Sea. *J. Geophys. Res.*, 100, 4585-4591.
- Warren, S.G., 1982: Optical properties of snow. *Rev. Geophys. Space Phys.*, 20, 67-89.
- Watanabe, T., and M. Wakatsuchi, 1998: Formation of 26.8-26.9  $\sigma_\theta$  water in the Kuril Basin of the Sea of Okhotsk as a possible origin of North Pacific Intermediate Water. *J. Geophys. Res.*, 103, 2849-2865.

- Weeks W.F., and S.F.Ackley, 1986: The growth, structure and properties of sea ice. *'The geophysics of sea ice'*, edited by N.Untersteiner,164pp.
- Weller,G. ,1972: Radiation flux investigation. *AIDJEX Bull.*,14,28-30.
- Weller,G. ,1980: Spatial and temporal variations in the south polar surface energy balance. *Mon. Wea.Rev.*,108,2006-2014.
- Wettlaufer,J.S., ,M.G.Worster, and H.E.Huppert, 1997: The phase evolution of young sea ice. *Geophys.Res.Let.*,24,1251-1254.
- Wettlaufer,J.S., 1991: Heat flux at the ice-ocean interface. *J.Geophys.Res.*,96,7215-7236.
- Worby,A.P., M.O.Jeffries, W.F.Weeks, K.Morris, R.Jana, 1996: The thickness distribution of sea ice and snow cover during late winter in the Bellingshausen and Amundsen Seas, Antarctica. *J.Geophys.Res.*,101,28441-28445.
- World Meteorological Organization (WMO), 1970: Sea Ice Nomenclature, Terminology, Codes, and Illustrated Glossary, WMO/OMM/BMO 259,TP 145,Secr. World Meteorol. Organ.,Geneva, Switzerland.
- Yen,Y.C., 1981: Review of thermal properties of snow, ice, and sea ice. *CRREL Rep.*,81-10,27pp.